Earth-Agent: Unlocking the Full Landscape of Earth Observation with Agents

Anonymous authors
Paper under double-blind review

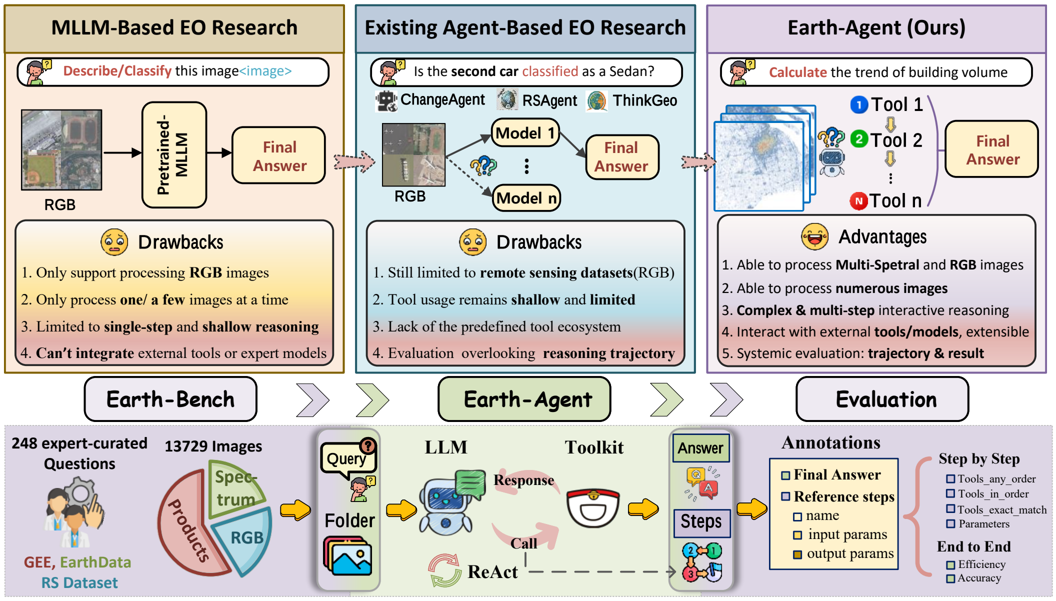
MLLM-Based EO Research
Describe/Classify this image<image>
RGB
Pretrained-MLLM
Final Answer
Drawbacks
1. Only support processing RGB images
2. Only process one/ a few images at a time
3. Limited to single-step and shallow reasoning
4. Can't integrate external tools or expert models
Existing Agent-Based EO Research
Is the second car classified as a Sedan?
ChangeAgent
RSAgent
ThinkGeo
RGB
Model 1
Model n
Final Answer
Drawbacks
1. Still limited to remote sensing datasets(RGB)
2. Tool usage remains shallow and limited
3. Lack of the predefined tool ecosystem
4. Evaluation overlooking reasoning trajectory
Earth-Agent (Ours)
Calculate the trend of building volume
1 Tool 1
2 Tool 2
N Tool n
Final Answer
Advantages
1. Able to process Multi-Spetral and RGB images
2. Able to process numerous images
3. Complex & multi-step interactive reasoning
4. Interact with external tools/models, extensible
5. Systemic evaluation: trajectory & result
Earth-Bench
Earth-Agent
Evaluation
248 expert-curated Questions
GEE, EarthData
RS Dataset
13729 Images
Spectrum
RGB
Products
Query
Folder
LLM
Response
Call
ReAct
Toolkit
Answer
Steps
Annotations
Final Answer
Reference steps
name
input params
output params
Step by Step
Tools_any_order
Tools_in_order
Tools_exact_match
Parameters
End to End
Efficiency
Accuracy

Figure 1: **Overview of our work:** The top panel contrasts prior paradigms: MLLM-based EO research (left), Existing agent-based EO research (middle), and our Earth-Agent (right). The bottom panel illustrates our contributions, including Earth-Bench construction, Earth-Agent ReAct with the predefined toolkit, and dual-level evaluation of both reasoning trajectories and final results.

Abstract

Earth observation (EO) is essential for understanding the evolving states of the Earth system. Although recent MLLMs have advanced EO research, they still lack the capability to tackle complex tasks that require multi-step reasoning and the use of domain-specific tools. Agent-based methods offer a promising direction, but current attempts remain in their infancy, confined to RGB perception, shallow reasoning, and lacking systematic evaluation protocols. To overcome these limitations, we introduce Earth-Agent, the first agentic framework that unifies RGB and spectral EO data within an MCP-based tool ecosystem, enabling cross-modal, multi-step, and quantitative spatiotemporal reasoning beyond pretrained MLLMs. Earth-Agent supports complex scientific tasks such as geophysical parameter retrieval and quantitative spatiotemporal analysis by dynamically invoking expert tools and models across modalities. To support comprehensive evaluation, we further propose Earth-Bench, a benchmark of 248 expert-curated tasks with 13,729 images, spanning spectrum, products and RGB modalities, and equipped with a dual-level evaluation protocol that assesses both reasoning trajectories and final outcomes. We conduct comprehensive experiments varying different LLM backbones, comparisons with general agent frameworks, and comparisons with MLLMs on remote sensing benchmarks, demonstrating both the effectiveness and potential of Earth-Agent. Earth-Agent establishes a new paradigm for EO analysis, moving the field toward scientifically grounded, next-generation applications of LLMs in Earth observation. Our code and dataset will be publicly released.

1 INTRODUCTION

Earth observation (EO) (Transon et al., 2018; Kokkoris et al., 2024; Li et al., 2023a) plays a critical role in understanding the evolving states of the Earth system in spatial and temporal dimensions (Anderson et al., 2017; Li et al., 2024a; Brown et al., 2025), and has been successfully applied to urban planning (Shaker et al., 2019), agriculture (Wójtowicz et al., 2016), resources management (Li et al., 2020), building extraction (Li et al., 2023b; 2024c), disaster monitoring (Joyce et al., 2009; Van Westen, 2000), etc. Typically, EO data is categorized into two types (Samadzadegan et al., 2025): **Perceptual data**, such as ***RGB Imagery (RGB)*** aligned with human vision, and **Raw Observational Data**, including ***Raw Spectral Data (Spectrum)*** and ***Processed Earth Products (Products)*** stored in geodatabases such as Google Earth Engine (GEE)* and NASA Earthdata†. Both types of data are indispensable for EO research: perceptual data provides intuitive and human-interpretable insights, while raw observational data offers rich spectral and spatiotemporal information that enables quantitative analysis (Valipour et al., 2025; Xiong et al., 2022).

In recent years, multimodal large language models (MLLMs) have achieved excellent performance on classical **remote sensing perceptual tasks** such as VQA (Kuckreja et al., 2024; Muhtar et al., 2024), scene classification (Kuckreja et al., 2024; Muhtar et al., 2024; Liu et al., 2024c; Wang et al., 2024e; Hu et al., 2025b; Zhan et al., 2025), object detection (Zhang et al., 2024b), and semantic segmentation (Mall et al., 2023; Guo et al., 2024a). However, despite their promising results, existing MLLM-based EO research still faces several fundamental drawbacks: **(1)** they cannot process diverse EO modalities beyond RGB, such as thermal infrared (TIR), synthetic aperture radar (SAR), or hyperspectral imagery (Zhang et al., 2024b); **(2)** they typically operate on only one or a few images at a time (Li et al., 2024b), making it difficult to scale to large EO corpora; **(3)** they are limited to executing only single-step or shallow reasoning like VQA and classification, struggling with complex multi-hop analytical tasks; and **(4)** their reasoning is bounded by the static knowledge encoded in pretrained parameters, without the ability to integrate external scientific tools or expert models, making it difficult to extend beyond the generic capabilities of the foundation model; This naturally raises the question: *how can we move beyond basic RGB perception and single-step reasoning to design models that integrate diverse EO modalities and support complex multi-step scientific analysis?*

Tool-augmented LLM agents represent a promising trajectory beyond MLLMs (Xi et al., 2025; Sun et al., 2025; Si et al., 2024; Tian et al., 2024; Tang et al., 2025). Unlike MLLMs that are restricted to RGB inputs, simple reasoning, and limited image contexts, agents are not inherently constrained by input modality or data volume (Xie et al., 2024; Gao et al., 2024). By leveraging the reasoning capabilities of LLMs and dynamically interacting with external tools (Xu et al., 2025), they can flexibly process diverse EO modalities, perform multi-step analytical reasoning, and integrate domain-specific tools and expert models that go beyond the scope of the pretrained MLLM model (Ding et al., 2025; Wang et al., 2024c). This mechanism directly tackles the core weaknesses of MLLMs, extending beyond RGB to diverse modalities, scaling from single-image inputs to tasks involving hundreds of images, advancing from shallow perception to multi-step reasoning, and bridging LLMs with external scientific tools for domain-specific analysis.

However, existing agent-based research in Earth science is still at an early stage (Pantiukhin et al., 2025), with existing attempts largely confined to perceptual tasks such as change detection (Liu et al., 2024b; 2025) and classification (Xu et al., 2024a; Hu et al., 2025a), often emphasizing caption ability rather than scientific analysis. Efforts on Raw Observational Data are even more limited. UnivEarth (Kao et al., 2025) considers EO data from GEE but operates essentially as a code generation agent, without implementing genuine tool calling, making it difficult to handle complex and realistic geoscientific analysis tasks that require professional tool use. These efforts reveal several key limitations: **(1)** current EO agents support only limited data modalities, with most efforts still centered on conventional remote sensing datasets dominated by RGB imagery (Xu et al., 2024a); **(2)** their tool usage remains shallow, limited to a few expert models and reasoning steps, even some agents lack a predefined tool ecosystem, making them insufficient for complex analytical workflows (Shabbir et al., 2025); and **(3)** their evaluation remains unsystematic, with emphasis only on final answers while overlooking reasoning trajectory. This raises another question: *how can we design an EO agent with a structured tool ecosystem and systematic evaluation, capable of bridging perceptual and spectral data like Earth scientists?*

---

[*] `https://earthengine.google.com`

[†] `https://search.earthdata.nasa.gov`

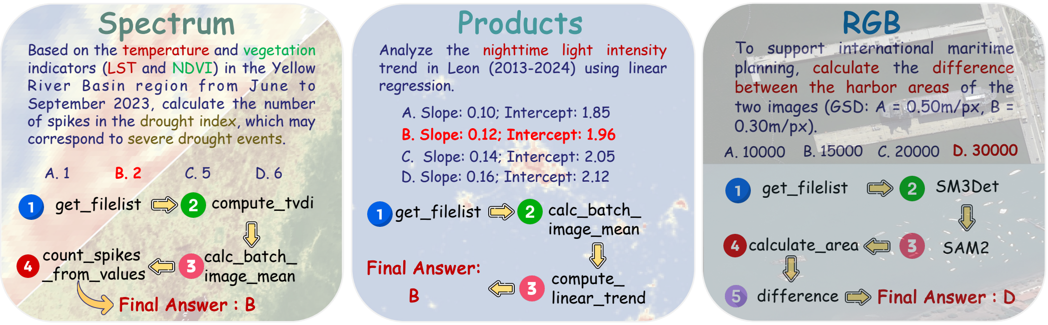

Based on the temperature and vegetation indicators (LST and NDVI) in the Yellow River Basin region from June to September 2023, calculate the number of spikes in the drought index, which may correspond to severe drought events.

A. 1 B. 2 C. 5 D. 6

Analyze the nighttime light intensity trend in Leon (2013-2024) using linear regression.

A. Slope: 0.10; Intercept: 1.85
B. Slope: 0.12; Intercept: 1.96
C. Slope: 0.14; Intercept: 2.05
D. Slope: 0.16; Intercept: 2.12

To support international maritime planning, calculate the difference between the harbor areas of the two images (GSD: A = 0.50m/px, B = 0.30m/px).

A. 10000 B. 15000 C. 20000 D. 30000

Figure 2: Earth-Agent solving tasks across Spectrum, Products, and RGB data through multi-step reasoning with expert tool calls.

To address these questions and unlock the full landscape of EO, we propose **Earth-Agent**, an agentic framework that unifies perceptual and spectral EO data within a single architecture in section 3. By coupling LLM reasoning with a structured toolkit in 3.2, Earth-Agent supports diverse modalities and complex multi-step analysis, enabling agents to tackle real-world geoscientific tasks beyond the limits of existing MLLMs and EO agents. Concretely, Earth-Agent integrates 104 specialized tools, built upon the **Model Context Protocol (MCP)** (Hou et al., 2025; Ray, 2025) for interoperability, and grouped into five domain-specific tool kits: **Index**, **Inversion**, **Perception**, **Analysis**, and **Statistics**. This structured design not only enables the agent to go beyond classical perceptual tasks toward quantitative analysis and spatiotemporal reasoning, but also makes the framework easily extensible with additional domain-specific tools. To systematically evaluate its effectiveness, we further introduce **Earth-Agent Benchmark (Earth-Bench)** in section 4, which reflects realistic EO workflows and supports both **Auto-Planning** and **Instruction-Following** query regimes, together with a **dual-level evaluation** protocol that measures reasoning trajectories as well as final outcomes. We comprehensively evaluate Earth-Agent by varying LLM backbones on Earth-Bench, comparing with general agents, and benchmarking against MLLMs on remote sensing datasets.

To sum up, our main contributions are summarized as follows:

- We propose Earth-Agent, the first agentic framework for EO, built upon the MCP and a ReAct (Yao et al., 2023) reasoning, integrating 104 specialized tools and expert models within predefined tool ecosystem, while remaining easily extensible with additional domain-specific tools and models.
- We construct Earth-Bench, a benchmark of 248 expert-curated questions with 13,729 images, spanning perceptual and spectral modalities beyond RGB. Each question requires multi-step reasoning with explicit tool use, and the benchmark supports a dual-level evaluation protocol that assesses both reasoning trajectories and final answers.
- Through comprehensive evaluation, we show that Earth-Agent substantially outperforms general agents such as Operator (OpenAI, 2025b) and Manus (Shen et al., 2025) on Earth-specific tasks in Earth-Bench, and also surpasses remote sensing MLLMs on remote sensing benchmarks, demonstrating both its effectiveness and potential for advancing EO research.

2 RELETED WORK

MLLM-based Earth Observation Research The rise of multimodal large language models (MLLMs) has stimulated growing interest in their use for Earth observation (EO) (Aleissaee et al., 2023; Lu et al., 2025; Li et al., 2024b). Early studies mainly explored captioning (Hu et al., 2025b) and question answering (Kuckreja et al., 2024) for single remote sensing images (Shi & Zou, 2017; Wang et al., 2020), aiming to align visual features with natural language. With the availability of larger datasets (Xiong et al., 2022; Zhou et al., 2025) and stronger backbones (Team, 2024; Liu et al., 2024d), subsequent works extended this paradigm to broader perception tasks: for instance, GeoChat (Kuckreja et al., 2024) enabled interactive scene understanding, while RS-GPT (Hu et al., 2025b) combined captioning with visual question answering. More recently, simple temporal reasoning has been introduced, with ChangeCLIP (Dong et al., 2024) addressing bi-temporal change captioning and SkyEye-GPT (Zhan et al., 2025) extending to video-based analysis. However, the scope of MLLM-based EO research remains narrow: existing approaches are still centered on RGB imagery and struggle with complex multi-step reasoning without domain-specific tool integration.

Agent-based Earth Observation Research. Tool-augmented agents have gained traction in general AI, achieving remarkable progress in domains such as code generation (Qian & Cong, 2023; Zhang et al., 2024a), web search (Xu et al., 2024b), and video understanding (Ren et al., 2025; Wang et al., 2024d), but their application to Earth observation (EO) is still at an early stage (Kao et al., 2025). Early systems such as Change-Agent (Liu et al., 2024b) focus on bi-temporal change detection, while RS-ChatGPT (Guo et al., 2024a) and RS-Agent (Xu et al., 2024a) combine LLMs with pretrained detectors or tool suites for scene classification, detection, and segmentation. More recently, ThinkGeo (Shabbir et al., 2025) introduces agentic workflows for simple geospatial calculations on perceptual data, and UnivEarth (Kao et al., 2025) requires LLMs to generate GEE code for spectral analysis, with high execution failure rates. Despite these advances, existing EO agents remain constrained: they operate mainly on RGB perception tasks, rely on remote sensing models for simple reasoning that does not extend to multi-step analysis, and lack a predefined tool ecosystem, making them insufficient for complex real-world geoscientific workflows. Moreover, current benchmarks cover limited task types and annotations, lacking systematic evaluation protocols that assess both the correctness of outcomes and the quality of reasoning trajectories. As a result, current frameworks remain limited in modality coverage, constrained to shallow reasoning with remote sensing models, and hindered by the absence of a predefined tool ecosystem, highlighting the necessity for EO agents and benchmarks that support diverse data, multi-step analytical workflows, and systematic evaluation.

3 EARTH-AGENT FRAMEWORK

In this section, we detail the operation mechanisms of Earth-Agent. We first formulate its operation pipeline as a ReAct-style (Yao et al., 2023) Partially Observable Markov Decision Processes (POMDP) formulation (Huang et al., 2024; Chala et al., 2025) in section 3.1 , including the observation process, policy reasoning and memory update, as shown in Figure 3. Then we introduce the functionality of the specialized tool kits that enable EO analysis across perceptual and spectral data in section 3.2. Finally, we define the dual-level evaluation protocol, which assesses EO agents in both end-to-end and step-by-step modes to evaluate not only final accuracy but also reasoning trajectories in section 3.3.

3.1 OPERATION MECHANISMS

Earth-Agent receives a task goal g, interprets user queries and intermediate tool outputs, and selects actions from a modular toolkit to progressively solve the task. This process is formulated as a POMDP, defined by the tuple $\langle g, \mathcal{S}, \mathcal{A}, \mathcal{O}, \mathcal{T} \rangle$, where g is the task goal, $\mathcal{S}$ is the state space (unobservable environment status such as geospatial data files or raster values), $\mathcal{A}$ is the action space (tool calls in the kit), $\mathcal{O}$ is the observation space (outputs returned by tools, including text, numerical values, and images), and $\mathcal{T} : \mathcal{S} \times \mathcal{A} \to \mathcal{S}$ is the state transition function.

At each time step t, given a policy π, the agent selects an action conditioned on the goal g and its interaction history, which records past observations and actions:

$$m_t = (o_0, a_0, o_1, a_1, \ldots, o_t),$$

The action distribution is modeled as:

$$a_t \sim \pi(a_t \mid g, m_t).$$

The full agent trajectory $\tau = [s_0, o_0, a_0, s_1, o_1, a_1, \ldots, s_T, o_T]$ is determined jointly by the policy π and the environment dynamics:

$$p_\pi(\tau) \;=\; \underbrace{p(s_0)\, Z(o_0 \mid s_0)}_{\text{Initial state}} \prod_{t=0}^{T-1} \underbrace{\pi(a_t \mid g, m_t)\, \overbrace{Z(o_{t+1} \mid s_{t+1})\, \mathcal{T}(s_{t+1} \mid s_t, a_t)}^{\text{① Tool calling}}}_{\text{③ Think \& ④ Action}} .$$

where Z denotes the observation distribution induced by tool outputs.

In this formulation, the LLM controller functions as the policy π, reasoning over the history m_t and task goal g to decide the next tool calling, while the Toolkit provides executable atomic actions

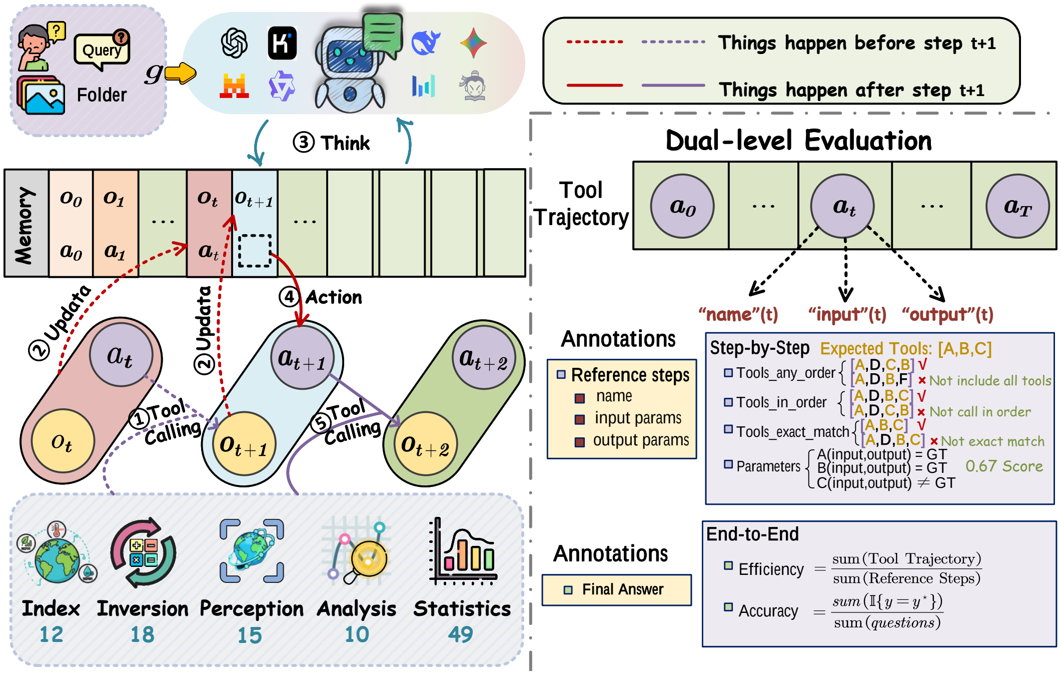
Query
Folder
g
③ Think
Things happen before step t+1
Things happen after step t+1
Memory
o_0 o_1 … o_t o_{t+1} …
a_0 a_1 a_t
② Updata
② Updata
④ Action
a_t a_{t+1} a_{t+2}
o_t o_{t+1} o_{t+2}
① Tool Calling
⑤ Tool Calling
Index 12
Inversion 18
Perception 15
Analysis 10
Statistics 49
Dual-level Evaluation
Tool Trajectory
a_0 … a_t … a_T
"name"(t) "input"(t) "output"(t)
Annotations
Reference steps
name
input params
output params
Step-by-Step Expected Tools: [A,B,C]
Tools_any_order [A,D,C,B] √ [A,D,B,F] × Not include all tools
Tools_in_order [A,D,B,C] √ [A,D,C,B] × Not call in order
Tools_exact_match [A,B,C] √ [A,D,B,C] × Not exact match
Parameters A(input,output) = GT B(input,output) = GT C(input,output) ≠ GT 0.67 Score
Annotations
Final Answer
End-to-End
Efficiency $= \frac{\mathrm{sum}(\text{Tool Trajectory})}{\mathrm{sum}(\text{Reference Steps})}$
Accuracy $= \frac{sum(\mathbb{I}\{y=y^*\})}{\mathrm{sum}(questions)}$

Figure 3: **Earth-Agent Framework:** The left part illustrates the ReAct-style workflow, where Earth-Agent iteratively performs tool calling, memory update, thinking, and action using domain-specific toolkits. The right panel presents the dual-level evaluation protocol, assessing both step-by-step reasoning trajectories and end-to-end outcomes.

categorized into ***Index, Inversion, Perception, Analysis,*** and ***Statistics***. Concretely, as illustrated in Figure 3, each loop proceeds as follows: ① **Tool calling** At step t, the agent invokes the most suitable tool conditioned on the current memory m_t and task goal g, which yields the tool response for observation o_{t+1}. ② **Memory update** At step t, the agent appends the pair (o_t, a_t) together with the resulting observation o_{t+1} into the memory stack, ensuring that the complete interaction history is preserved for subsequent reasoning. ③ **Think** At step $t{+}1$, the LLM controller reasons over the updated memory m_t together with the task goal g to plan the next action, determining which tool to invoke and how to configure its inputs. ④ **Action** Selecting and executing the subsequent tool call a_{t+1} that produces o_{t+2}. The ReAct loop continues until the stopping condition is satisfied, yielding both the final answer and a reproducible sequence of tool calling trajectory.

3.2 TOOL KIT

To enable comprehensive EO analysis, Earth-Agent integrates 104 specialized tools organized into five functional kits. The ***Index kit*** provides implementations of widely used EO indices (e.g., NDVI, NDWI, NBR) (Montero et al., 2023) for rapid environmental characterization. The ***Inversion kit*** focuses on geophysical parameter retrieval, including land surface temperature (LST) (Li et al., 2013), precipitable water vapor (PWV) (He & Liu, 2020), vegetation water content (Ceccato et al., 2001), sea ice concentration (DiGirolamo et al., 2022), and others. The ***Perception kit*** supports vision-oriented tasks such as scene classification (Ma et al., 2025), object detection (Li et al., 2024e), and segmentation (Ravi et al., 2024). The ***Analysis kit*** targets spatiotemporal reasoning, offering trend detection, seasonality decomposition, change point analysis, and spatial autocorrelation. Finally, the ***Statistics kit*** provides large-scale data preprocessing and statistical computation (e.g., variance, skewness, batch operations, cloud masking). Together, these tool kits cover the diverse types of EO tasks from perceptual to spectral, and from descriptive to quantitative analysis. The detailed list and description of tools can be found in Appendix G.

3.3 EVALUATION PROTOCOL

Prior benchmarks have primarily emphasized final accuracy, overlooking the reasoning trajectory that leads to the final output (Mialon et al., 2023; Jimenez et al., 2024; Chen et al., 2025). To address this, we adopt a **dual-level evaluation protocol**: agents are assessed in a ***step-by-step*** mode to capture the quality of their reasoning trajectories, and in an ***end-to-end*** mode to measure final task performance. This dual perspective enables fine-grained diagnostics of both reasoning and outcomes. The detailed calculation formulas can be found in Appendix B.2.

End-to-End evaluation measures task-level performance, including ***Accuracy*** of the final answer and ***Efficiency*** of the trajectory relative to expert solutions.

Step-by-Step evaluation assesses the quality of intermediate reasoning. We consider four complementary aspects: ***Tool-Any-Order***, which checks whether all necessary tools are used in LLM planning; ***Tool-In-Order***, which evaluates whether tools are invoked in the correct sequence; ***Tool-Exact-Match***, which evaluates the exact prefix-level accuracy between the predicted and expert trajectories; and ***Parameter Accuracy***, which verifies whether both tool identifiers and their arguments are correctly matched.

4 EARTH-AGENT BENCHMARK

4.1 OVERVIEW OF EARTH-AGENT BENCHMARK

We introduce **Earth-Agent Benchmark (Earth-Bench)**, a dataset designed to evaluate tool-augmented EO agents in realistic Earth science analysis scenarios. The benchmark integrates three major types of Earth observation data: ***RGB Imagery (RGB)***, ***Raw Spectral Data (Spectrum)***, and ***Processed Earth Products (Products)***. It supports 14 representative tasks, including classification, detection, temperature monitoring, weather forecasting, etc., with a particular emphasis on scientific analysis that requires quantitative reasoning rather than qualitative description.

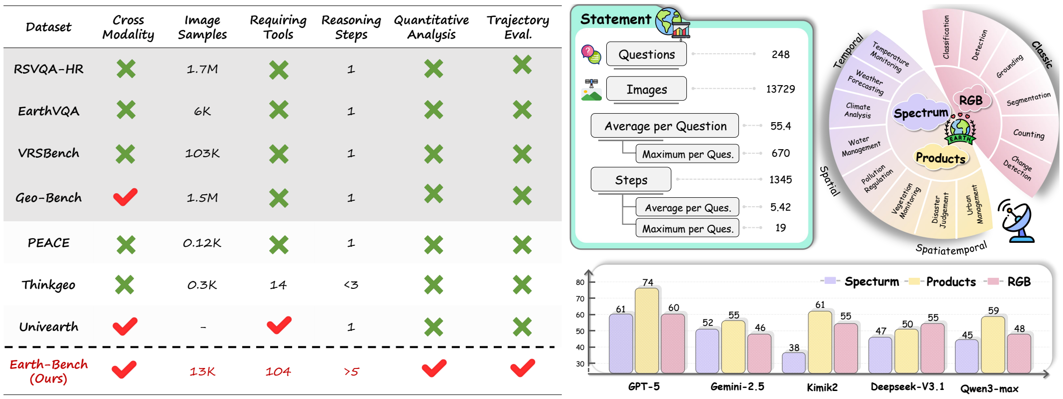

Dataset	Cross Modality	Image Samples	Requiring Tools	Reasoning Steps	Quantitative Analysis	Trajectory Eval.
RSVQA-HR	✗	1.7M	✗	1	✗	✗
EarthVQA	✗	6K	✗	1	✗	✗
VRSBench	✗	103K	✗	1	✗	✗
Geo-Bench	✓	1.5M	✗	1	✗	✗
PEACE	✗	0.12K	✗	1	✗	✗
Thinkgeo	✗	0.3K	14	<3	✗	✗
Univearth	✓	-	✓	1	✗	✗
Earth-Bench (Ours)	✓	13K	104	>5	✓	✓

Figure 4: **Dataset Comparison and Overview:** The left panel compares Earth-Bench with prior MLLM and agentbased EO benchmarks. The right panel presents the statistics of Earth-Bench and its evaluation with SOTA LLMs using Earth-Agent, highlighting the difficulty of Earth-Bench.

As shown in Figure 4, **MLLM-based benchmarks** including RSVQA-HR (Lobry et al., 2020), EarthVQA (Wang et al., 2024b), VRSBench (Li et al., 2024d) and Geo-Bench (Lacoste et al., 2023) are mainly limited to single-step perceptual for RGB data using pretrained MLLMs (Liu et al., 2024d; Team, 2024; OpenAI, 2024), without requiring external tool use for scientific quantitative analysis (e.g., spatiotemporal trend estimation), not to mention reasoning trajectory evaluation. On the other hand, **Earth-Bench** advances beyond prior **Agent-based EO benchmarks**, such as PEACE (Huang et al., 2025), Thinkgeo (Shabbir et al., 2025) and UnivEarth (Kao et al., 2025), by incorporating 13K+ images across spectrum, product and RGB modalities, while requiring interaction with 104 domain tools. It consists of 248 expert-curated questions, requiring an average of 5.4 reasoning steps of quantitative analysis. Even with the state-of-the-art (SOTA) LLM backbones, performance remains limited, which underscores not only the benchmark's difficulty and diagnostic value but also the necessity of reasoning trajectory evaluation. Therefore, we need to annotate on both trajectories and final answers in section 4.2.

4.2 DATA ANNOTATION PIPELINE

To construct Earth-Bench, we collected raw data from platforms such as Google Earth Engine, NASA EarthData, and public remote sensing datasets (Xia et al., 2017; Zhan et al., 2023; Xia et al., 2018; Su et al., 2019). From these data sources, a team of domain experts curated 248 problems that require multi-step quantitative reasoning. The annotation team was composed of **2** computer science experts, **7** remote sensing specialists, and **3** Earth science specialists. Each problem is accompanied by a step-by-step Python solution and is designed to reflect the complexity of real-world Earth science workflows, which demand the coordinated use of multiple tool kits.

In prior benchmarks, queries have been designed either as *step-implicit*, where no intermediate step guidance is provided (Mialon et al., 2023; Wang et al., 2024a), or as *step-explicit*, where the query itself contains step guidance (Guo et al., 2024b; Ma et al., 2024). Motivated by the complexity of EO workflows, which often require multi-step processing, Earth-Bench incorporates both regimes: **Auto-Planning** corresponds to the step-implicit setting and evaluates the agent's ability to autonomously plan its solution trajectory, while **Instruction-Following** corresponds to the step-explicit setting and evaluates the agent's ability to follow and translate human instructions into executable actions. Both regimes contain 248 complete questions for evaluation. Together, these two regimes provide a comprehensive assessment of both autonomous reasoning and guided execution in EO contexts. Details can refer to Appendix A.4.

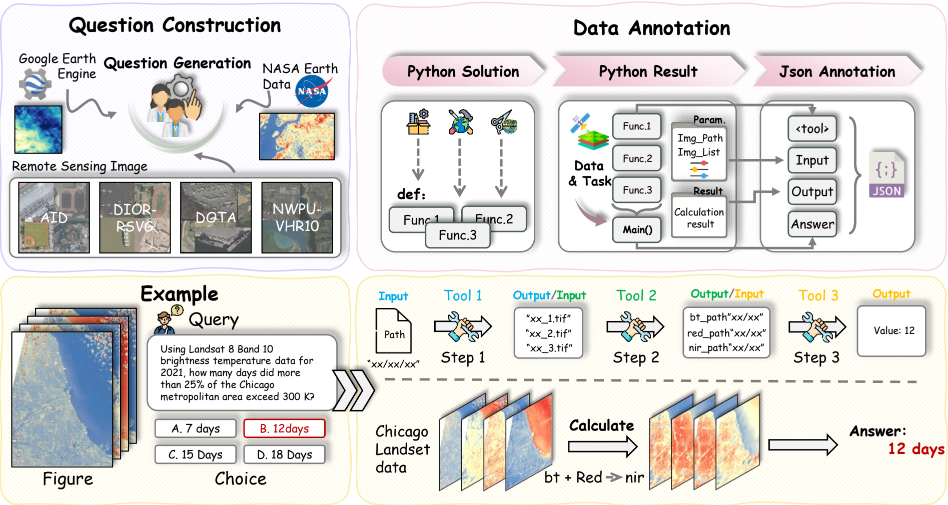

Using Landsat 8 Band 10 brightness temperature data for 2021, how many days did more than 25% of the Chicago metropolitan area exceed 300 K?

Figure 5: **Construction and Annotation of Earth-Bench.** The left shows question generation from EO data, the right illustrates the data annotation pipeline that simulates ReAct-style trajectories, and the bottom provides an example explaining the multi-step annotation process.

To enable dual-level evaluation, we explicitly annotated both the final answers and the full reasoning trajectories. As illustrated in Fig. 5, the annotation process was designed to mimic the ReAct loop of agents: **Python Solution.** Annotators first identify the domain tools such as compute_ndwi and split_window) required to solve a problem and then assemble them into a step-by-step main() program. Each tool is represented as a Python function, and the functions are planned in the correct order to form an executable workflow that mirrors the agent's reasoning trajectory. **Python Result.** When executed, the program produces explicit input and output arguments for each function call, as well as the final output of the main() function. **JSON Annotation.** Each function call is then translated into a structured JSON record to align with the ReAct-style trajectory annotation. The function name corresponds to the action tool name, the function input arguments corresponds to the action passed by the agent, and the function output arguments corresponds to the tool responses returned to the agent. The final output of the main() function is recorded as the ground-truth answer for the problem. This provides a complete record of both the reasoning trajectory and the final answer.

5 EXPERIMENTS

5.1 EXPERIMENTAL SETUP

Evaluated Models. We evaluate 3 closed-source and 10 leading open-source LLMs. For ***closed-source models***, we consider GPT-5 (OpenAI, 2025a), GPT-4o (OpenAI, 2024), and Gemini-2.5 (Comanici et al., 2025). For ***open-source models***, including Deepseek-V3.1 (Liu et al., 2024a), Kimik2 (Team et al., 2025), Qwen3-max-Preview, Qwen3-32B (Yang et al., 2025), and InternVL3.5 (Wang et al., 2025), which represent the smartest open LLMs available to date.

5.2 EARTH-AGENT WITH DIFFERENT LLM BACKBONES

As shown in Table 1, we evaluate the impact of different LLM backbones on Earth-Bench. Results are reported under both ***step-by-step*** and ***end-to-end*** evaluation protocols, allowing us to jointly assess the quality of reasoning trajectories and final outcomes. The following observations can be made:

Table 1: Performance of different LLM backbones on Earth-Bench under both *Auto-Planning (AP)* and *Instruction-Following (IF)* regimes. Results are reported with dual-level evaluation, covering Tool-Any-Order, Tool-In-Order, Tool-Exact-Match, Parameters for trajectory quality and Efficiency, Accuracy for final outcomes. We **bold** the best results and underline the runner-ups.

Model	Tool-Any-Order		Tool-In-Order		Tool-Exact-Match		Parameters		Efficiency		Accuracy	
	AP	IF	AP	IF	AP	IF	AP	IF	AP	IF	AP	IF
GPT-5	68.74	71.41↑	57.71	61.06↑	44.97	46.01↑	26.11	25.91↓	2.3560	2.9093	**65.99**	**62.35**↓
Gemini-2.5	58.04	61.63↑	45.31	50.72↑	31.32	41.04↑	17.26	23.43↑	2.9958	2.4595	52.23	53.04↑
GPT-4o	65.65	67.02↑	50.76	53.04↑	46.26	47.41↑	26.55	27.92↑	2.1211	2.6007	43.72	44.94↑
Kimik2	71.03	**78.86**↑	57.57	**68.83**↑	42.11	**51.15**↑	25.90	30.45↑	1.8542	2.1793	50.61	56.68↑
DeepSeek-V3.1	**78.31**	78.66↑	**62.73**	64.50↑	**48.54**	49.58↑	**30.81**	**31.36**↑	2.6116	2.6303	51.42	52.23↑
Qwen3-Max	69.56	70.14↑	53.28	56.02↑	37.02	42.74↑	21.83	26.27↑	1.8810	1.9511↓	50.20	47.37↓
Seed-1.6	55.43	59.44↑	40.67	46.79↑	28.39	35.47↑	18.32	23.13↑	1.3110	1.3408↓	52.48	59.51↑
LLaMA-4	16.51	22.41↑	2.45	12.05↑	1.70	9.05↑	1.30	6.46↑	0.2886	0.3211↓	44.94	38.46↓
Qwen-Plus	52.04	55.96↑	30.75	39.77↑	11.69	25.51↑	9.12	16.95↑	1.5119	1.5854↓	42.51	38.46↓
GLM-4.5v	42.48	46.69↑	28.57	35.24↑	14.12	19.95↑	11.02	15.37↑	1.7123	2.0129↓	32.86	35.25↑
Mistral	27.73	29.64↑	11.78	20.90↑	9.13	18.13↑	7.24	11.66↑	0.9552	0.8802↑	29.96	22.67↓
Qwen3-32B	39.76	42.39↑	21.56	33.79↑	9.51	26.10↑	8.17	17.73↑	2.7274	1.9010↑	20.65	24.80↑
InternVL-3.5	8.83	16.62↑	3.87	10.59↑	2.02	9.32↑	1.46	5.32↑	0.1206	0.1750↓	26.72	26.72

Obs.1. LLM models pretrained with tool calling, such as GPT-5, Gemini-2.5, DeepSeek-V3.1, Kimik2, and Qwen3, demonstrate **strong** performance across both ***step-by-step*** and ***end-to-end*** evaluations. Further, closed-source models like GPT-5 typically achieve **higher** ***final accuracy***, while open-source models, particularly DeepSeek-V3.1 and Kimik2, **outperform** GPT-5 in ***tool-use accuracy***, demonstrating superior performance in reasoning trajectory alignment. We have provided a detailed analysis of the LLMs' performance across the Spectrum, Products, and RGB modalities, which can be found in Appendix C.

Obs.2. Instruction-following regimes enhance tool calling by providing explicit step guidance in the query, leading to **improved** ***tool calling accuracy*** across nearly all models. Interestingly, despite the improved reasoning trajectories, this does **not necessarily** lead to ***higher final accuracy***. In fact, for some advanced models, this added complexity may even result in a **decrease** in ***final accuracy***. We have conducted a detailed ***error analysis*** of Earth-Agent's performance in the Earth-Bench benchmark, focusing on representative models such as GPT-5, DeepSeek-V3.1, Kimik2, and Qwen3-max. This can be found in Appendix D.

Obs.3. Across nearly all models, the ability to identify the correct set of tools, as reflected in ***Tool-Any-Order*** and ***Tool-In-Order*** metrics, remains **consistently strong**. However, models often introduce irrelevant steps during reasoning, which **undermines** their accuracy on ***Tool-Exact-Match*** and ***parameter*** execution. Crucially, these two fine-grained capabilities are indispensable in real EO analysis workflows. For example, if additional transformations are mistakenly applied to the EO data process, it becomes extremely difficult to obtain correct results in the subsequent steps. Their weakness therefore exposes a **key bottleneck** that prevents EO Agents from achieving higher final ***accuracy*** in EO data processing.

5.3 COMPARISON WITH GENERAL AGENTS

Since many Earth-Bench tasks involve processing hundreds of images, existing open-source agent frameworks cannot handle these questions due to input size constraints. To enable fair comparison, we construct **Earth-Bench-Lite**, a reduced yet representative subset that preserves modality diversity while remaining within the capacity of general-purpose agents. It consists of 60 questions evenly distributed across the three EO modalities: Spectrum, Products, and RGB. As shown in Table 2, we report results across three modalities: *Spectrum*, *Products*, and *RGB*.

Table 2: Comparison with general agents on Earth-Bench-Lite. Results are reported across Spectrum, Products, RGB modalities. We **bold** the best results and underline the runner-ups.

Method	Spectrum	Products	RGB	Avg.	Latency
GPT-Agent	45.00	31.60	45.26	40.42	≈ 300 min
MGX	40.00	15.80	0.00	18.60	**≈ 60 min**
Manus	15.00	15.80	47.62	26.14	≈ 150 min
Coze	35.00	10.50	0.00	15.30	≈ 120 min
Earth-Agent(GPT5)	**65.00**	**36.84**	**65.71**	**55.83**	158 min
Earth-Agent(Deepseek-V3.1)	50.00	42.11	51.43	47.84	79 min
Earth-Agent(Kimik2)	36.84	50.00	50.00	45.95	131 min

By comparison, general agents show limited modality coverage. They can handle relatively simple *Spectrum* tasks by writing ad-hoc code, but perform poorly on *Products* tasks due to the lack of domain-specific spatiotemporal analysis tools. For the *RGB* modality, MGX and Coze even fail to complete any tasks. In contrast, by interacting with 104 predefined geoscience tools, Earth-Agent consistently achieves superior performance across all three modalities, whether driven by the closed-source GPT-5 or the open-source DeepSeek-V3.1. We also compared the latency of our Earth-Agent framework with that of the baseline agents. The latency remains within a reasonable range when compared to existing general agents. The substantial performance improvements in task completion more than justify the additional computational cost. A detailed discussion can be found in the Appendix E.

5.4 COMPARISON WITH MLLM-BASED EO METHODS

We further compare Earth-Agent with remote sensing large models on classification, detection, and segmentation tasks. The results are summarized in Table 3.

Table 3: Comparison with MLLMs on Remote sense benchmarks. Results are reported on classification, detection, and segmentation tasks. We **bold** the best results and underline the runner-ups.

Model	Classification		Detection		Grounding
	AID	WHU-RS19	DOTA	HRSC2016	DIOR-RSVG
MiniGPT-v2 (Chen et al., 2023)	32.96	64.80	14.8	24.8	29.892
LLaVA-1.5 (Liu et al., 2024d)	51.00	74.52	17.5	22.1	12.085
Sphinx (Lin et al., 2023)	58.20	-	15.1	25.7	0.939
Geochat (Kuckreja et al., 2024)	72.03	86.47	16.5	24.0	10.024
VHM (Pang et al., 2025)	91.70	95.80	-	-	-
LHRS-Bot (Muhtar et al., 2024)	91.26	93.17	17.1	24.4	11.826
Earth-Agent (ours)	**93.42**	**96.12**	**60.88**	**65.60**	**60.46**

Earth-Agent demonstrates clear superiority over existing MLLMs across classification, detection, and segmentation benchmarks (Table 3). Prior MLLM-based approaches often lack generalization across diverse EO tasks: for example, LHRS-Bot achieves strong results in classification but struggles on detection and grounding, while VHM attains high classification accuracy but cannot even handle detection or segmentation tasks. In contrast, Earth-Agent interacts with a predefined toolkit of 104 geoscience functions and expert models, allowing it to adaptively invoke specialized tools or models for each task type. This modular design enables Earth-Agent to maintain robust performance across modalities, overcoming the limited extensibility of previous MLLM-based EO systems.

6 CONCLUSION

Earth-Agent marks a significant advancement in applying (M)LLMs to EO analysis, extending RGB perception to Spectrum, Products and RGB modalities. By shifting from single-step inference with pretrained MLLMs to multi-step reasoning through external tool/model integration, it overcomes key limitations of prior MLLM-based approaches, such as handling numerous image inputs and quantitative spatiotemporal analysis. To support rigorous evaluation, we introduced Earth-Bench, which requires multi-step quantitative reasoning and dual-level evaluation, which evaluate both reasoning trajectories and final outcomes. Our experiments further reveal the current bottlenecks of Earth-Agent in EO applications and provide detailed diagnostics. Finally, by comparing with both general agents and domain MLLMs, we highlight the transformative potential of Earth-Agent as a foundation for the revolutio of LLM applications in Earth observation.

REFERENCES

Abdulaziz Amer Aleissaee, Amandeep Kumar, Rao Muhammad Anwer, Salman Khan, Hisham Cholakkal, Gui-Song Xia, and Fahad Shahbaz Khan. Transformers in remote sensing: A survey. *Remote Sensing*, 15(7):1860, 2023.

Katherine Anderson, Barbara Ryan, William Sonntag, Argyro Kavvada, and Lawrence Friedl. Earth observation in service of the 2030 agenda for sustainable development. *Geo-spatial Information Science*, 20(2):77–96, 2017.

Christopher F Brown, Michal R Kazmierski, Valerie J Pasquarella, William J Rucklidge, Masha Samsikova, Chenhui Zhang, Evan Shelhamer, Estefania Lahera, Olivia Wiles, Simon Ilyushchenko, et al. Alphaearth foundations: An embedding field model for accurate and efficient global mapping from sparse label data. *arXiv preprint arXiv:2507.22291*, 2025.

Pietro Ceccato, Stéphane Flasse, Stefano Tarantola, Stéphane Jacquemoud, and Jean-Marie Grégoire. Detecting vegetation leaf water content using reflectance in the optical domain. *Remote Sensing of Environment*, 77(1):22–33, 2001. ISSN 0034-4257. doi: https://doi.org/10.1016/S0034-4257(01)00191-2. URL `https://www.sciencedirect.com/science/article/pii/S0034425701001912`.

Olena Chala, Vladyslav Yevsieiev, Svitlana Maksymova, and Amer Abu-Jassar. Mathematical model based on multi-agent reinforcement learning (marl) and partially observable markov decision process (pomdp) for modeling cargo movement for a mobile robots group. *Multidisciplinary Journal of Science and Technology*, 5(4):480–489, 2025.

Chen Chen, Xinlong Hao, Weiwen Liu, Xu Huang, Xingshan Zeng, Shuai Yu, Dexun Li, Shuai Wang, Weinan Gan, Yuefeng Huang, et al. Acebench: Who wins the match point in tool usage? *arXiv preprint arXiv:2501.12851*, 2025.

Jun Chen, Deyao Zhu, Xiaoqian Shen, Xiang Li, Zechun Liu, Pengchuan Zhang, Raghuraman Krishnamoorthi, Vikas Chandra, Yunyang Xiong, and Mohamed Elhoseiny. Minigpt-v2: large language model as a unified interface for vision-language multi-task learning. *arXiv preprint arXiv:2310.09478*, 2023.

Gheorghe Comanici, Eric Bieber, Mike Schaekermann, Ice Pasupat, Noveen Sachdeva, Inderjit Dhillon, Marcel Blistein, Ori Ram, Dan Zhang, Evan Rosen, et al. Gemini 2.5: Pushing the frontier with advanced reasoning, multimodality, long context, and next generation agentic capabilities. *arXiv preprint arXiv:2507.06261*, 2025.

N. DiGirolamo, C. L. Parkinson, D. J. Cavalieri, P. Gloersen, and H. J. Zwally. Sea ice concentrations from nimbus-7 smmr and dmsp ssm/i-ssmis passive microwave data, 2022. URL `https://doi.org/10.5067/MPYG15WAA4WX`. NSIDC-0051. [Data Set]. Accessed: 2025-09-23.

Keyan Ding, Jing Yu, Junjie Huang, Yuchen Yang, Qiang Zhang, and Huajun Chen. Scitoolagent: a knowledge-graph-driven scientific agent for multitool integration. *Nature Computational Science*, pp. 1–11, 2025.

Sijun Dong, Libo Wang, Bo Du, and Xiaoliang Meng. Changeclip: Remote sensing change detection with multimodal vision-language representation learning. *ISPRS Journal of Photogrammetry and Remote Sensing*, 208:53–69, 2024.

Chen Gao, Xiaochong Lan, Nian Li, Yuan Yuan, Jingtao Ding, Zhilun Zhou, Fengli Xu, and Yong Li. Large language models empowered agent-based modeling and simulation: A survey and perspectives. *Humanities and Social Sciences Communications*, 11(1):1–24, 2024.

Haonan Guo, Xin Su, Chen Wu, Bo Du, Liangpei Zhang, and Deren Li. Remote sensing chatgpt: Solving remote sensing tasks with chatgpt and visual models. In *IGARSS 2024-2024 IEEE International Geoscience and Remote Sensing Symposium*, pp. 11474–11478. IEEE, 2024a.

Zhicheng Guo, Sijie Cheng, Hao Wang, Shihao Liang, Yujia Qin, Peng Li, Zhiyuan Liu, Maosong Sun, and Yang Liu. Stabletoolbench: Towards stable large-scale benchmarking on tool learning of large language models. *arXiv preprint arXiv:2403.07714*, 2024b.

Jia He and Zhizhao Liu. Water vapor retrieval from modis nir channels using ground-based gps data. *IEEE Transactions on Geoscience and Remote Sensing*, 58(5):3726–3737, 2020. doi: 10.1109/TGRS.2019.2962057.

Xinyi Hou, Yanjie Zhao, Shenao Wang, and Haoyu Wang. Model context protocol (mcp): Landscape, security threats, and future research directions. *arXiv preprint arXiv:2503.23278*, 2025.

Huiyang Hu, Peijin Wang, Yingchao Feng, Kaiwen Wei, Wenxin Yin, Wenhui Diao, Mengyu Wang, Hanbo Bi, Kaiyue Kang, Tong Ling, et al. Ringmo-agent: A unified remote sensing foundation model for multi-platform and multi-modal reasoning. *arXiv preprint arXiv:2507.20776*, 2025a.

Yuan Hu, Jianlong Yuan, Congcong Wen, Xiaonan Lu, Yu Liu, and Xiang Li. Rsgpt: A remote sensing vision language model and benchmark. *ISPRS Journal of Photogrammetry and Remote Sensing*, 224:272–286, 2025b.

Yangyu Huang, Tianyi Gao, Haoran Xu, Qihao Zhao, Yang Song, Zhipeng Gui, Tengchao Lv, Hao Chen, Lei Cui, Scarlett Li, et al. Peace: Empowering geologic map holistic understanding with mllms. In *Proceedings of the Computer Vision and Pattern Recognition Conference*, pp. 3899–3908, 2025.

Zhiyu Huang, Chen Tang, Chen Lv, Masayoshi Tomizuka, and Wei Zhan. Learning online belief prediction for efficient pomdp planning in autonomous driving. *arXiv preprint arXiv:2401.15315*, 2024.

Carlos E Jimenez, John Yang, Alexander Wettig, Shunyu Yao, Kexin Pei, Ofir Press, and Karthik R Narasimhan. SWE-bench: Can language models resolve real-world github issues? In *The Twelfth International Conference on Learning Representations*, 2024. URL `https://openreview.net/forum?id=VTF8yNQM66`.

Karen E Joyce, Kim C Wright, Sergey V Samsonov, and Vincent G Ambrosia. Remote sensing and the disaster management cycle. *Advances in geoscience and remote sensing*, 48(7):317–346, 2009.

Chia Hsiang Kao, Wenting Zhao, Shreelekha Revankar, Samuel Speas, Snehal Bhagat, Rajeev Datta, Cheng Perng Phoo, Utkarsh Mall, Carl Vondrick, Kavita Bala, et al. Towards llm agents for earth observation. *arXiv preprint arXiv:2504.12110*, 2025.

Ioannis P. Kokkoris, Bruno Smets, Lars Hein, Giorgos Mallinis, Marcel Buchhorn, Stefano Balbi, Ján Černecký, Marc Paganini, and Panayotis Dimopoulos. The role of earth observation in ecosystem accounting: A review of advances, challenges and future directions. *Ecosystem Services*, 70:101659, 2024. ISSN 2212-0416. doi: https://doi.org/10.1016/j.ecoser.2024.101659. URL `https://www.sciencedirect.com/science/article/pii/S2212041624000664`.

Kartik Kuckreja, Muhammad Sohail Danish, Muzammal Naseer, Abhijit Das, Salman Khan, and Fahad Shahbaz Khan. Geochat: Grounded large vision-language model for remote sensing. In *Proceedings of the IEEE/CVF Conference on Computer Vision and Pattern Recognition*, pp. 27831–27840, 2024.

Alexandre Lacoste, Nils Lehmann, Pau Rodriguez, Evan Sherwin, Hannah Kerner, Björn Lütjens, Jeremy Irvin, David Dao, Hamed Alemohammad, Alexandre Drouin, et al. Geo-bench: Toward foundation models for earth monitoring. *Advances in Neural Information Processing Systems*, 36:51080–51093, 2023.

Jinpeng Li, Jun He, Weijia Li, Jiabin Chen, and Jinhua Yu. Roadcorrector: A structure-aware road extraction method for road connectivity and topology correction. *IEEE Transactions on Geoscience and Remote Sensing*, 62:1–18, 2024a.

Ming Li, Keyu Chen, Ziqian Bi, Ming Liu, Benji Peng, Qian Niu, Junyu Liu, Jinlang Wang, Sen Zhang, Xuanhe Pan, et al. Surveying the mllm landscape: A meta-review of current surveys. *arXiv preprint arXiv:2409.18991*, 2024b.

Weijia Li, Runmin Dong, Haohuan Fu, Jie Wang, Le Yu, and Peng Gong. Integrating google earth imagery with landsat data to improve 30-m resolution land cover mapping. *Remote Sensing of Environment*, 237:111563, 2020.

Weijia Li, Yawen Lai, Linning Xu, Yuanbo Xiangli, Jinhua Yu, Conghui He, Gui-Song Xia, and Dahua Lin. Omnicity: Omnipotent city understanding with multi-level and multi-view images. In *Proceedings of the IEEE/CVF Conference on Computer Vision and Pattern Recognition*, pp. 17397–17407, 2023a.

Weijia Li, Wenqian Zhao, Jinhua Yu, Juepeng Zheng, Conghui He, Haohuan Fu, and Dahua Lin. Joint semantic–geometric learning for polygonal building segmentation from high-resolution remote sensing images. *ISPRS Journal of Photogrammetry and Remote Sensing*, 201:26–37, 2023b.

Weijia Li, Haote Yang, Zhenghao Hu, Juepeng Zheng, Gui-Song Xia, and Conghui He. 3d building reconstruction from monocular remote sensing images with multi-level supervisions. In *Proceedings of the IEEE/CVF Conference on Computer Vision and Pattern Recognition*, pp. 27728–27737, 2024c.

Xiang Li, Jian Ding, and Mohamed Elhoseiny. Vrsbench: A versatile vision-language benchmark dataset for remote sensing image understanding. *Advances in Neural Information Processing Systems*, 37:3229–3242, 2024d.

Yuxuan Li, Xiang Li, Yunheng Li, Yicheng Zhang, Yimian Dai, Qibin Hou, Ming-Ming Cheng, and Jian Yang. Sm3det: A unified model for multi-modal remote sensing object detection. *arXiv preprint arXiv:2412.20665*, 2024e.

Zhao-Liang Li, Bo-Hui Tang, Hua Wu, Huazhong Ren, Guangjian Yan, Zhengming Wan, Isabel F. Trigo, and José A. Sobrino. Satellite-derived land surface temperature: Current status and perspectives. *Remote Sensing of Environment*, 131:14–37, 2013. ISSN 0034-4257. doi: https://doi.org/10.1016/j.rse.2012.12.008. URL `https://www.sciencedirect.com/science/article/pii/S0034425712004749`.

Ziyi Lin, Chris Liu, Renrui Zhang, Peng Gao, Longtian Qiu, Han Xiao, Han Qiu, Chen Lin, Wenqi Shao, Keqin Chen, et al. Sphinx: The joint mixing of weights, tasks, and visual embeddings for multi-modal large language models. *arXiv preprint arXiv:2311.07575*, 2023.

Aixin Liu, Bei Feng, Bing Xue, Bingxuan Wang, Bochao Wu, Chengda Lu, Chenggang Zhao, Chengqi Deng, Chenyu Zhang, Chong Ruan, et al. Deepseek-v3 technical report. *arXiv preprint arXiv:2412.19437*, 2024a.

Chenyang Liu, Keyan Chen, Haotian Zhang, Zipeng Qi, Zhengxia Zou, and Zhenwei Shi. Change-agent: Toward interactive comprehensive remote sensing change interpretation and analysis. *IEEE Transactions on Geoscience and Remote Sensing*, 62:1–16, 2024b. doi: 10.1109/TGRS.2024.3425815.

Fan Liu, Delong Chen, Zhangqingyun Guan, Xiaocong Zhou, Jiale Zhu, Qiaolin Ye, Liyong Fu, and Jun Zhou. Remoteclip: A vision language foundation model for remote sensing. *IEEE Transactions on Geoscience and Remote Sensing*, 2024c.

Haotian Liu, Chunyuan Li, Yuheng Li, and Yong Jae Lee. Improved baselines with visual instruction tuning. In *Proceedings of the IEEE/CVF conference on computer vision and pattern recognition*, pp. 26296–26306, 2024d.

Zhuoran Liu, Danpei Zhao, Bo Yuan, and Zhiguo Jiang. Rescueadi: adaptive disaster interpretation in remote sensing images with autonomous agents. *IEEE Transactions on Geoscience and Remote Sensing*, 2025.

Sylvain Lobry, Diego Marcos, Jesse Murray, and Devis Tuia. Rsvqa: Visual question answering for remote sensing data. *IEEE Transactions on Geoscience and Remote Sensing*, 58(12):8555–8566, 2020.

Siqi Lu, Junlin Guo, James R Zimmer-Dauphinee, Jordan M Nieusma, Xiao Wang, Steven A Wernke, Yuankai Huo, et al. Vision foundation models in remote sensing: A survey. *IEEE Geoscience and Remote Sensing Magazine*, 2025.

Jingjing Ma, Wei Jiang, Xu Tang, Xiangrong Zhang, Fang Liu, and Licheng Jiao. Multiscale sparse cross-attention network for remote sensing scene classification. *IEEE Transactions on Geoscience and Remote Sensing*, 2025.

Zixian Ma, Weikai Huang, Jieyu Zhang, Tanmay Gupta, and Ranjay Krishna. m & m's: A benchmark to evaluate tool-use for m ulti-step m ulti-modal tasks. In *European Conference on Computer Vision*, pp. 18–34. Springer, 2024.

Utkarsh Mall, Cheng Perng Phoo, Meilin Kelsey Liu, Carl Vondrick, Bharath Hariharan, and Kavita Bala. Remote sensing vision-language foundation models without annotations via ground remote alignment. *arXiv preprint arXiv:2312.06960*, 2023.

Grégoire Mialon, Clémentine Fourrier, Thomas Wolf, Yann LeCun, and Thomas Scialom. Gaia: a benchmark for general ai assistants. In *The Twelfth International Conference on Learning Representations*, 2023.

David Montero, Cesar Aybar, Miguel D. Mahecha, Sebastian Wieneke, et al. A standardized catalogue of spectral indices to advance the use of remote sensing in earth system research. *Scientific Data*, 10(1):197, 2023. doi: 10.1038/s41597-023-02096-0. URL `https://doi.org/10.1038/s41597-023-02096-0`.

Dilxat Muhtar, Zhenshi Li, Feng Gu, Xueliang Zhang, and Pengfeng Xiao. Lhrs-bot: Empowering remote sensing with vgi-enhanced large multimodal language model. In *European Conference on Computer Vision*, pp. 440–457. Springer, 2024.

OpenAI. Hello gpt-4o. `https://openai.com/index/hello-gpt-4o/`, 2024.

OpenAI. Gpt-5 is here. `https://openai.com/gpt-5/`, 2025a.

OpenAI. Introducingoperator. `https://openai.com/index/introducing-operator/`, 2025b.

Chao Pang, Xingxing Weng, Jiang Wu, Jiayu Li, Yi Liu, Jiaxing Sun, Weijia Li, Shuai Wang, Litong Feng, Gui-Song Xia, et al. Vhm: Versatile and honest vision language model for remote sensing image analysis. In *Proceedings of the AAAI Conference on Artificial Intelligence*, volume 39, pp. 6381–6388, 2025.

Dmitrii Pantiukhin, Boris Shapkin, Ivan Kuznetsov, Antonia Anna Jost, and Nikolay Koldunov. Accelerating earth science discovery via multi-agent llm systems. *arXiv preprint arXiv:2503.05854*, 2025.

Chen Qian and Xin Cong. Communicative agents for software development. *arXiv preprint arXiv:2307.07924*, 6(3):1, 2023.

Nikhila Ravi, Valentin Gabeur, Yuan-Ting Hu, Ronghang Hu, Chaitanya Ryali, Tengyu Ma, Haitham Khedr, Roman Rädle, Chloe Rolland, Laura Gustafson, et al. Sam 2: Segment anything in images and videos. *arXiv preprint arXiv:2408.00714*, 2024.

Partha Pratim Ray. A survey on model context protocol: Architecture, state-of-the-art, challenges and future directions. *Authorea Preprints*, 2025.

Xubin Ren, Lingrui Xu, Long Xia, Shuaiqiang Wang, Dawei Yin, and Chao Huang. Videorag: Retrieval-augmented generation with extreme long-context videos. *arXiv preprint arXiv:2502.01549*, 2025.

Farhad Samadzadegan, Ahmad Toosi, and Farzaneh Dadrass Javan. A critical review on multi-sensor and multi-platform remote sensing data fusion approaches: current status and prospects. *International journal of remote sensing*, 46(3):1327–1402, 2025.

Akashah Shabbir, Muhammad Akhtar Munir, Akshay Dudhane, Muhammad Umer Sheikh, Muhammad Haris Khan, Paolo Fraccaro, Juan Bernabe Moreno, Fahad Shahbaz Khan, and Salman Khan. Thinkgeo: Evaluating tool-augmented agents for remote sensing tasks. *arXiv preprint arXiv:2505.23752*, 2025.

Ahmed Shaker, Wai Yeung Yan, and Paul E LaRocque. Automatic land-water classification using multispectral airborne lidar data for near-shore and river environments. *ISPRS journal of photogrammetry and remote sensing*, 152:94–108, 2019.

Minjie Shen, Yanshu Li, Lulu Chen, and Qikai Yang. From mind to machine: The rise of manus ai as a fully autonomous digital agent. *arXiv preprint arXiv:2505.02024*, 2025.

Zhenwei Shi and Zhengxia Zou. Can a machine generate humanlike language descriptions for a remote sensing image? *IEEE Transactions on Geoscience and Remote Sensing*, 55(6):3623–3634, 2017.

Chenglei Si, Diyi Yang, and Tatsunori Hashimoto. Can llms generate novel research ideas? a large-scale human study with 100+ nlp researchers. *arXiv preprint arXiv:2409.04109*, 2024.

Hao Su, Shunjun Wei, Min Yan, Chen Wang, Jun Shi, and Xiaoling Zhang. Object detection and instance segmentation in remote sensing imagery based on precise mask r-cnn. In *IGARSS 2019-2019 IEEE International Geoscience and Remote Sensing Symposium*, pp. 1454–1457. IEEE, 2019.

Qiushi Sun, Zhoumianze Liu, Chang Ma, Zichen Ding, Fangzhi Xu, Zhangyue Yin, Haiteng Zhao, Zhenyu Wu, Kanzhi Cheng, Zhaoyang Liu, et al. Scienceboard: Evaluating multimodal autonomous agents in realistic scientific workflows. *arXiv preprint arXiv:2505.19897*, 2025.

Jiabin Tang, Lianghao Xia, Zhonghang Li, and Chao Huang. Ai-researcher: Autonomous scientific innovation. *arXiv preprint arXiv:2505.18705*, 2025.

Kimi Team, Yifan Bai, Yiping Bao, Guanduo Chen, Jiahao Chen, Ningxin Chen, Ruijue Chen, Yanru Chen, Yuankun Chen, Yutian Chen, et al. Kimi k2: Open agentic intelligence. *arXiv preprint arXiv:2507.20534*, 2025.

Qwen Team. Qwen2 technical report. *arXiv preprint arXiv:2407.10671*, 2, 2024.

Minyang Tian, Luyu Gao, Shizhuo Zhang, Xinan Chen, Cunwei Fan, Xuefei Guo, Roland Haas, Pan Ji, Kittithat Krongchon, Yao Li, et al. Scicode: A research coding benchmark curated by scientists. *Advances in Neural Information Processing Systems*, 37:30624–30650, 2024.

Julie Transon, Raphaël D'Andrimont, Alexandre Maugnard, and Pierre Defourny. Survey of hyperspectral earth observation applications from space in the sentinel-2 context. *Remote Sensing*, 10(2), 2018. ISSN 2072-4292. doi: 10.3390/rs10020157. URL `https://www.mdpi.com/2072-4292/10/2/157`.

Mojtaba Valipour, Kelly Zheng, James Lowman, Spencer Szabados, Mike Gartner, and Bobby Braswell. Agi for the earth, the path, possibilities and how to evaluate intelligence of models that work with earth observation data? *arXiv preprint arXiv:2508.06057*, 2025.

CJ Van Westen. Remote sensing for natural disaster management. *International archives of photogrammetry and remote sensing*, 33(B7/4; PART 7):1609–1617, 2000.

Jize Wang, Ma Zerun, Yining Li, Songyang Zhang, Cailian Chen, Kai Chen, and Xinyi Le. Gta: a benchmark for general tool agents. *Advances in Neural Information Processing Systems*, 37: 75749–75790, 2024a.

Junjue Wang, Zhuo Zheng, Zihang Chen, Ailong Ma, and Yanfei Zhong. Earthvqa: Towards queryable earth via relational reasoning-based remote sensing visual question answering. In *Proceedings of the AAAI conference on artificial intelligence*, volume 38, pp. 5481–5489, 2024b.

Lei Wang, Chen Ma, Xueyang Feng, Zeyu Zhang, Hao Yang, Jingsen Zhang, Zhiyuan Chen, Jiakai Tang, Xu Chen, Yankai Lin, et al. A survey on large language model based autonomous agents. *Frontiers of Computer Science*, 18(6):186345, 2024c.

Qi Wang, Wei Huang, Xueting Zhang, and Xuelong Li. Word–sentence framework for remote sensing image captioning. *IEEE Transactions on Geoscience and Remote Sensing*, 59(12):10532–10543, 2020.

Weiyun Wang, Zhangwei Gao, Lixin Gu, Hengjun Pu, Long Cui, Xingguang Wei, Zhaoyang Liu, Linglin Jing, Shenglong Ye, Jie Shao, et al. Internvl3. 5: Advancing open-source multimodal models in versatility, reasoning, and efficiency. *arXiv preprint arXiv:2508.18265*, 2025.

Xiaohan Wang, Yuhui Zhang, Orr Zohar, and Serena Yeung-Levy. Videoagent: Long-form video understanding with large language model as agent. In *European Conference on Computer Vision*, pp. 58–76. Springer, 2024d.

Zhecheng Wang, Rajanie Prabha, Tianyuan Huang, Jiajun Wu, and Ram Rajagopal. Skyscript: A large and semantically diverse vision-language dataset for remote sensing. In *Proceedings of the AAAI Conference on Artificial Intelligence*, volume 38, pp. 5805–5813, 2024e.

Marek Wójtowicz, Andrzej Wójtowicz, Jan Piekarczyk, et al. Application of remote sensing methods in agriculture. *Communications in biometry and crop science*, 11(1):31–50, 2016.

Zhiheng Xi, Wenxiang Chen, Xin Guo, Wei He, Yiwen Ding, Boyang Hong, Ming Zhang, Junzhe Wang, Senjie Jin, Enyu Zhou, et al. The rise and potential of large language model based agents: A survey. *Science China Information Sciences*, 68(2):121101, 2025.

Gui-Song Xia, Jingwen Hu, Fan Hu, Baoguang Shi, Xiang Bai, Yanfei Zhong, Liangpei Zhang, and Xiaoqiang Lu. Aid: A benchmark data set for performance evaluation of aerial scene classification. *IEEE Transactions on Geoscience and Remote Sensing*, 55(7):3965–3981, 2017.

Gui-Song Xia, Xiang Bai, Jian Ding, Zhen Zhu, Serge Belongie, Jiebo Luo, Mihai Datcu, Marcello Pelillo, and Liangpei Zhang. Dota: A large-scale dataset for object detection in aerial images. In *Proceedings of the IEEE conference on computer vision and pattern recognition*, pp. 3974–3983, 2018.

Junlin Xie, Zhihong Chen, Ruifei Zhang, Xiang Wan, and Guanbin Li. Large multimodal agents: A survey. *arXiv preprint arXiv:2402.15116*, 2024.

Zhitong Xiong, Fahong Zhang, Yi Wang, Yilei Shi, and Xiao Xiang Zhu. Earthnets: Empowering ai in earth observation. *arXiv preprint arXiv:2210.04936*, 2022.

Weikai Xu, Chengrui Huang, Shen Gao, and Shuo Shang. Llm-based agents for tool learning: A survey: W. xu et al. *Data Science and Engineering*, pp. 1–31, 2025.

Wenjia Xu, Zijian Yu, Boyang Mu, Zhiwei Wei, Yuanben Zhang, Guangzuo Li, and Mugen Peng. Rs-agent: Automating remote sensing tasks through intelligent agent. *arXiv preprint arXiv:2406.07089*, 2024a.

Yiheng Xu, Dunjie Lu, Zhennan Shen, Junli Wang, Zekun Wang, Yuchen Mao, Caiming Xiong, and Tao Yu. Agenttrek: Agent trajectory synthesis via guiding replay with web tutorials. *arXiv preprint arXiv:2412.09605*, 2024b.

An Yang, Anfeng Li, Baosong Yang, Beichen Zhang, Binyuan Hui, Bo Zheng, Bowen Yu, Chang Gao, Chengen Huang, Chenxu Lv, et al. Qwen3 technical report. *arXiv preprint arXiv:2505.09388*, 2025.

Shunyu Yao, Jeffrey Zhao, Dian Yu, Nan Du, Izhak Shafran, Karthik Narasimhan, and Yuan Cao. React: Synergizing reasoning and acting in language models. In *International Conference on Learning Representations (ICLR)*, 2023.

Yang Zhan, Zhitong Xiong, and Yuan Yuan. Rsvg: Exploring data and models for visual grounding on remote sensing data. *IEEE Transactions on Geoscience and Remote Sensing*, 61:1–13, 2023.

Yang Zhan, Zhitong Xiong, and Yuan Yuan. Skyeyegpt: Unifying remote sensing vision-language tasks via instruction tuning with large language model. *ISPRS Journal of Photogrammetry and Remote Sensing*, 221:64–77, 2025.

Kechi Zhang, Jia Li, Ge Li, Xianjie Shi, and Zhi Jin. Codeagent: Enhancing code generation with tool-integrated agent systems for real-world repo-level coding challenges. *arXiv preprint arXiv:2401.07339*, 2024a.

Wei Zhang, Miaoxin Cai, Tong Zhang, Yin Zhuang, and Xuerui Mao. Earthgpt: A universal multimodal large language model for multi-sensor image comprehension in remote sensing domain. *IEEE Transactions on Geoscience and Remote Sensing*, 2024b.

Baichuan Zhou, Haote Yang, Dairong Chen, Junyan Ye, Tianyi Bai, Jinhua Yu, Songyang Zhang, Dahua Lin, Conghui He, and Weijia Li. Urbench: A comprehensive benchmark for evaluating large multimodal models in multi-view urban scenarios. In *Proceedings of the AAAI Conference on Artificial Intelligence*, volume 39, pp. 10707–10715, 2025.

A DATASET ILLUSTRATION

A.1 DATASET COMPOSITION

The remote sensing imagery used in our dataset primarily comes from Landsat and MODIS, with additional high-resolution imagery sourced from open datasets. All the remote sensing data products are obtained through Google Earth Engine (GEE). The following Table 4 is a more detailed breakdown of the data sources, products, and their distribution:

Table 4: Sensor and Data Source Statistics

Category	Sensor/Data Source	Dataset	Samples
Spectrum	Landsat	Landsat 8 / 9	1684
	MODIS	-	10273
	ASTER	-	110
Products	GEE	LST	183
		NDVI	369
		GPM	160
		VIIRS	164
		GHSL	68
		QA PIXEL	212
		NDWI	69
		fire MaxFRP	194
RGB	Public Datasets	AID	169
		DIOR-RSVG	7
		DOTA	22
		NWPU-VHR-10	21
		xBD	32
Total	-	-	13737

This table provides an overview of the data sources and the distribution of samples across three categories (Spectrum, Product, RGB). It includes a diverse set of remote sensing products, such as Landsat, MODIS, ASTER, and various other publicly available high-resolution datasets, ensuring comprehensive coverage for a wide range of Earth observation tasks.

A.2 BENCHMARK STATISTICS

Table 5: Statistics of the benchmark dataset, including average verification code length, number of images, query length, reasoning steps, and question counts for different task types.

Type	Avg. Code Lines	Avg. Images	Avg. Query Length AP	Avg. Query Length IF	Avg. Steps	Question Count
Spectrum	361.19	96.82	331.54	497.94	4.38	100
Products	283.64	43.23	505.72	648.09	6.35	88
RGB	176.42	4.18	333.80	464.70	5.77	60
Avg.	288.97	55.39	393.89	543.18	5.42	-
Total	71664	13737	97685	134708	1343	248

As illustrated in Table 5, Earth-Bench consists of 248 questions associated with approximately 13.7K images. We recruited a team of domain experts to annotate these questions. The annotation process was as follows: experts first designed solution steps based on their expertise, then selected appropriate tools from the Agent Toolkit, implemented the steps by writing Python code to invoke the selected tools for data processing, and finally generated the corresponding answers. In total, the expert team annotated 1345 solution steps and produced 71,664 lines of verification code for the 248 benchmark questions.

A.3 QUESTION TYPES AND CATEGORY

As shown in Figure 5, Earth-Bench questions are categorized into three types based on their data sources: ***Spectrum***, ***Products***, and ***RGB***. The Table 6 below summarizes the number and proportion of questions within each category:

Table 6: Distribution of Question Types and Their Proportions

Question Types	**Number**	**Proportion (%)**
Temperature Monitoring	44	17.74
Weather Forecasting	11	4.44
Climate Analysis	20	8.06
Water Management	22	8.87
Pollution Regulation	14	5.65
Vegetation Monitoring	28	11.29
Disaster Judgement	24	9.68
Urban Management	25	10.08
Classification	15	6.05
Detection	15	6.05
Grounding	7	2.82
Segmentation	3	1.21
Counting	7	2.82
Change Detection	13	5.24

This table provides a detailed distribution of question types within Earth-Bench, reflecting the variety of Earth observation tasks addressed by the dataset.

A.4 QUERY REGIMES

Earth-Bench categorizes each task into two regimes: Auto-Planning and Instruction-Following. The key distinction is that in Instruction-Following, the query explicitly provides the Agent with a solution approach, while preserving the original intent of the task. As shown in Table 5, the statistics of query length highlight this difference: on average, queries in the Instruction-Following regime are about 150 characters longer than those in Auto-Planning, due to the inclusion of solution guidance. For illustration, Appendix H presents examples of the same task under both regimes, along with the performance of different LLMs. In summary, Instruction-Following emphasizes LLMs' instruction-following and tool-use capabilities, whereas Auto-Planning additionally evaluates their ability to decompose and plan Earth observation tasks.

A.5 DATASET QUALITY CONTROL

Our annotation team was composed of **2** computer science experts, **7** remote sensing specialists (including one professor) and **3** Earth science specialists (including one professor).

Three core authors who served as senior reviewers led the pipeline of dataset construction. Each senior reviewer was responsible for guiding the development of the question sets and templates for the ***Spectrum***, ***Products***, and ***RGB*** categories. They played a key role in providing strategic direction for the overall question pool.

The remaining 7 team members, consisting of graduate students and senior undergraduates, contributed in the following areas:

- Creation of initial questions (approximately 400 questions)
- Raw data collection
- Development of Python-based solution scripts

Once the questions were created, they were thoroughly reviewed by the 3 senior reviewers. The review process focused on two key criteria:

1. **Data Integrity**: Ensuring that the raw data involved (e.g., Landsat or MODIS) has complete band information within the task's time range and does not contain anomalies. Any questions and TIF files with missing or anomalous large values were discarded.
2. **Task Difficulty Assessment**: Senior reviewers assessed the difficulty of questions based on the number and complexity of the functions defined in the Python solutions. For simpler tasks (e.g., only calculating NDVI index to finish a task), these were removed to ensure an appropriate challenge across questions.

This collaborative structure ensured that the dataset was curated by a diverse team with expertise from the full landscape of Earth observation fields, enabling a well-rounded and comprehensive dataset for evaluation.

A.6 BIAS ABLATION EXPERIMENT

To examine whether Earth-Bench exhibits bias toward specific models, i.e., whether certain models inherently find its tasks easier and thus risk skewing conclusions, we conducted an ablation study. Specifically, we removed all tools and allowed LLMs to directly answer questions given only the Query and Folder, then compared the results with those of tool-augmented Agents that had access to both Query and Data.

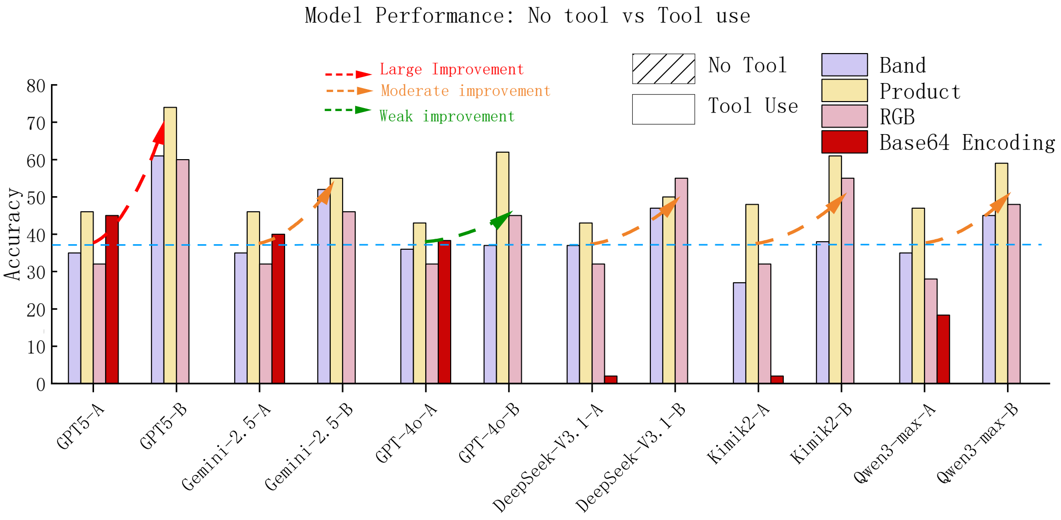

Figure 6: Dataset Ablation Experiment

As shown in Fig. 6, without tool access, mainstream LLMs achieved comparable performance across the three task types, with an overall Accuracy of about 37%. This indicates that the dataset is fair in its raw form and that models cannot rely solely on parametric knowledge to solve all benchmark questions. In contrast, with tool access, different models exhibited varying degrees of improvement:

GPT-5 achieved the largest gain, whereas GPT-4o showed a more modest increase. These results highlight differences in problem decomposition and tool-use capabilities among LLMs, and further corroborate the conclusions presented in the main experiments.

In the *No Tool* setting, LLMs/MLLMs were restricted from using any tools, and base64 encoding was not applied in RGB tasks specifically. To ensure integrity in the comparison, we added experiments with base64 encoding for RGB tasks. We observed that while models like GPT-5 showed some improvement in accuracy (compared with not applying base64 encoding), the performance remained at relatively low levels. DeepSeek and Kimik2 were unable to handle RGB tasks yet. The conclusions derived from the ablation study remain unchanged.

B EVALUATION

B.1 EVALUATION MODEL

Our evaluation covers 13 recent LLMs, including both closed-source and open-source ones, to understand their capabilities across multiple Earth observation tasks. The baseline models are listed in Table 7.

Table 7: Models evaluated in our benchmark and their corresponding API references.

Model	**Model Version**	**API Links**
GPT5	GPT-5	`https://platform.openai.com/docs/models/gpt-5`
GPT4	GPT-4o	`https://platform.openai.com/docs/models/gpt-4o`
Gemini	Gemini-2.5-Flash	`https://ai.google.dev/gemini-api/docs/models#gemini-2.5-flash`
Mistral	Mistral-Large	`https://docs.mistral.ai/getting-started/models/`
Qwen	Qwen3-Max-Previous Qwen3-32B Qwen-Plus	`https://www.alibabacloud.com/help/en/model-studio/use-qwen-by-calling-api`
Kimi	Kimi-K2	`https://platform.moonshot.ai/docs/guide/start-using-kimi-api`
Deepseek	Deepseek-V3.1	`https://api-docs.deepseek.com`
Seed	Seed-1.6	`https://www.volcengine.com/docs/82379/1099455`
LLaMA	LLaMA-4-Maverick	`https://www.llama.com/products/llama-api/`
GLM	GLM-4.5v	`https://docs.z.ai/guides/vlm/glm-4.5v`
InternVL	InternVL-3.5	`https://internlm.intern-ai.org.cn/api/document`

B.2 EVALUATION METRIC

Formally, for each task goal g, our geoscience experts provide (i) a ground-truth final answer $y^\star$, and (ii) an expert-annotated reasoning trajectory.

$$\tau^\star = \big[(o_0^\star, a_0^\star),\ (o_1^\star, a_1^\star),\ \ldots,\ (o_m^\star, a_m^\star)\big],$$

where each action is defined as

$$a_k^\star = (t_k^\star,\ in_k^\star,\ out_k^\star),$$

with $t_k^\star \in \mathcal{V}$ denoting the tool identifier (from the tool vocabulary), $in_k^\star \in \mathcal{X}$ the input arguments, and $out_k^\star \in \mathcal{O}$ the corresponding output. In other words, each tool is characterized by its name in the vocabulary, its input arguments, and its output results.

Given a policy π, the agent generates an output trajectory

$$\tau = \big[(o_0, a_0),\, (o_1, a_1),\, \dots,\, (o_n, a_n)\big],$$

together with a predicted final answer y.

To comprehensively evaluate the performance of the Agent on the Earth Benchmark, we assess its execution process from two perspectives: End-to-End and Step-by-Step. The corresponding evaluation metrics are defined as follows:

End-to-End protocol. End-to-end metrics evaluate the task-level performance of the agent, independent of its intermediate reasoning. We consider two complementary measures:

(1) Accuracy. The correctness of the final answer is computed as

$$\text{Acc} \;=\; \mathbb{E}_{g\sim\mathcal{G}}\big[\mathbb{I}\{y = y^\star\}\big], \tag{1}$$

where $\mathbb{I}\{\cdot\}$ is the indicator function and $\mathcal{G}$ is the distribution of benchmark tasks.

(2) Efficiency. To penalize unnecessarily long trajectories, we measure the relative optimality of tool usage:

$$\text{Eff}(\tau, \tau^\star) \;=\; \frac{|\tau|}{|\tau^\star|}, \tag{2}$$

where $|\tau|$ and $|\tau^\star|$ denote the number of tool calls in the predicted and ground-truth trajectories, respectively.

Step-by-Step protocol. In addition to outcome-based metrics, we also evaluate the fidelity of the reasoning trajectory relative to expert annotations. Let $\mathbf{t}^\star = (t_1^\star, \dots, t_m^\star)$ and $\mathbf{t} = (t_1, \dots, t_n)$ denote the tool sequences, and $\mathbf{in}^\star = (in_1^\star, \dots, in_m^\star)$, $\mathbf{in} = (in_1, \dots, in_n)$ the corresponding parameter sequences. We define four metrics:

(1) Tools-Any-Order (TAO). Coverage of required tools, ignoring order and duplicates:

$$TAO(\tau, \tau^\star) \;=\; \frac{\big|\, Set(\mathbf{t}^\star) \cap Set(\mathbf{t}) \,\big|}{|\, Set(\mathbf{t}^\star)\,|}, \tag{3}$$

where $Set(\cdot)$ extracts the set of unique tools.

(2) Tools-In-Order(TIO). Fraction of ground-truth tools matched as a subsequence in the predicted sequence:

$$k^\star \;=\; \max\big\{\, k : \exists\, 1 \le j_1 < \cdots < j_k \le n,\; t_{j_i} = t_i^\star,\; \forall i \le k \big\}, \quad TIO(\tau, \tau^\star) \;=\; \frac{k^\star}{m}. \tag{4}$$

(3) Tool-Exact-Match(TEM). Length of the longest common prefix (LCP), normalized by the ground-truth length:

$$\ell_{\text{lcp}} \;=\; \max\big\{\, \ell \le \min(m, n) : t_i = t_i^\star,\; \forall i \le \ell \big\}, \quad TEM(\tau, \tau^\star) \;=\; \frac{\ell_{\text{lcp}}}{m}. \tag{5}$$

(4) Parameter Accuracy. Exact match of both tool identifiers and arguments under the prefix rule:

$$\ell_{\text{param}} \;=\; \max\big\{\, \ell \le \min(m, n) : t_i = t_i^\star \wedge in_i \equiv in_i^\star,\; \forall i \le \ell \big\}, \quad S_{\text{param}} \;=\; \frac{\ell_{\text{param}}}{m}. \tag{6}$$

Here $in_i \equiv in_i^\star$ denotes structural equality of arguments (e.g., dictionary match).

C BREAKDOWN RESULTS ON DIFFERENT MODALITIES

Table 8, Table 9, and Table 10 present the detailed evaluation results on different subsets of Earth-Bench. In the main analysis, we report only the overall performance across the entire benchmark to ensure clarity and comparability. Nevertheless, the breakdown results of individual subsets provide valuable insights into potential directions for improving LLMs in Earth Observation tasks.

Table 8: Performance of different LLM-based agents on the **Spectrum** subset of Earth-Bench. We **bold** the best results and underline the runner-ups.

Model	Tool-Any-Order		Tool-In-Order		Tool-Exact-Match		Parameters		Efficiency		Accuracy	
	AP	IF	AP	IF	AP	IF	AP	IF	AP	IF	AP	IF
GPT-5	72.67	78.37↑	65.80	74.71↑	49.64	52.07↑	21.74	24.97↑	3.5510	4.6657↓	**61.00**	**64.00**↑
Gemini-2.5	71.35	71.90↑	65.14	64.84↓	40.12	49.89↑	17.57	21.41↑	4.3584	4.5585↑	52.00	52.00
GPT-4o	69.55	72.83↑	56.12	62.07↑	48.27	51.02↑	21.62	24.08↑	3.7736	4.5726↓	37.00	42.00↑
Kimik2	71.92	**86.02**↑	62.27	**78.91**↑	43.04	**54.81**↑	20.73	25.67↑	2.5758	3.1005↓	38.00	50.00↑
DeepSeek-V3.1	76.48	75.97↓	**67.64**	66.57↓	**50.22**	50.52↑	**26.32**	**26.13**↓	3.9014	4.0685↓	47.00	45.00↓
Qwen3-Max	**77.67**	74.27↓	66.47	65.58↓	33.97	48.54↑	16.04	24.43↑	3.1981	3.2864↓	45.00	40.00↓
Seed-1.6	55.07	63.92↑	42.00	54.94↑	24.53	34.37↓	12.56	16.83↑	1.7525	1.9186↓	40.00	57.00↑
LLaMA-4	16.89	25.20↑	3.57	18.26↑	2.69	13.58↑	2.02	8.17↑	0.3648	0.4275↓	36.00	37.00↑
Qwen-Plus	55.95	57.38↑	36.27	48.89↑	5.67	35.14↑	2.87	17.47↑	2.2833	2.4157↓	33.00	36.00↑
GLM-4.5v	47.53	49.87↑	41.93	45.63↑	14.26	25.22↑	9.13	16.41↑	3.1121	3.0709↑	33.33	28.28↓
Mistral	23.73	19.58↓	4.58	16.13↑	1.87	13.37↑	1.33	6.15↑	1.3825	0.8316↑	24.00	18.00↓
Qwen3-32B	45.02	65.25↑	26.60	57.17↑	5.53	38.86↑	3.43	20.52↑	4.3328	3.4380↑	12.00	29.00↑
InternVL-3.5	7.50	18.77↑	3.58	16.09↑	0.58	13.02↑	0.33	5.65↑	**0.1127**	**0.2411**↓	19.00	25.00↑

On the Spectrum subset, the accuracy of the Agent's responses is generally below the average, and the overall efficiency is also lower than the benchmark mean. This indicates that the Agent encounters significant difficulties when addressing tasks in this subset. A likely reason is that the LLMs involved in the evaluation have limited familiarity with processing raw Earth Observation data. Furthermore, tasks in this subset often require analyzing a larger number of images, making them inherently more challenging compared to tasks in other subsets.

In contrast, on the Product subset, the Agent's responses are substantially above the average in terms of accuracy, and its efficiency is comparable to that of expert annotations. This suggests that LLMs are more adept at handling structured, product-level information, where tasks often align with general reasoning and statistical capabilities rather than requiring specialized domain expertise.

Table 9: Performance of different LLM-based agents on the **Products** subset of Earth-Bench. We **bold** the best results and underline the runner-ups.

Model	Tool-Any-Order		Tool-In-Order		Tool-Exact-Match		Parameters		Efficiency		Accuracy	
	AP	IF	AP	IF	AP	IF	AP	IF	AP	IF	AP	IF
GPT-5	60.04	62.35↑	38.43	40.44↑	31.52	34.03↑	17.62	16.75↓	1.7154	1.6190↑	**75.00**	**71.59**↓
Gemini-2.5	48.94	51.46↑	33.82	35.26↑	29.54	27.63↓	16.33	17.11↑	3.0055	1.1600↑	62.50	63.64↑
GPT-4o	57.27	60.11↑	33.89	37.80↑	31.31	35.02↑	19.13	18.71↓	1.1800	1.5270↓	54.55	54.55
Kimik2	66.91	69.83↑	42.99	**49.96**↑	**34.75**	**38.84**↑	20.23	**21.32**↑	1.2489	1.6481↓	62.50	60.23↓
DeepSeek-V3.1	**73.48**	**72.75**↓	**43.35**	46.16↑	32.18	33.32↑	**20.50**	19.92↓	1.8111	1.6449↑	50.00	59.09↑
Qwen3-Max	63.24	66.80↑	40.30	44.78↑	33.22	30.24↓	20.23	16.52↓	1.0688	1.0859↓	56.82	61.36↑
Seed-1.6	54.02	55.57↑	36.75	37.20↑	28.84	31.27↑	16.79	19.82↑	0.8776	0.9359↓	65.06	67.05↑
LLaMA-4	8.92	9.83↑	2.51	2.61↑	1.39	1.65↑	1.05	1.31↑	0.1641	0.1614↑	60.23	47.73↓
Qwen-Plus	47.71	51.57↑	25.33	27.37↑	10.16	4.14↓	6.52	2.97↓	0.9972	1.0016↓	53.41	40.91↓
GLM-4.5v	35.06	41.97↑	19.36	24.68↑	8.77	9.04↑	6.60	7.77↑	0.9342	1.1979↓	43.18	47.67↑
Mistral	26.61	30.36↑	12.80	13.43↑	8.83	10.40↑	5.42	4.40↓	0.6263	1.0206↓	36.36	22.73↓
Qwen3-32B	29.66	6.97↓	11.81	1.93↓	2.70	1.14↓	2.07	1.14↓	2.2108	0.6987↑	27.27	18.39↓
InternVL-3.5	4.91	5.27↑	1.94	2.32↑	0.52	2.26↑	0.52	0.55↑	**0.0495**	**0.0424**↑	36.36	28.41↓

For the RGB subset, the Agent demonstrates above-average performance in tool utilization and achieves efficiency close to that of expert annotations. However, its response accuracy remains substantially below the average. This limitation is closely tied to the capabilities of the tools within the Perception Toolkit. In certain cases, even when the Agent selects the same tools as those used in expert annotations, the outputs still diverge from the ground-truth answers due to the constraints of the underlying expert models. As the first attempt to develop an Agent framework for Earth Observation, our work highlights this challenge and encourages future EO Agent research to adopt more advanced expert models in order to overcome these limitations.

Table 10: Performance of different LLM-based agents on the **RGB** subset of Earth-Bench. We **bold** the best results and underline the runner-ups.

Model	Tool-Any-Order		Tool-In-Order		Tool-Exact-Match		Parameters		Efficiency		Accuracy	
	AP	IF	AP	IF	AP	IF	AP	IF	AP	IF	AP	IF
GPT-5	76.61	72.09↓	75.04	67.08↓	59.60	52.71↓	46.15	40.73↓	1.5312	1.5784↓	**59.32**	49.15↓
Gemini-2.5	48.70	60.11↑	29.38	50.11↑	21.33	45.54↑	19.07	36.75↑	0.7926	0.8878↓	47.46	47.46
GPT-4o	71.86	66.89↓	66.60	61.13↓	64.76	60.00↓	46.65	47.54↑	0.8779	0.8939↓	45.76	35.59↓
Kimik2	75.65	80.62↑	71.37	79.90↑	51.48	63.32↑	43.12	**52.19**↑	1.5341	1.4104↑	54.24	**62.71**↑
DeepSeek-V3.1	**88.98**	**89.21**↑	**85.49**	**87.64**↑	**71.54**	**74.05**↑	**53.57**	57.22↑	1.6895	1.7966↓	55.93	54.24↓
Qwen3-Max	65.25	68.14↑	50.28	56.58↑	47.88	51.55↑	34.04	43.93↑	0.8601	0.9785↓	49.15	38.98↓
Seed-1.6	57.99	57.59↓	44.00	47.30↑	34.11	43.74↑	29.93	39.02↑	1.1948	0.9589↑	55.93	52.54↓
LLaMA-4	27.20	36.52↑	0.47	15.61↑	0.47	12.43↑	0.47	11.25↑	0.3464	0.3790↓	37.29	27.12↓
Qwen-Plus	51.89	60.11↑	29.51	42.80↑	24.18	41.07↑	23.62	36.89↑	0.9721	1.0488↓	42.37	38.98↓
GLM-4.5v	47.91	48.42↑	27.36	33.54↑	21.93	27.38↑	19.73	24.98↑	1.3070	1.4535↓	16.95	28.81↑
Mistral	36.16	45.59↑	22.46	40.11↑	21.89	37.71↑	19.97	31.84↑	0.7215	0.7531↓	30.51	30.51
Qwen3-32B	45.93	56.47↑	27.54	41.69↑	26.41	41.69↑	25.28	37.74↑	0.7767	1.0891↓	25.42	27.12↑
InternVL-3.5	16.95	29.92↑	7.23	13.58↑	6.67	13.58↑	4.75	11.88↑	**0.2398**	**0.2606**↓	25.42	27.12↑

Overall, the comparative analysis across subsets highlights both the strengths and limitations of LLM-based Agents in Earth Observation. While LLMs achieve relatively strong performance on Product tasks, where success relies more on general reasoning and statistical skills, they remain less effective on tasks that demand specialized knowledge, such as those in the Spectrum subset, which involve interpreting raw spectral data. Moreover, Earth-Agent incorporates expert models within the Perception Toolkit for tasks such as segmentation and object detection, which significantly improves performance in the corresponding scenarios. However, the generalization ability of these expert models remains limited, as their outputs do not always align with ground-truth answers, even when the correct tools are selected. These findings suggest that future progress in EO Agents will depend not only on enhancing LLMs with domain-specific knowledge, but also on developing more robust and versatile expert models to ensure reliable performance across the diverse spectrum of Earth Observation tasks.

D ERROR ANALYSIS

To analyze the errors made by Agents with different LLM backbones on Earth-Bench tasks, we selected GPT-5 as a representative closed-source model, and Kimi-K2, Qwen3-Max, and Deepseek-V3.1 as representative open-source models. We counted the number of errors and categorized them into five types:

- Unaware of Termination Conditions: failure to recognize the task's termination condition, leading to repeated tool calls until reaching the maximum step limit;
- Tool Hallucination: attempts to invoke non-existent tools;
- File Hallucination: attempts to process non-existent files, i.e., providing invalid file or folder paths as tool inputs;
- Invalid Parameters: inputs that do not conform to the expected parameter format or are otherwise invalid;
- System Error: system-level failures caused by the runtime environment or external dependencies.

Figure 7 presents the frequency and distribution of these error types. Results show that GPT-5 produced the largest number of errors, while Kimi-K2 had the fewest. Except for GPT-5, the other models exhibited similar error counts across different regimes, and their error distributions did not vary significantly, suggesting that providing more detailed execution steps does not substantially improve tool-use proficiency.

In terms of error types, GPT-5 errors were dominated by Invalid Parameters, with occasional System Errors and File Hallucinations, but no Tool Hallucinations. In contrast, the three open-source models demonstrated different error patterns: while Invalid Parameters remained a notable factor, it was not the primary source of errors. Instead, nearly 60% of their errors stemmed from Hallucinations and Unaware of Termination Conditions. We hypothesize that this difference is related to training strategies. Open-source models are often trained with reinforcement learning, which may encourage more exploratory outputs, thereby increasing the likelihood of hallucinations. Moreover, their reward functions are typically designed to shape behavioral style and output preferences rather than enhance factual knowledge, which could make models more prone to generating divergent or repetitive outputs and to overlooking termination conditions.

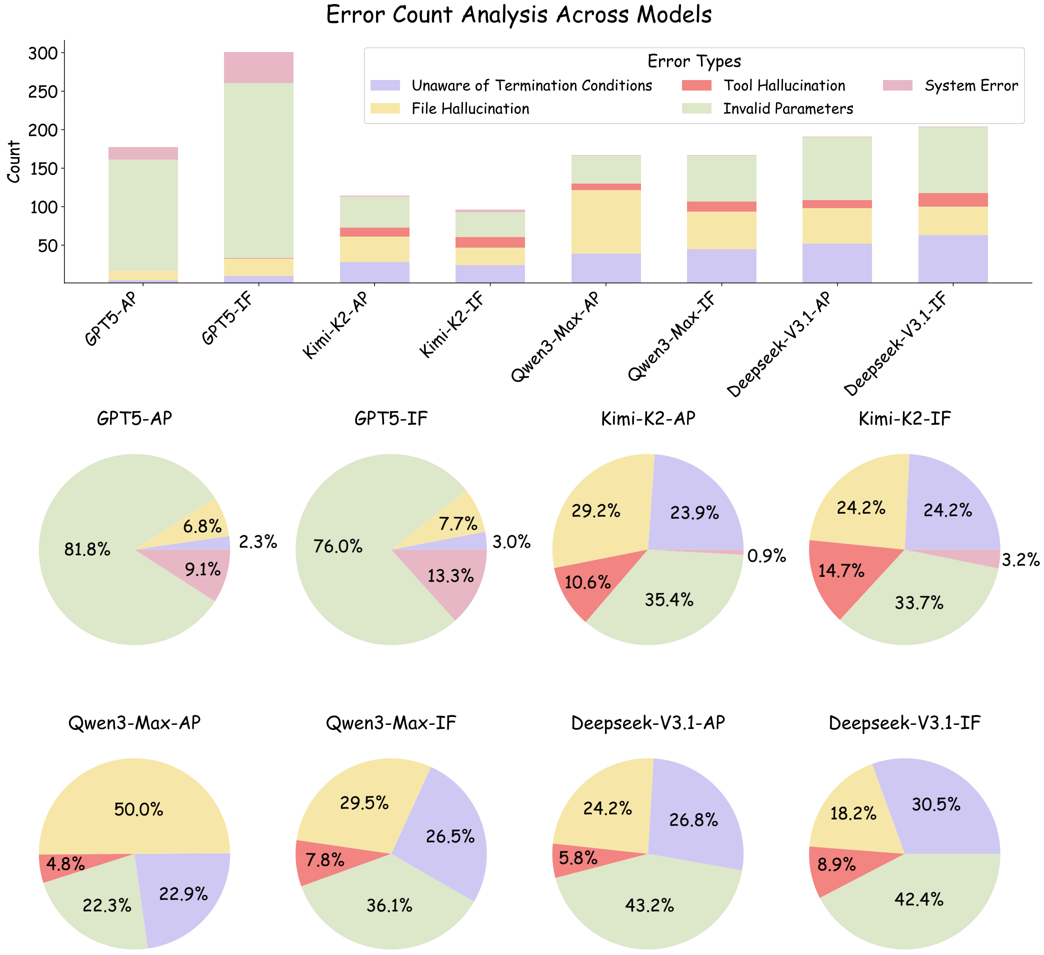

Figure 7: Error analysis.

E LATENCY EXPERIMENT

E.1 BREAKDOWN RESULTS ON LATENCY

We further break down the latency into ***LLM Latency*** and ***Tool Latency***. It is evident that the majority of the latency is spent on model calls (LLM Latency), rather than on external tool calls (Tool Latency). This suggests that reducing the frequency of model calls could further improve latency. The results are shown in Table 11.

We observe that the majority of the latency is attributed to ***LLM Latency***, while the impact of ***Tool Latency*** is relatively minimal. Therefore, reducing the frequency of model calls could significantly improve overall latency. This suggests that optimizing the model call frequency would further enhance system performance.

Table 11: Latency Breakdown for Different Models on Earth-Bench-Lite

Model	Latency	Tool Call Number	LLM Latency	Tool Latency
Earth-Agent (GPT)	9494.92s	669	6969.26s	2525.66s
Earth-Agent (DeepSeek-V3.1)	4716.99s	540	3066.76s	1650.23s
Earth-Agent (Kimik2)	7903.07s	502	6306.59s	1596.47s

E.2 OUR PROPOSED STRATEGY

We addressed this issue in the design of the Earth-Agent architecture. Specifically, we optimized the tool design to minimize unnecessary interactions with the model. For instance, by leveraging batch calculations for Earth indices, such as the NDVI calculation, we significantly reduce the frequency of model interactions, thereby lowering the overall latency. Below is an example of our approach:

Batch Computing Strategy

```
def calculate_ndvi(input_nir_path, input_red_path, output_path):
    with rasterio.open(input_nir_path) as nir_src:
        nir_band = nir_src.read(1)  # Read the first band (assuming single-band rasters)
        nir_profile = nir_src.profile  # Get the metadata profile
    with rasterio.open(input_red_path) as red_src:
        red_band = red_src.read(1)  # Read the first band (assuming single-band rasters)
    nir_band = np.array(nir_band, dtype=np.float32)
    red_band = np.array(red_band, dtype=np.float32)
    nir_band = np.clip(nir_band, 0, 10000)
    red_band = np.clip(red_band, 0, 10000)
    valid_mask = (nir_band >= 0) & (nir_band <= 10000) & (red_band >= 0) & (red_band <= 10000)
    denominator = nir_band + red_band + 1e-6
    ndvi = (nir_band - red_band) / denominator
    # Set invalid pixels to -9999
    ndvi[~valid_mask] = -9999
    ndvi_profile = nir_profile.copy()
    ndvi_profile.update(
        dtype=rasterio.float32,  # NDVI values are floating-point numbers
        nodata=-9999,  # Set a NoData value
        compress='lzw'  # Optional: compress the output file
    )
    # Save the NDVI result to the specified output path
    os.makedirs((TEMP_DIR / output_path).parent, exist_ok=True)
    with rasterio.open(TEMP_DIR / output_path, 'w', **ndvi_profile) as dst:
        dst.write(ndvi.astype(rasterio.float32), 1)

    return f'Result save at {TEMP_DIR / output_path}'
@mcp.tool(description="""
Batch-calculate NDVI from multiple pairs of NIR/Red raster files and save results.

Parameters:
    input_nir_paths (list[str]): Paths to Near-Infrared (NIR) band raster files.
    input_red_paths (list[str]): Paths to Red band raster files.
    output_paths (list[str]): Relative output paths (e.g., "question17/ndvi_2022-01-16.tif") for each pair.

Returns:
    list[str]: A list of result messages (one per output), as returned by `calculate_ndvi`.
""")
def calculate_batch_ndvi(
    input_nir_paths: list[str],
    input_red_paths: list[str],
    output_paths: list[str]
) -> list[str]:
    return [
        calculate_ndvi(nir_path, red_path, out_path)
        for nir_path, red_path, out_path in zip(input_nir_paths, input_red_paths, output_paths)
    ]
```

F SCALABILITY DISCUSSION

Understanding the performance trends as the number of tool calls increases is crucial for evaluating the system's behavior, particularly in terms of latency and scalability under increasing task complexity.

F.1 PERFORMANCE WITH RESPECT TO TOOL NUMBER

To address this, we conducted an ablation study examining the relationship between the **number of tools** used and **the system's performance** across three SOTA models: GPT5, DeepSeek-V3.1, and Kimik2. The following Table 12 presents the results, highlighting the high performance range for each model:

Table 12: Performance of Earth-Agent Models with respect to Tool Numbers. The **high performance range** is highlighted.

Tool Numbers	**GPT5**		**DeepSeek-V3.1**		**Kimik2**	
	Questions	Accuracy (%)	Questions	Accuracy (%)	Questions	Accuracy (%)
0	25	8.00	-	-	25	4.00
1	3	**66.67**	2	0.00	1	0.00
2	8	**75.00**	-	-	5	40.00
3	42	**80.95**	23	**73.91**	17	**76.47**
4	29	**89.66**	23	**86.96**	21	**66.67**
5	30	**60.00**	19	**68.42**	21	**71.43**
6	7	**85.71**	15	**60.00**	27	**70.37**
7	10	**90.00**	15	40.00	16	**56.25**
8	10	**80.00**	8	**87.50**	20	**65.00**
9	4	**75.00**	10	**60.00**	4	25.00
10	10	**70.00**	11	**54.55**	5	**40.00**
11	4	**50.00**	8	**75.00**	11	**54.55**
12	3	33.33	8	**75.00**	9	**66.67**
13	6	**100.00**	17	**70.59**	20	**80.00**
14	4	**75.00**	4	**50.00**	3	33.33
15	2	0.00	5	**100.00**	4	50.00
16	2	100.00	3	66.67	1	0.00
17	4	50.00	4	25.00	3	66.67
18	4	50.00	4	25.00	2	50.00
19	3	0.00	3	0.00	1	0.00
20	3	33.33	3	33.33	1	100.00
...	...	...	...	...	...	...
159	1	100.00	-	-	-	-

From the results, we observe distinct performance trends for each model:

- For Earth-Agent driven by GPT5, high accuracy is primarily concentrated within **the tool number range of 1 to 14**.
- For Earth-Agent driven by DeepSeek-V3.1, the high-performance range is within **the tool number range of 3 to 15**.
- For Earth-Agent driven by Kimik2, the high-performance range falls within **the tool number range of 3 to 13**.

These high performance ranges align with expectations and indicate that task complexity plays a key role in system performance. Using too few tools (with the extreme case being zero tools) results in low accuracy, as the agent is unable to solve the task effectively, often leading to early errors. Conversely, performance tends to degrade when too many tools are employed, suggesting that the current capabilities of the base LLMs may not be sufficient to handle long chains of reasoning efficiently.

F.2 PERFORMANCE WITH RESPECT TO UNIQUE TOOL NUMBER

We also investigated the relationship between the **unique number of tools** used and **performance trends**. Below is a visual representation using a bubble chart, where the size of each bubble is proportional to the number of questions.

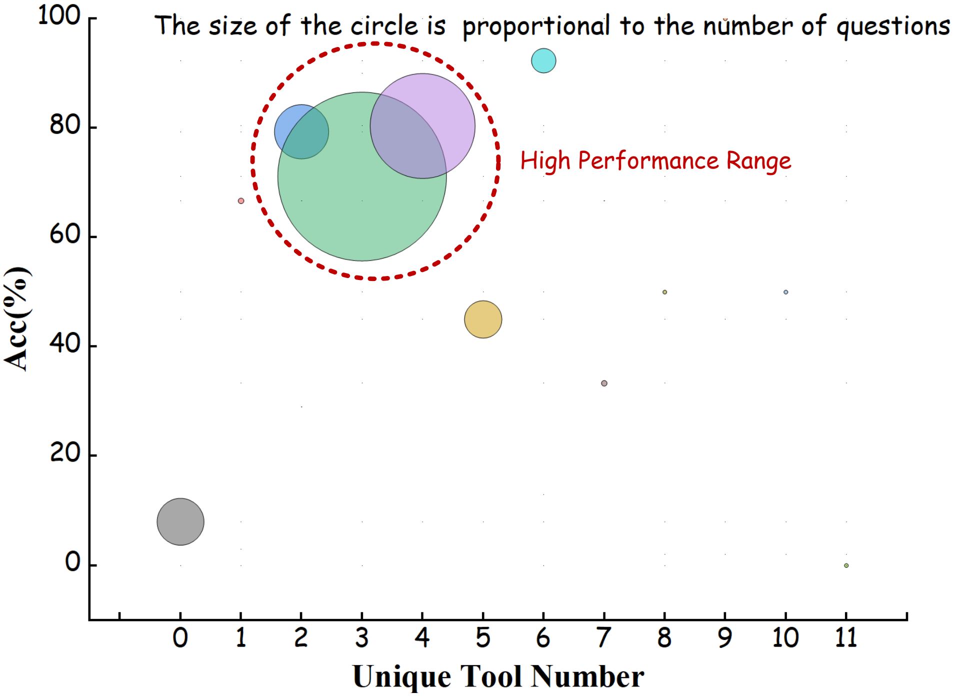

Figure 8: **GPT5: Performance with respect to Unique Tool Number**

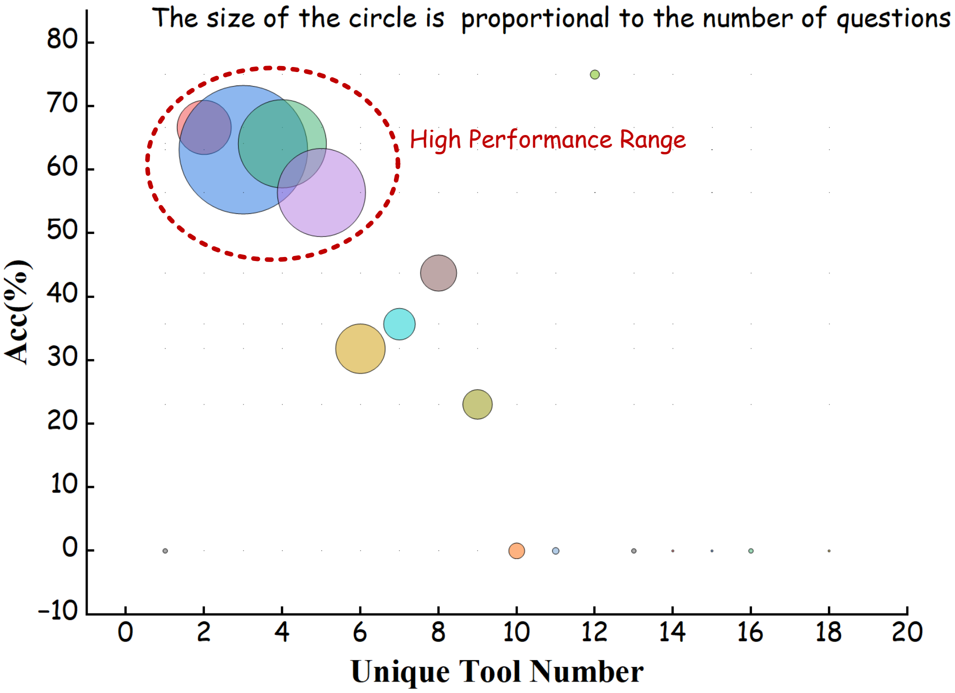

Figure 9: **DeepSeek-V3.1: Performance with respect to Unique Tool Number**

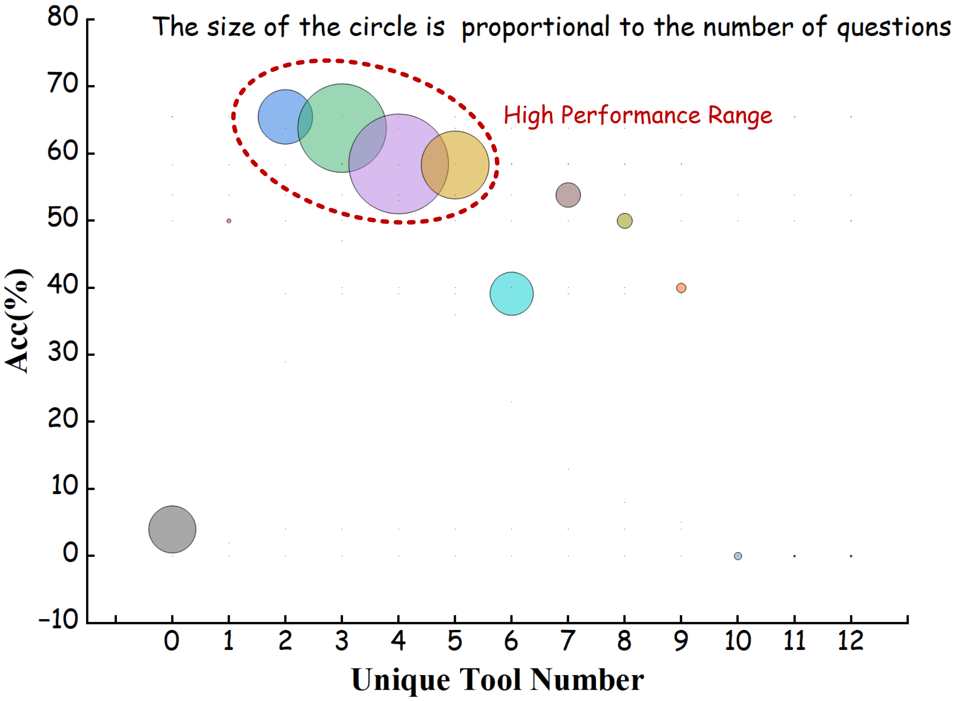

Figure 10: **Kimik2: Performance with respect to Unique Tool Number**

Based on Figures 8, 9, and 10, we observed the following trends in the Earth-Agent system: When driven by GPT5, high accuracy is primarily observed within the range of 2 to 5 unique tool calls. For DeepSeek, the optimal accuracy is concentrated in the range of 2 to 6 unique tool calls, while for Kimik2, high accuracy is predominantly found in the range of 1 to 6 unique tool calls. We also observed a performance decline when the number of tool calls becomes excessive. These findings align with our expectations, highlighting the current limitations of LLMs in handling tasks that involve long chains of reasoning or excessive tool interactions.

This analysis provides valuable insights into the scalability of the system as task complexity increases. It also offers important directions for future agent training, including (1) optimizing the agent's startup phase and (2) developing datasets for long-chain reasoning to enhance the agent's ability to handle multiple tool calls effectively.

G TOOL KIT LIST

The Index Toolkit offers a comprehensive suite of automated functions for computing a wide range of remote sensing indices directly from raster data. It supports efficient batch processing and covers commonly used indices related to vegetation, water, soil, snow, and burn severity, such as NDVI, NDWI, and NDBI. A detailed list of the implemented indices is provided in Table 13.

Table 13: List of detailed information of Index Toolkit.

Tool Name	**Category**	**Description Summary**
calculate_batch_ndvi	Index	Batch-calculate NDVI from multiple pairs of NIR/Red raster files and save results.
calculate_batch_ndwi	Index	Batch-calculate NDWI from multiple pairs of NIR/SWIR raster files and save results.
calculate_batch_ndbi	Index	Batch-calculate NDBI from multiple pairs of SWIR/NIR raster files and save results.

calculate_batch_evi	Index	Batch-calculate EVI from multiple sets of NIR/Red/Blue raster files and save results.
calculate_batch_nbr	Index	Batch-calculate NBR from multiple pairs of NIR/SWIR raster files and save results.
calculate_batch_fvc	Index	Batch-calculate FVC from multiple pairs of NIR/Red raster files and save results.
calculate_batch_wri	Index	Batch-calculate WRI from multiple sets of Green/Red/NIR/SWIR raster files and save results.
calculate_batch_ndti	Index	Batch-calculate NDTI from multiple pairs of Red/Green raster files and save results.
calculate_batch_frp	Index	Batch-calculate Fire Radiative Power (FRP) masks from multiple raster files and save results.
calculate_batch_ndsi	Index	Calculate NDSI for multiple pairs of Green and SWIR band images.
calc_extreme_snow_loss_percentage_from_binary_map	Index	Calculate the percentage of extreme snow and ice loss areas from a binary map.
compute_tvdi	Index	Compute TVDI (Temperature Vegetation Dryness Index) using NDVI and LST from local raster files.

The Inversion Toolkit integrates a collection of algorithms for retrieving key geophysical and environmental parameters from optical, thermal infrared, and microwave remote sensing data. It supports multiple retrieval methods for parameters such as land surface temperature (LST), land surface emissivity, and precipitable water vapor (PWV), including single-channel, multi-channel, and split-window approaches. By enabling flexible, efficient, and reproducible parameter estimation across multi-source Earth Observation data, the toolkit provides a versatile foundation for quantitative remote sensing applications. A detailed list of the implemented algorithms is provided in Table 14.

Table 14: List of detailed information of Inversion Toolkit.

Tool Name	**Category**	**Description Summary**
band_ratio	Inversion	Compute Precipitable Water Vapor (PWV) image from local MODIS surface reflectance band files using the band ratio method.
lst_single_channel	Inversion	Estimate Land Surface Temperature (LST) using the Single-Channel method, with NDVI-based emissivity estimation from RED and NIR bands.
lst_multi_channel	Inversion	Estimate Land Surface Temperature (LST) using the multi-channel algorithm.
split_window	Inversion	Estimate Land Surface Temperature (LST) or Precipitable Water Vapor (PWV) using the split-window algorithm.
temperature_emissivity_separation	Inversion	Estimate Land Surface Temperature (LST) using an enhanced Temperature Emissivity Separation (TES) algorithm with empirical emissivity estimation.

modis_day_night_lst	Inversion	Estimate land surface temperature (LST) from local MODIS Day and Night brightness temperatures using a single-channel correction method.
ttm_lst	Inversion	Estimate land surface temperature (LST) and emissivity using improved Three-Temperature Method (TTM) from three local thermal band GeoTIFF files. Uses all three bands to form a system of equations and solves per-pixel with physical constraints.
calculate_mean_lst_by_ndvi	Inversion	Calculate the average Land Surface Temperature (LST) across multiple images where NDVI is either above or below a given threshold.
calculate_max_lst_by_ndvi	Inversion	Calculate the maximum Land Surface Temperature (LST) in areas where NDVI is above or below a given threshold.
ATI	Inversion	Estimate Apparent Thermal Inertia (ATI) using the Thermal Inertia Method. This method calculates ATI as $(1 - albedo)/(day\_temp - night\_temp)$, which serves as a proxy for land surface temperature stability over diurnal cycles.
dual_polarization_differential	Inversion	Dual-Polarization Differential Method (DPDM) for microwave remote sensing parameter inversion. Supports soil moisture and vegetation index estimation with improved data handling and flexible parameters.
dual_frequency_diff	Inversion	Dual-frequency Differential Method (DDM) for parameter inversion using local raster data. Supports inversion of multiple parameters via empirical linear models: Soil Moisture (SM): param = alpha*(band1 - band2) + beta; Vegetation Index (VI): param = alpha*(band1 - band2) + beta; Leaf Area Index (LAI): param = alpha*(band1 - band2) + beta
multi_freq_bt	Inversion	Multi-frequency Brightness Temperature Method for parameter inversion using local raster data.
chang_single_param_inversion	Inversion	Chang algorithm for inversion of a single parameter using multi-frequency dual-polarized microwave brightness temperatures from local raster files.
nasa_team_sea_ice_concentration	Inversion	Estimate Sea Ice Concentration using NASA Team Algorithm from local passive microwave brightness temperature GeoTIFF files.
dual_polarization_ratio	Inversion	Estimate Vegetation Water Content (VWC) or Soil Moisture (SM) using Dual-Polarization Ratio Method (PRM) from local passive microwave brightness temperature GeoTIFF files. The polarization ratio is computed as: (V - H) / (V + H), where V and H are brightness temperatures of vertical and horizontal polarizations.

calculate_water_turbidity_ntu	Inversion	Calculate water turbidity in NTU (Nephelometric Turbidity Units) from red band raster file and save the result to a specified output path.

The Perception Toolkit provides a comprehensive set of remote sensing perception tools, covering a wide range of tasks such as scene classification, object detection, and change detection. In addition, it supports threshold-based segmentation and offers a series of post-processing utilities for bounding box and contour refinement. Overall, the toolkit enables diverse perception tasks on RGB remote sensing imagery, including scene recognition, semantic segmentation, and spatiotemporal change detection. A detailed list of the implemented tools is provided in Table 15.

Table 15: List of detailed information of Perception Toolkit.

Tool Name	**Category**	**Description Summary**
MSCN	Perception	MSCN is a scene and land-use image classifier, effective for categories such as Airport, BareLand, BaseballField, Beach, Bridge, Center, Church, Commercial, DenseResidential, Desert, Farmland, Forest, Industrial, Meadow, MediumResidential, Mountain, Park, Parking, Playground, Pond, Port, RailwayStation, Resort, River, School, SparseResidential, Square, Stadium, StorageTanks, and Viaduct.
RemoteCLIP	Perception	RemoteCLIP is a scene and land-use image classifier, specialized for categories such as Airport, Beach, Bridge, Commercial, Desert, Farmland, FootballField, Forest, Industrial, Meadow, Mountain, Park, Parking, Pond, Port, RailwayStation, Residential, River, and Viaduct.
Strip_R_CNN	Perception	Strip_R_CNN is a remote sensing object detection model with a strong focus on maritime and ship-related targets. Compared to SM3Det, it is particularly specialized in detecting and localizing different types of ships and naval vessels. This model is highly effective at detecting the following categories: L3 ship, L3 warcraft, L3 merchant ship, L3 aircraft carrier, Arleigh Burke, Container, Ticonderoga, Perry, Tarawa, WhidbeyIsland, CommanderA, Austen, Nimitz, Sanantonio, Container, Car carrierB, Enterprise, Car carrierA, Medical

SM3Det	Perception	SM3Det is a remote sensing object detection model. Given an input image and a natural language prompt specifying the target object (e.g., “plane”, “ship”, “storage tank”), it detects all instances of that object and returns their bounding boxes. This model is particularly strong at detecting and localizing the following categories:plane, ship, storage tank, baseball diamond, tennis court, basketball court, ground track field, harbor, bridge, large vehicle, small vehicle, helicopter, roundabout, soccer ball field, swimming pool.
RemoteSAM	Perception	RemoteSAM is a remote sensing visual grounding model. Given an input image and a text prompt describing a region of interest (e.g., “the football field located on the westernmost side”), it outputs the corresponding bounding box coordinates.
InstructSAM	Perception	InstructSAM is an instruction-guided counting model for remote sensing images. Given an input image and a natural language prompt specifying the target object (e.g., “storage tank”, “football field”), it detects and counts the number of instances matching the description.
SAM2	Perception	Use SAM2 to segment the input image and return the path of the segmented image.
ChangeOS	Perception	Use ChangeOS to detect the change between two images and return the change mask. Can also be used to segment building by providing same image path in pre_image_path and post_image_path.
threshold_segmentation	Perception	Perform threshold-based segmentation on a single-band raster image. The function reads a raster image from the specified path, converts it to a binary mask by applying a fixed threshold, and writes the resulting binary image to a new file. Pixel values greater than the threshold are set to 255 (white), and values less than or equal to the threshold are set to 0 (black).
bbox_expansion	Perception	Expands bounding boxes by a given radius and returns the expanded bounding boxes.
count_above_threshold	Perception	Count the number of pixels in an image whose values are greater than the specified threshold.
count_connected_components	Perception	Read a binary image and return the count of connected components.
bboxes2centroids	Perception	Convert bounding boxes from [x_min, y_min, x_max, y_max] format to centroid coordinates (x, y).
centroid_distance_extremes	Perception	Compute pairwise distances between centroids and return both the closest and farthest pairs with their indices and distances.
calculate_bbox_area	Perception	Calculate the total area of a list of bounding boxes in [x, y, w, h] format.

The Analysis Toolkit provides a suite of statistical and spatiotemporal analysis methods tailored for remote sensing and geoscience data. Its functionalities include classical time-series trend detection and decomposition techniques such as linear regression, the Mann–Kendall test, Sen's slope estimation, and STL decomposition. It also supports change-point detection and seasonal analysis based on autocorrelation. In addition, the toolkit integrates spatial statistical approaches, including hotspot direction analysis, as well as methods for spike detection in numerical sequences. A detailed list of the implemented tools is provided in Table 16.

Table 16: List of detailed information of Analysis Toolkit.

Tool Name	**Category**	**Description Summary**
compute_linear_trend	Analysis	Computes the linear trend (slope and intercept) of a time series by fitting a line of the form: $y = a \cdot x + b$ using the least squares method.
mann_kendall_test	Analysis	Perform the non-parametric Mann-Kendall trend test on a univariate time series. The test evaluates whether there is a monotonic upward or downward trend without requiring the data to conform to any particular distribution.
sens_slope	Analysis	Compute Sen's Slope estimator for a univariate time series. Sen's Slope is a robust non-parametric method for estimating the median rate of change over time, often used with the Mann-Kendall test to assess both trend and magnitude.
stl_decompose	Analysis	Apply Seasonal-Trend decomposition using LOESS (STL) to a univariate time series. Decomposes the series into trend, seasonal, and residual components.
detect_change_points	Analysis	Detect structural change points in a univariate time series using the ruptures library with the PELT algorithm. A change point marks a location where the statistical properties of the signal shift (e.g., mean or variance).
autocorrelation_function	Analysis	Compute the Autocorrelation Function (ACF) for a univariate time series. The ACF measures the correlation of the series with its own lags, which is useful for detecting seasonality, persistence, and lag dependence.
detect_seasonality_acf	Analysis	Detect the dominant seasonality (period) in a univariate time series using the Autocorrelation Function (ACF). The method searches for significant peaks in the ACF beyond lag=1 to identify repeating cycles.
getis_ord_gi_star	Analysis	Compute the Getis-Ord Gi* statistic for local spatial autocorrelation on a raster image. This method identifies statistically significant spatial clusters of high (hot spots) or low (cold spots) values using a user-specified spatial weight kernel.

analyze_hotspot_direction	Analysis	Analyze the main directional concentration of hotspots in a binary hotspot map. The function counts the number of hotspot pixels (value=1) in each cardinal direction relative to the map center, and returns the dominant direction.
count_spikes_from_values	Analysis	Count the number of upward spikes in a sequence of numerical values. A spike is defined as a positive difference between consecutive valid values greater than the given threshold.

The Statistics Toolkit offers a comprehensive set of functions for descriptive statistics, image-based statistical analysis, and geospatial data processing. Its capabilities cover the calculation of classical statistical measures such as mean, variance, and skewness, as well as the extraction of statistical information from imagery and intersection-based threshold analysis. In addition, the toolkit provides fundamental arithmetic operations, temperature unit conversions, and image differencing functions. It also supports essential preprocessing tasks, including radiometric correction and cloud masking. Overall, the toolkit enables flexible and efficient extraction and analysis of statistical features from geoscience and remote sensing data. A detailed list of the implemented tools is provided in Table 17.

Table 17: List of detailed information of Statistics Toolkit.

Tool Name	**Category**	**Description Summary**
coefficient_of_variation	Statistics	Compute the Coefficient of Variation (CV) for a dataset. The CV is defined as the ratio of the standard deviation to the mean and is commonly used as a normalized measure of dispersion.
skewness	Statistics	Compute the skewness of a dataset, which measures the asymmetry of the probability distribution.
kurtosis	Statistics	Compute the kurtosis of a dataset, which measures the ẗailednessöf the distribution.
calc_batch_image_mean	Statistics	Compute mean value of an batch of images.
calc_batch_image_std	Statistics	Compute the standard deviation (spread of pixel values) for a batch of images.
calc_batch_image_median	Statistics	Compute the median pixel value for a batch of images.
calc_batch_image_min	Statistics	Compute the minimum pixel value for a batch of images.
calc_batch_image_max	Statistics	Compute the maximum pixel value for a batch of images.
calc_batch_image_skewness	Statistics	Compute the skewness of pixel value distributions for a batch of images. Skewness quantifies the asymmetry of the distribution:1. Positive skew → longer right tail; 2. Negative skew → longer left tail; 3. Zero skew → symmetric distribution.
calc_batch_image_kurtosis	Statistics	Compute the kurtosis of pixel value distributions for a batch of images. Kurtosis measures the ẗailednessöf the distribution relative to a normal distribution.

calc_batch_image_sum	Statistics	Compute the sum of pixel values for a batch of images.
calc_batch_image_hotspot _percentage	Statistics	Compute the hotspot percentage (fraction of pixels above a threshold) for a batch of images.
calc_batch_image_hotspot_tif	Statistics	Create binary hotspot maps for a batch of images, where pixels below a specified threshold are set to 1 (hotspot) and others set to 0. The output is saved as GeoTIFF files, preserving georeference metadata from the input images.
difference	Statistics	Compute the absolute difference between two numbers.
division	Statistics	Perform division between two numbers.
percentage_change	Statistics	Calculate the percentage change between two numbers, useful for comparing relative growth or decline.
kelvin_to_celsius	Statistics	Convert temperature from Kelvin to Celsius.
celsius_to_kelvin	Statistics	Convert temperature from Celsius to Kelvin.
max_value_and_index	Statistics	Find the maximum value in a list and return both the maximum value and its index.
min_value_and_index	Statistics	Find the minimum value in a list and return both the minimum value and its index.
ceil_number	Statistics	Return the ceiling (rounded up integer) of a given number.
multiply	Statistics	Multiply two numbers and return their product.
get_list_object_via_indexes	Statistics	Retrieve elements from a list using a list or tuple of indices.
mean	Statistics	Compute the arithmetic mean (average) of a dataset.
calculate_threshold_ratio	Statistics	Calculate the average percentage of pixels above a given threshold for one or more images and a specified band.
calc_batch_fire_pixels	Statistics	Compute the number of fire pixels (FRP ¿ threshold) for a batch of images.
create_fire_increase_map	Statistics	Create a binary map highlighting areas where fire increase exceeds a specified threshold.
identify_fire_prone_areas	Statistics	Identify fire-prone areas from a hotspot map based on a given percentile threshold.
get_percentile_value_from_image	Statistics	Calculate the N-th percentile value of pixel values in a raster image, and return it as a native Python type matching the image's data type.
image_division_mean	Statistics	Calculate the mean of pixel-wise division between two images or between two bands of the same image.
calculate_intersection_percentage	Statistics	Calculate the percentage of pixels that simultaneously satisfy threshold conditions in two raster images.

calc_batch_image_mean_mean	Statistics	Compute the average of mean pixel values across a batch of images.
calc_batch_image_mean_max	Statistics	Compute the mean pixel values of a batch of images and return the maximum mean.
calc_batch_image_mean_max_min	Statistics	Compute the batch-wise statistics across multiple images, including: Mean of mean values, Maximum of maximum values, Minimum of minimum values.
calc_batch_image_mean_threshold	Statistics	Calculate the percentage or count of images whose mean pixel values (in a specified band) are above or below a given threshold.
calculate_multi_band_threshold _ratio	Statistics	Calculate the percentage of pixels that simultaneously satisfy multiple band threshold conditions.
count_pixels_satisfying_conditions	Statistics	Count the number of pixels that simultaneously satisfy multiple band threshold conditions.
count_images_exceeding_threshold _ratio	Statistics	Count how many images have a percentage of pixels above or below a threshold that exceeds a specified ratio.
average_ratio_exceeding_threshold	Statistics	Calculate the average percentage of pixels exceeding a value threshold, considering only images where the ratio is greater than a specified ratio threshold.
count_images_exceeding_mean _multiplier	Statistics	Count how many images have a mean pixel value above or below a multiple of the overall mean pixel value across all images.
calculate_band_mean_by_condition	Statistics	Calculate the mean value of a target band over pixels where a condition band satisfies a threshold.
calc_threshold_value_mean	Statistics	Calculate the mean value of corresponding raster pixels in path2 where the raster values in path1 exceed the given threshold.
calculate_tif_difference	Statistics	Calculate difference between two tif files (image_b - image_a) and save result.
subtract	Statistics	Subtract two images and save result.
calculate_area	Statistics	This function calculates the area of non-zero pixels in the input image and returns the result.
grayscale_to_colormap	Statistics	Apply a colormap to a grayscale image and save as a color image.
get_filelist	Statistics	Returns a list of files in the specified directory.
radiometric_correction_sr	Statistics	Apply Landsat 8 surface reflectance (SR_B*) radiometric correction.
apply_cloud_mask	Statistics	Apply cloud / shadow mask to a single Landsat 8 surface reflectance band using QA_PIXEL band.

G.1 TOOL PROMPT

To better illustrate the functionality of the toolkits, we provide a representative example. Specifically, we focus on the `lst_multi_channel` tool, which estimates LST using a multi-channel algorithm. This method leverages multiple thermal infrared bands from remote sensing imagery and applies empirical formulas to derive accurate LST values. The corresponding implementation is provided below:

Tool Example

```python
@mcp.tool(description='''
Estimate Land Surface Temperature (LST) using the multi-channel algorithm.
Requires local input files:
- Two thermal infrared bands (e.g., Band 31 and Band 32) as GeoTIFF files.

Parameters:
    band31_path (str): Path to local GeoTIFF file for thermal band 31 (~11 \mu m}).
    band32_path (str): Path to local GeoTIFF file for thermal band 32 (~12 \mu m).
    output_path (str): Relative path for the output raster file, e.g. "question17/lst_2022-01-16.tif"

Returns:
    str: Local file path of the exported LST image.
''')
def lst_multi_channel(band31_path: str, band32_path: str, output_path: str) -> str:
    """
    Description:
        Estimate Land Surface Temperature (LST) using the multi-channel algorithm.
        This method combines two thermal infrared bands to reduce atmospheric effects.

    Parameters:
        band31_path (str): Path to GeoTIFF file for thermal band 31 (~11 \mu m)
        band32_path (str): Path to GeoTIFF file for thermal band 32 (~12 \mu m)
        output_path (str): Relative path for the output LST GeoTIFF

    Returns:
        str: Full path to the saved LST GeoTIFF
    """
    import os, rasterio
    import numpy as np

    with rasterio.open(band31_path) as src31:
        band31 = src31.read(1).astype(np.float32)
        profile = src31.profile

    with rasterio.open(band32_path) as src32:
        band32 = src32.read(1).astype(np.float32)

    a = 1.022
    b = 0.47
    c = 0.43

    lst = a * band31 + b * (band31 - band32) + c

    profile.update(dtype=rasterio.float32, count=1, compress='lzw')

    os.makedirs((TEMP_DIR / output_path).parent, exist_ok=True)

    with rasterio.open(TEMP_DIR / output_path, 'w', **profile) as dst:
        dst.write(lst.astype(np.float32), 1)

    return f'Result saved at {TEMP_DIR / output_path}'
```

H EARTH-AGENT WITH DIFFERENT LLM BACKBONES

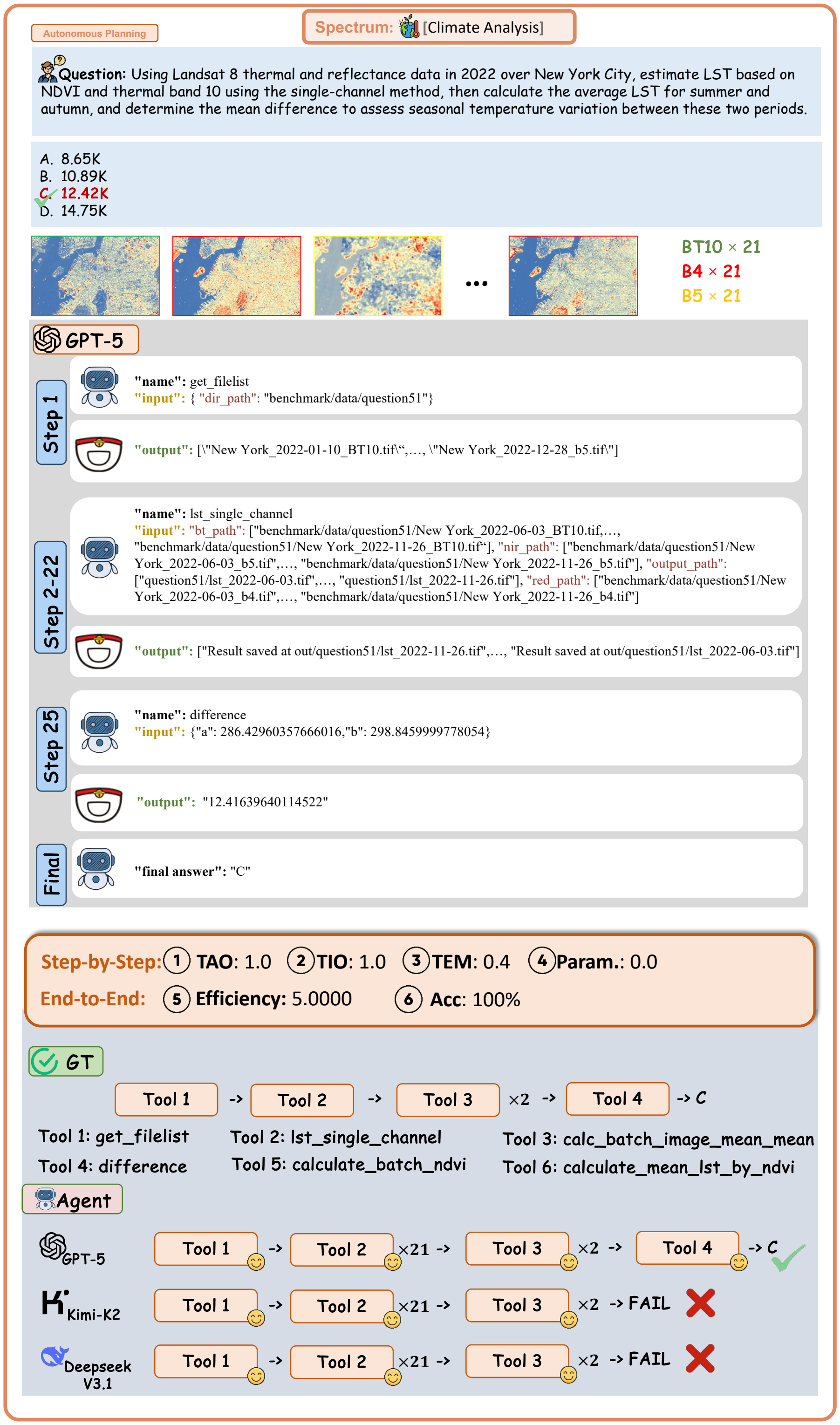

Question: Using Landsat 8 thermal and reflectance data in 2022 over New York City, estimate LST based on NDVI and thermal band 10 using the single-channel method, then calculate the average LST for summer and autumn, and determine the mean difference to assess seasonal temperature variation between these two periods.

A. 8.65K
B. 10.89K
C. 12.42K ✓
D. 14.75K

```
"name": get_filelist
"input": { "dir_path": "benchmark/data/question51"}
"output": [\"New York_2022-01-10_BT10.tif\“,…, \"New York_2022-12-28_b5.tif\"]
```

```
"name": lst_single_channel
"input": "bt_path": ["benchmark/data/question51/New York_2022-06-03_BT10.tif,…, "benchmark/data/question51/New York_2022-11-26_BT10.tif“], "nir_path": ["benchmark/data/question51/New York_2022-06-03_b5.tif",…, "benchmark/data/question51/New York_2022-11-26_b5.tif"], "output_path": ["question51/lst_2022-06-03.tif",…, "question51/lst_2022-11-26.tif"], "red_path": ["benchmark/data/question51/New York_2022-06-03_b4.tif",…, "benchmark/data/question51/New York_2022-11-26_b4.tif"]
"output": ["Result saved at out/question51/lst_2022-11-26.tif",…, "Result saved at out/question51/lst_2022-06-03.tif"]
```

```
"name": difference
"input": {"a": 286.42960357666016,"b": 298.8459999778054}
"output": "12.41639640114522"
```

```
"final answer": "C"
```

Step-by-Step: ① **TAO**: 1.0 ② **TIO**: 1.0 ③ **TEM**: 0.4 ④ **Param.**: 0.0
End-to-End: ⑤ **Efficiency:** 5.0000 ⑥ **Acc**: 100%

GT

Tool 1 -> Tool 2 -> Tool 3 ×2 -> Tool 4 -> C

Tool 1: get_filelist
Tool 2: lst_single_channel
Tool 3: calc_batch_image_mean_mean
Tool 4: difference
Tool 5: calculate_batch_ndvi
Tool 6: calculate_mean_lst_by_ndvi

Agent

GPT-5: Tool 1 -> Tool 2 ×21 -> Tool 3 ×2 -> Tool 4 -> C ✓
Kimi-K2: Tool 1 -> Tool 2 ×21 -> Tool 3 ×2 -> FAIL ✗
Deepseek V3.1: Tool 1 -> Tool 2 ×21 -> Tool 3 ×2 -> FAIL ✗

Figure 11: **Example of Climate Analysis with Spectrum Data under the Auto-Planning Regime.**

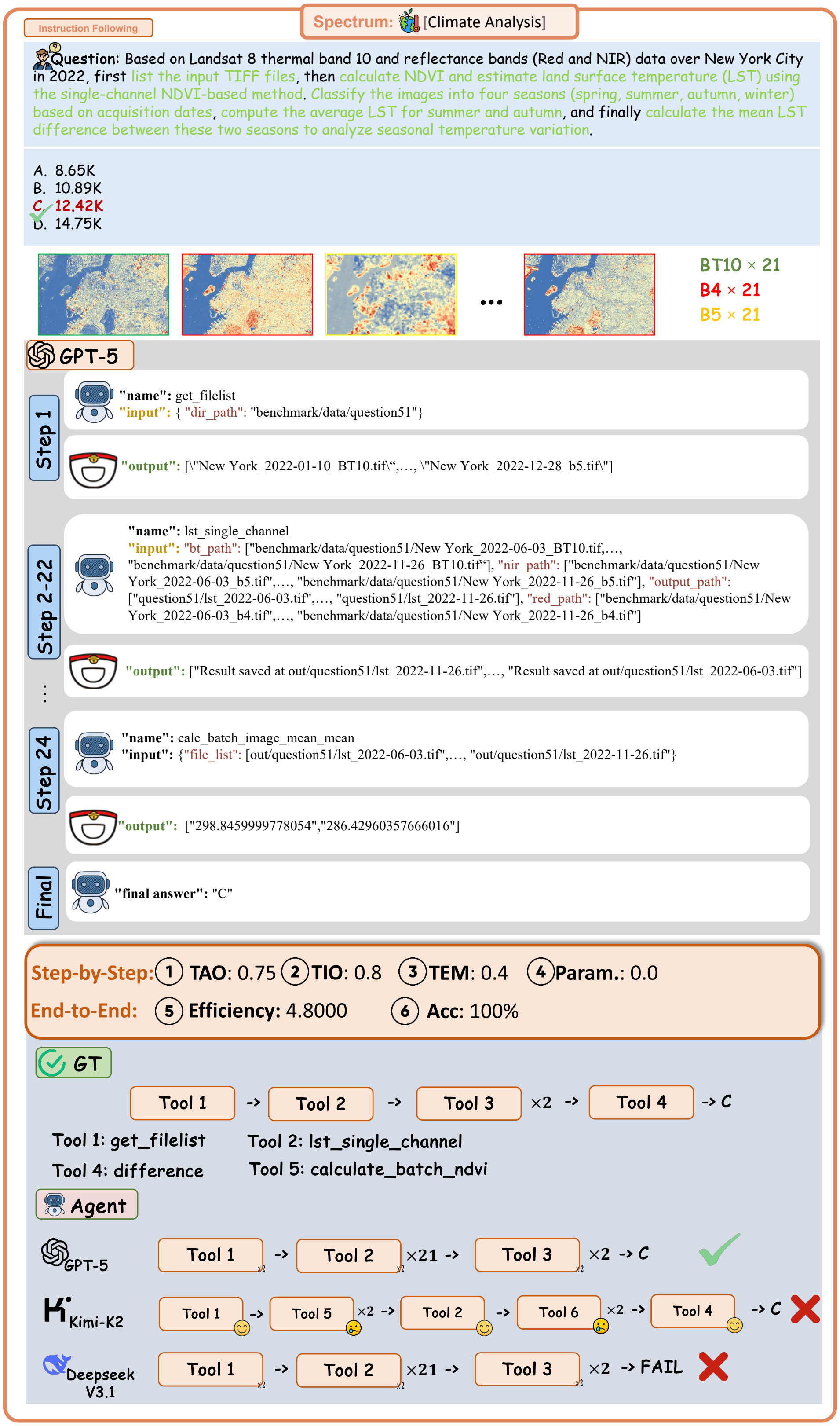

Question: Based on Landsat 8 thermal band 10 and reflectance bands (Red and NIR) data over New York City in 2022, first list the input TIFF files, then calculate NDVI and estimate land surface temperature (LST) using the single-channel NDVI-based method. Classify the images into four seasons (spring, summer, autumn, winter) based on acquisition dates, compute the average LST for summer and autumn, and finally calculate the mean LST difference between these two seasons to analyze seasonal temperature variation.

A. 8.65K
B. 10.89K
C. 12.42K ✓
D. 14.75K

Step 1

```
"name": get_filelist
"input": { "dir_path": "benchmark/data/question51"}
"output": [\"New York_2022-01-10_BT10.tif\“,…, \"New York_2022-12-28_b5.tif\"]
```

Step 2-22

```
"name": lst_single_channel
"input": "bt_path": ["benchmark/data/question51/New York_2022-06-03_BT10.tif,…, "benchmark/data/question51/New York_2022-11-26_BT10.tif“], "nir_path": ["benchmark/data/question51/New York_2022-06-03_b5.tif",…, "benchmark/data/question51/New York_2022-11-26_b5.tif"], "output_path": ["question51/lst_2022-06-03.tif",…, "question51/lst_2022-11-26.tif"], "red_path": ["benchmark/data/question51/New York_2022-06-03_b4.tif",…, "benchmark/data/question51/New York_2022-11-26_b4.tif"]
"output": ["Result saved at out/question51/lst_2022-11-26.tif",…, "Result saved at out/question51/lst_2022-06-03.tif"]
```

⋮

Step 24

```
"name": calc_batch_image_mean_mean
"input": {"file_list": [out/question51/lst_2022-06-03.tif",…, "out/question51/lst_2022-11-26.tif"}
"output":  ["298.8459999778054","286.42960357666016"]
```

Final

```
"final answer": "C"
```

Step-by-Step: ① **TAO**: 0.75 ② **TIO**: 0.8 ③ **TEM**: 0.4 ④ **Param.**: 0.0

End-to-End: ⑤ **Efficiency**: 4.8000 ⑥ **Acc**: 100%

GT
Tool 1 -> Tool 2 -> Tool 3 ×2 -> Tool 4 -> C
Tool 1: get_filelist
Tool 2: lst_single_channel
Tool 4: difference
Tool 5: calculate_batch_ndvi
Agent
GPT-5
Tool 1 -> Tool 2 ×21 -> Tool 3 ×2 -> C ✓
Kimi-K2
Tool 1 -> Tool 5 ×2 -> Tool 2 -> Tool 6 ×2 -> Tool 4 -> C ✗
Deepseek V3.1
Tool 1 -> Tool 2 ×21 -> Tool 3 ×2 -> FAIL ✗

Figure 12: **Example of Climate Analysis with Spectrum Data under the Instruction-Following Regime.**

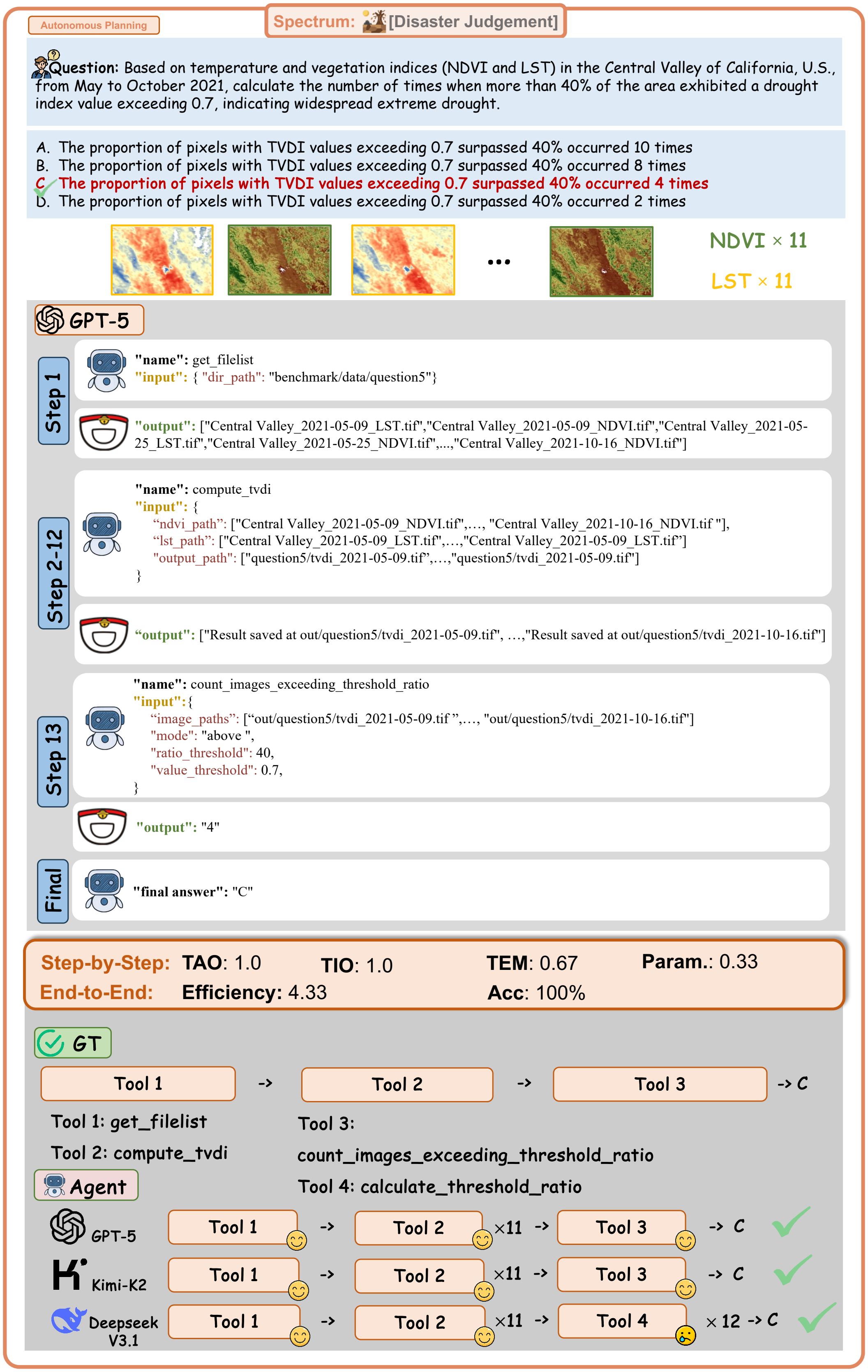

Question: Based on temperature and vegetation indices (NDVI and LST) in the Central Valley of California, U.S., from May to October 2021, calculate the number of times when more than 40% of the area exhibited a drought index value exceeding 0.7, indicating widespread extreme drought.

A. The proportion of pixels with TVDI values exceeding 0.7 surpassed 40% occurred 10 times
B. The proportion of pixels with TVDI values exceeding 0.7 surpassed 40% occurred 8 times
C. The proportion of pixels with TVDI values exceeding 0.7 surpassed 40% occurred 4 times ✓
D. The proportion of pixels with TVDI values exceeding 0.7 surpassed 40% occurred 2 times

```
"name": get_filelist
"input": { "dir_path": "benchmark/data/question5"}
```

```
"output": ["Central Valley_2021-05-09_LST.tif","Central Valley_2021-05-09_NDVI.tif","Central Valley_2021-05-25_LST.tif","Central Valley_2021-05-25_NDVI.tif",...,"Central Valley_2021-10-16_NDVI.tif"]
```

```
"name": compute_tvdi
"input": {
    "ndvi_path": ["Central Valley_2021-05-09_NDVI.tif",…, "Central Valley_2021-10-16_NDVI.tif "],
    "lst_path": ["Central Valley_2021-05-09_LST.tif",…,"Central Valley_2021-05-09_LST.tif"]
    "output_path": ["question5/tvdi_2021-05-09.tif",…,"question5/tvdi_2021-05-09.tif"]
}
```

```
"output": ["Result saved at out/question5/tvdi_2021-05-09.tif", …,"Result saved at out/question5/tvdi_2021-10-16.tif"]
```

```
"name": count_images_exceeding_threshold_ratio
"input":{
    "image_paths": ["out/question5/tvdi_2021-05-09.tif ",…, "out/question5/tvdi_2021-10-16.tif"]
    "mode": "above ",
    "ratio_threshold": 40,
    "value_threshold": 0.7,
}
```

```
"output": "4"
```

```
"final answer": "C"
```

Step-by-Step: **TAO**: 1.0 **TIO**: 1.0 **TEM**: 0.67 **Param.**: 0.33
End-to-End: **Efficiency:** 4.33 **Acc**: 100%

GT
Tool 1 -> Tool 2 -> Tool 3 -> C
Tool 1: get_filelist
Tool 2: compute_tvdi
Tool 3: count_images_exceeding_threshold_ratio
Tool 4: calculate_threshold_ratio
Agent
GPT-5 Tool 1 -> Tool 2 ×11 -> Tool 3 -> C ✓
Kimi-K2 Tool 1 -> Tool 2 ×11 -> Tool 3 -> C ✓
Deepseek V3.1 Tool 1 -> Tool 2 ×11 -> Tool 4 × 12 -> C ✓

Figure 13: **Example of Disaster Judgement with Spectrum Data under the Auto-Planning Regime.**

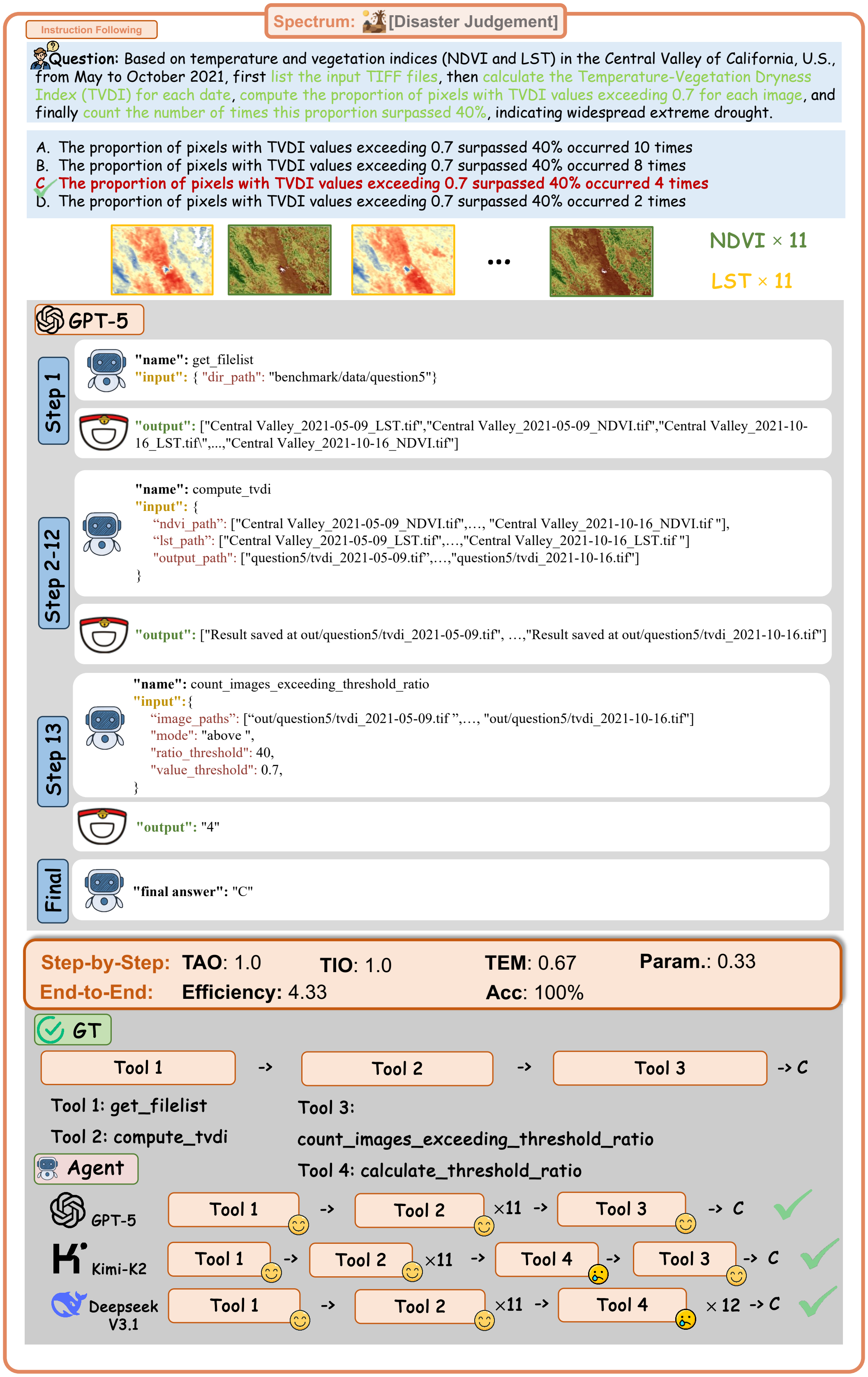

Question: Based on temperature and vegetation indices (NDVI and LST) in the Central Valley of California, U.S., from May to October 2021, first list the input TIFF files, then calculate the Temperature-Vegetation Dryness Index (TVDI) for each date, compute the proportion of pixels with TVDI values exceeding 0.7 for each image, and finally count the number of times this proportion surpassed 40%, indicating widespread extreme drought.

A. The proportion of pixels with TVDI values exceeding 0.7 surpassed 40% occurred 10 times
B. The proportion of pixels with TVDI values exceeding 0.7 surpassed 40% occurred 8 times
✓ C. The proportion of pixels with TVDI values exceeding 0.7 surpassed 40% occurred 4 times
D. The proportion of pixels with TVDI values exceeding 0.7 surpassed 40% occurred 2 times

Step 1

```
"name": get_filelist
"input": { "dir_path": "benchmark/data/question5"}
```

```
"output": ["Central Valley_2021-05-09_LST.tif","Central Valley_2021-05-09_NDVI.tif","Central Valley_2021-10-16_LST.tif\",...,"Central Valley_2021-10-16_NDVI.tif"]
```

Step 2-12

```
"name": compute_tvdi
"input": {
    "ndvi_path": ["Central Valley_2021-05-09_NDVI.tif",…, "Central Valley_2021-10-16_NDVI.tif "],
    "lst_path": ["Central Valley_2021-05-09_LST.tif",…,"Central Valley_2021-10-16_LST.tif "]
    "output_path": ["question5/tvdi_2021-05-09.tif",…,"question5/tvdi_2021-10-16.tif"]
}
```

```
"output": ["Result saved at out/question5/tvdi_2021-05-09.tif", …,"Result saved at out/question5/tvdi_2021-10-16.tif"]
```

Step 13

```
"name": count_images_exceeding_threshold_ratio
"input":{
    "image_paths": ["out/question5/tvdi_2021-05-09.tif ",…, "out/question5/tvdi_2021-10-16.tif"]
    "mode": "above ",
    "ratio_threshold": 40,
    "value_threshold": 0.7,
}
```

```
"output": "4"
```

Final

```
"final answer": "C"
```

Step-by-Step: **TAO**: 1.0 **TIO**: 1.0 **TEM**: 0.67 **Param.**: 0.33
End-to-End: **Efficiency:** 4.33 **Acc**: 100%

GT

Tool 1 -> Tool 2 -> Tool 3 -> C

Tool 1: get_filelist
Tool 2: compute_tvdi
Tool 3: count_images_exceeding_threshold_ratio
Tool 4: calculate_threshold_ratio

Agent

GPT-5: Tool 1 🙂 -> Tool 2 🙂 ×11 -> Tool 3 🙂 -> C ✓
Kimi-K2: Tool 1 🙂 -> Tool 2 🙂 ×11 -> Tool 4 😢 -> Tool 3 🙂 -> C ✓
Deepseek V3.1: Tool 1 🙂 -> Tool 2 🙂 ×11 -> Tool 4 😢 × 12 -> C ✓

Figure 14: **Example of Disaster Judgement with Spectrum Data under the Instruction-Following Regime.**

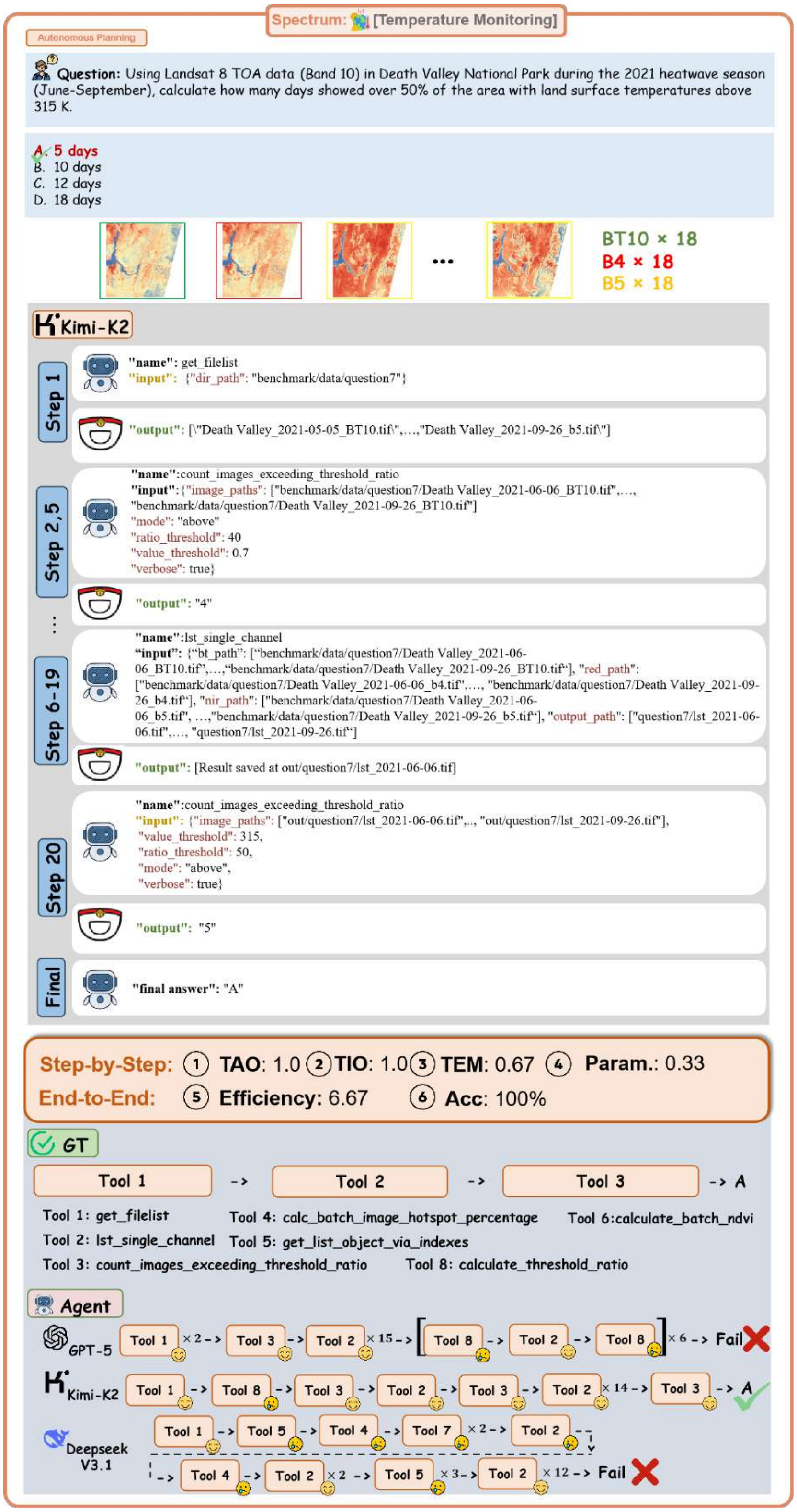

Question: Using Landsat 8 TOA data (Band 10) in Death Valley National Park during the 2021 heatwave season (June-September), calculate how many days showed over 50% of the area with land surface temperatures above 315 K.

A. 5 days
B. 10 days
C. 12 days
D. 18 days

Step 1

```
"name": get_filelist
"input":  {"dir_path": "benchmark/data/question7"}
"output": [\"Death Valley_2021-05-05_BT10.tif\",…,"Death Valley_2021-09-26_b5.tif\"]
```

Step 2,5

```
"name":count_images_exceeding_threshold_ratio
"input":{"image_paths": ["benchmark/data/question7/Death Valley_2021-06-06_BT10.tif",…,
"benchmark/data/question7/Death Valley_2021-09-26_BT10.tif"]
"mode": "above"
"ratio_threshold": 40
"value_threshold": 0.7
"verbose": true}
"output": "4"
```

Step 6-19

```
"name":lst_single_channel
"input": {"bt_path": ["benchmark/data/question7/Death Valley_2021-06-06_BT10.tif",…,"benchmark/data/question7/Death Valley_2021-09-26_BT10.tif"], "red_path": ["benchmark/data/question7/Death Valley_2021-06-06_b4.tif",…, "benchmark/data/question7/Death Valley_2021-09-26_b4.tif"], "nir_path": ["benchmark/data/question7/Death Valley_2021-06-06_b5.tif", …,"benchmark/data/question7/Death Valley_2021-09-26_b5.tif"], "output_path": ["question7/lst_2021-06-06.tif",…, "question7/lst_2021-09-26.tif"]
"output": [Result saved at out/question7/lst_2021-06-06.tif]
```

Step 20

```
"name":count_images_exceeding_threshold_ratio
"input": {"image_paths": ["out/question7/lst_2021-06-06.tif",.., "out/question7/lst_2021-09-26.tif"],
 "value_threshold": 315,
 "ratio_threshold": 50,
 "mode": "above",
 "verbose": true}
"output":  "5"
```

Final

```
"final answer": "A"
```

Step-by-Step: ① **TAO**: 1.0 ② **TIO**: 1.0 ③ **TEM**: 0.67 ④ **Param.**: 0.33

End-to-End: ⑤ **Efficiency:** 6.67 ⑥ **Acc**: 100%

GT: Tool 1 -> Tool 2 -> Tool 3 -> A

Tool 1: get_filelist
Tool 2: lst_single_channel
Tool 3: count_images_exceeding_threshold_ratio
Tool 4: calc_batch_image_hotspot_percentage
Tool 5: get_list_object_via_indexes
Tool 6:calculate_batch_ndvi
Tool 8: calculate_threshold_ratio

Agent:

GPT-5: Tool 1 × 2 -> Tool 3 -> Tool 2 × 15 -> [Tool 8 -> Tool 2 -> Tool 8] × 6 -> Fail ✗

Kimi-K2: Tool 1 -> Tool 8 -> Tool 3 -> Tool 2 -> Tool 3 -> Tool 2 × 14 -> Tool 3 -> A ✓

Deepseek V3.1: Tool 1 -> Tool 5 -> Tool 4 -> Tool 7 × 2 -> Tool 2 -> Tool 4 -> Tool 2 × 2 -> Tool 5 × 3 -> Tool 2 × 12 -> Fail ✗

Figure 15: Example of Temperature Monitoring with Spectrum Data under the Auto-Planning Regime.

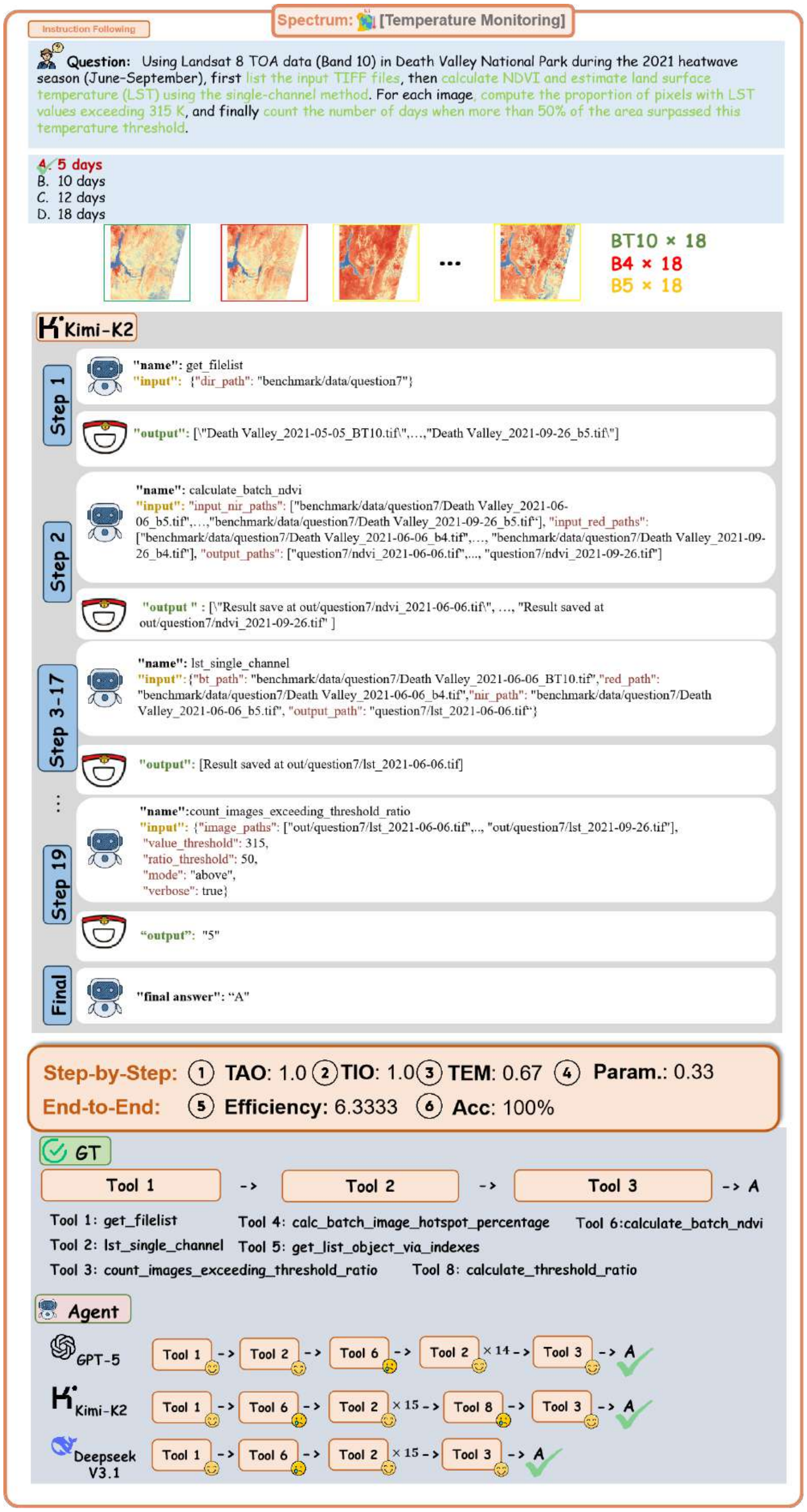
Instruction Following
Spectrum: [Temperature Monitoring]
BT10 × 18
B4 × 18
B5 × 18
Kimi-K2
Step 1
Step 2
Step 3-17
Step 19
Final
GT
Tool 1 -> Tool 2 -> Tool 3 -> A
Agent
GPT-5
Tool 1 -> Tool 2 -> Tool 6 -> Tool 2 × 14 -> Tool 3 -> A ✓
Kimi-K2
Tool 1 -> Tool 6 -> Tool 2 × 15 -> Tool 8 -> Tool 3 -> A ✓
Deepseek V3.1
Tool 1 -> Tool 6 -> Tool 2 × 15 -> Tool 3 -> A ✓

Question: Using Landsat 8 TOA data (Band 10) in Death Valley National Park during the 2021 heatwave season (June-September), first list the input TIFF files, then calculate NDVI and estimate land surface temperature (LST) using the single-channel method. For each image, compute the proportion of pixels with LST values exceeding 315 K, and finally count the number of days when more than 50% of the area surpassed this temperature threshold.

A. 5 days ✓
B. 10 days
C. 12 days
D. 18 days

Step 1

```
"name": get_filelist
"input":  {"dir_path": "benchmark/data/question7"}
```

```
"output": [\"Death Valley_2021-05-05_BT10.tif\",…,"Death Valley_2021-09-26_b5.tif\"]
```

Step 2

```
"name": calculate_batch_ndvi
"input": "input_nir_paths": ["benchmark/data/question7/Death Valley_2021-06-06_b5.tif",…,"benchmark/data/question7/Death Valley_2021-09-26_b5.tif"], "input_red_paths": ["benchmark/data/question7/Death Valley_2021-06-06_b4.tif",…, "benchmark/data/question7/Death Valley_2021-09-26_b4.tif"], "output_paths": ["question7/ndvi_2021-06-06.tif",..., "question7/ndvi_2021-09-26.tif"]
```

```
"output " : [\"Result save at out/question7/ndvi_2021-06-06.tif\", …, "Result saved at out/question7/ndvi_2021-09-26.tif" ]
```

Step 3-17

```
"name": lst_single_channel
"input":{"bt_path": "benchmark/data/question7/Death Valley_2021-06-06_BT10.tif","red_path": "benchmark/data/question7/Death Valley_2021-06-06_b4.tif","nir_path": "benchmark/data/question7/Death Valley_2021-06-06_b5.tif", "output_path": "question7/lst_2021-06-06.tif"}
```

```
"output": [Result saved at out/question7/lst_2021-06-06.tif]
```

⋮

Step 19

```
"name":count_images_exceeding_threshold_ratio
"input": {"image_paths": ["out/question7/lst_2021-06-06.tif",.., "out/question7/lst_2021-09-26.tif"],
 "value_threshold": 315,
 "ratio_threshold": 50,
 "mode": "above",
 "verbose": true}
```

```
"output":  "5"
```

Final

```
"final answer": "A"
```

Step-by-Step: ① **TAO**: 1.0 ② **TIO**: 1.0 ③ **TEM**: 0.67 ④ **Param.**: 0.33

End-to-End: ⑤ **Efficiency**: 6.3333 ⑥ **Acc**: 100%

Tool 1: get_filelist
Tool 2: lst_single_channel
Tool 3: count_images_exceeding_threshold_ratio
Tool 4: calc_batch_image_hotspot_percentage
Tool 5: get_list_object_via_indexes
Tool 6:calculate_batch_ndvi
Tool 8: calculate_threshold_ratio

Figure 16: **Example of Temperature Monitoring with Spectrum Data under the Instruction-Following Regime.**

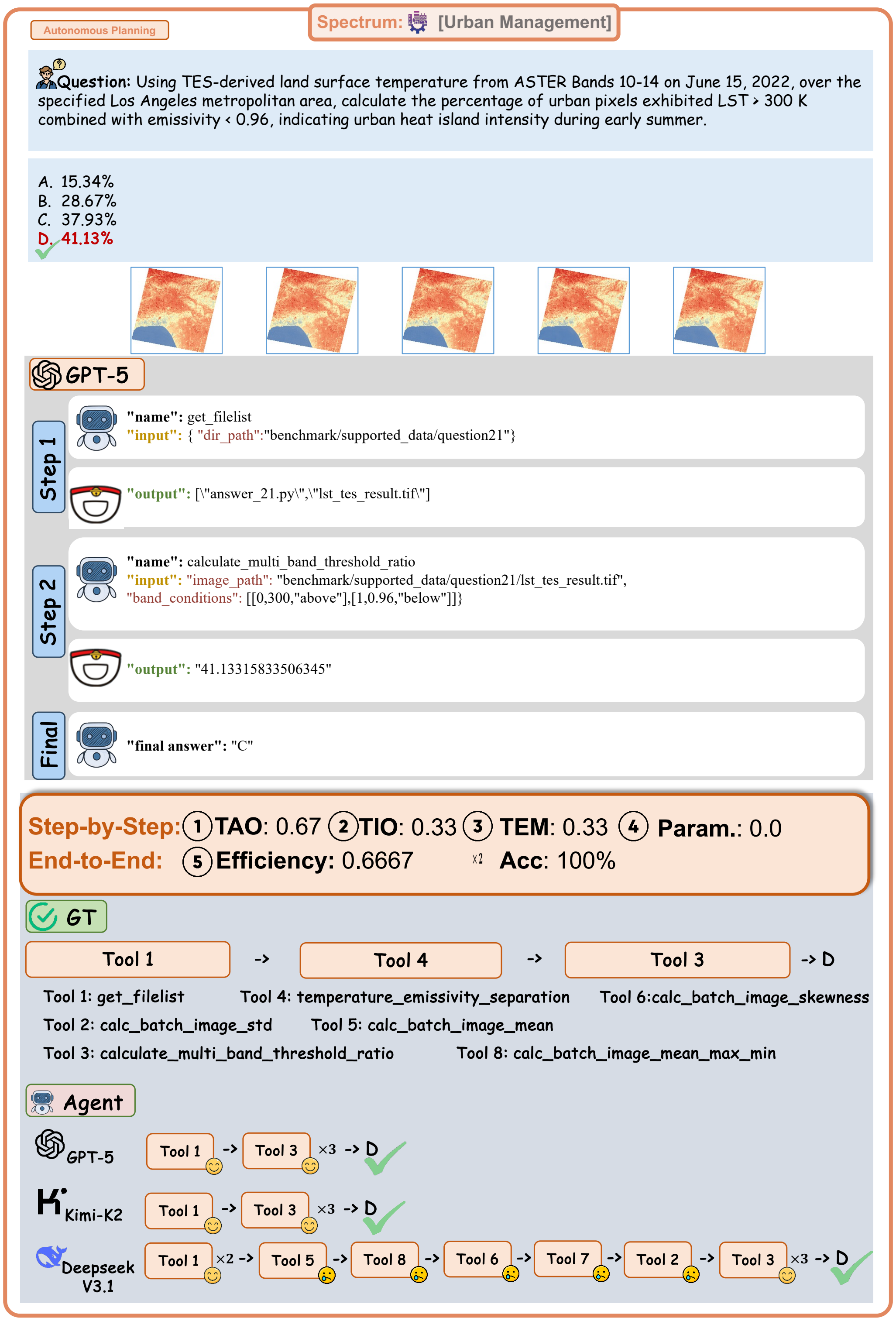
Autonomous Planning
Spectrum: [Urban Management]
GPT-5
Step 1
Step 2
Final
GT
Tool 1 -> Tool 4 -> Tool 3 -> D
Agent
GPT-5
Tool 1 -> Tool 3 ×3 -> D
Kimi-K2
Tool 1 -> Tool 3 ×3 -> D
Deepseek V3.1
Tool 1 ×2 -> Tool 5 -> Tool 8 -> Tool 6 -> Tool 7 -> Tool 2 -> Tool 3 ×3 -> D

Question: Using TES-derived land surface temperature from ASTER Bands 10-14 on June 15, 2022, over the specified Los Angeles metropolitan area, calculate the percentage of urban pixels exhibited LST > 300 K combined with emissivity < 0.96, indicating urban heat island intensity during early summer.

A. 15.34%
B. 28.67%
C. 37.93%
D. 41.13% ✓

```
"name": get_filelist
"input": { "dir_path":"benchmark/supported_data/question21"}
"output": [\"answer_21.py\",\"lst_tes_result.tif\"]
```

```
"name": calculate_multi_band_threshold_ratio
"input": "image_path": "benchmark/supported_data/question21/lst_tes_result.tif",
"band_conditions": [[0,300,"above"],[1,0.96,"below"]]}
"output": "41.13315833506345"
```

```
"final answer": "C"
```

Step-by-Step: ① **TAO**: 0.67 ② **TIO**: 0.33 ③ **TEM**: 0.33 ④ **Param.**: 0.0
End-to-End: ⑤ **Efficiency:** 0.6667 ×2 **Acc**: 100%

Tool 1: get_filelist
Tool 4: temperature_emissivity_separation
Tool 6:calc_batch_image_skewness
Tool 2: calc_batch_image_std
Tool 5: calc_batch_image_mean
Tool 3: calculate_multi_band_threshold_ratio
Tool 8: calc_batch_image_mean_max_min

Figure 17: **Example of Urban Management with Spectrum Data under the Auto-Planning Regime.**

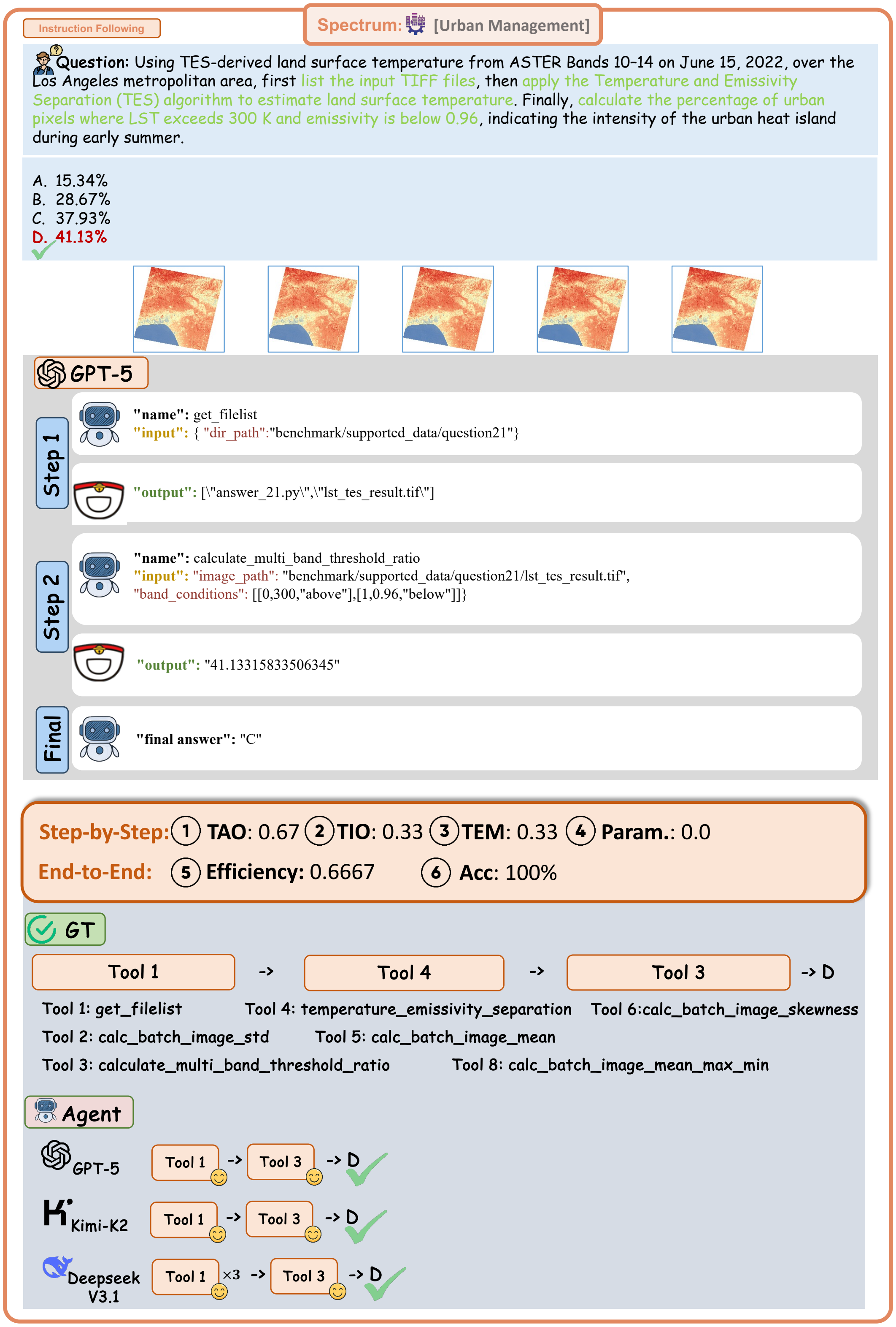

Question: Using TES-derived land surface temperature from ASTER Bands 10–14 on June 15, 2022, over the Los Angeles metropolitan area, first list the input TIFF files, then apply the Temperature and Emissivity Separation (TES) algorithm to estimate land surface temperature. Finally, calculate the percentage of urban pixels where LST exceeds 300 K and emissivity is below 0.96, indicating the intensity of the urban heat island during early summer.

A. 15.34%
B. 28.67%
C. 37.93%
D. 41.13% ✓

Step 1

"name": get_filelist
"input": { "dir_path":"benchmark/supported_data/question21"}

"output": [\"answer_21.py\",\"lst_tes_result.tif\"]

Step 2

"name": calculate_multi_band_threshold_ratio
"input": "image_path": "benchmark/supported_data/question21/lst_tes_result.tif", "band_conditions": [[0,300,"above"],[1,0.96,"below"]]}

"output": "41.13315833506345"

Final

"final answer": "C"

Step-by-Step: ① **TAO**: 0.67 ② **TIO**: 0.33 ③ **TEM**: 0.33 ④ **Param.**: 0.0

End-to-End: ⑤ **Efficiency:** 0.6667 ⑥ **Acc**: 100%

Tool 1: get_filelist
Tool 4: temperature_emissivity_separation
Tool 6:calc_batch_image_skewness
Tool 2: calc_batch_image_std
Tool 5: calc_batch_image_mean
Tool 3: calculate_multi_band_threshold_ratio
Tool 8: calc_batch_image_mean_max_min

Figure 18: **Example of Urban Management with Spectrum Data under the Instruction-Following Regime.**

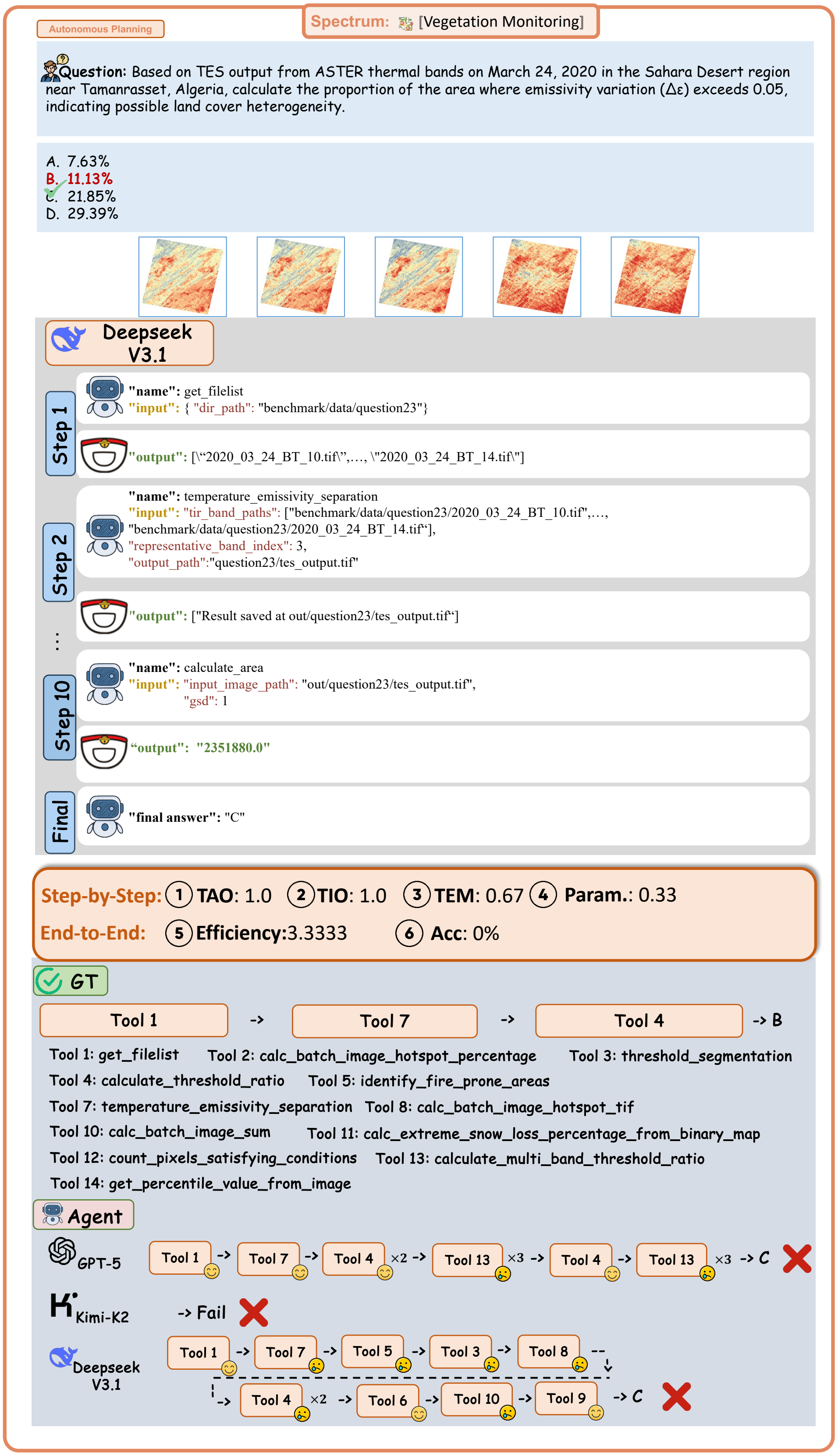

Autonomous Planning

Spectrum: [Vegetation Monitoring]

Question: Based on TES output from ASTER thermal bands on March 24, 2020 in the Sahara Desert region near Tamanrasset, Algeria, calculate the proportion of the area where emissivity variation (Δε) exceeds 0.05, indicating possible land cover heterogeneity.

A. 7.63%
B. 11.13% ✓
C. 21.85%
D. 29.39%

Deepseek V3.1

Step 1

"name": get_filelist
"input": { "dir_path": "benchmark/data/question23"}

"output": [\“2020_03_24_BT_10.tif\”,…, \"2020_03_24_BT_14.tif\"]

Step 2

"name": temperature_emissivity_separation
"input": "tir_band_paths": ["benchmark/data/question23/2020_03_24_BT_10.tif",…, "benchmark/data/question23/2020_03_24_BT_14.tif"],
"representative_band_index": 3,
"output_path":"question23/tes_output.tif"

"output": ["Result saved at out/question23/tes_output.tif"]

⋮

Step 10

"name": calculate_area
"input": "input_image_path": "out/question23/tes_output.tif",
"gsd": 1

“output": "2351880.0"

Final

"final answer": "C"

Step-by-Step: ① **TAO**: 1.0 ② **TIO**: 1.0 ③ **TEM**: 0.67 ④ **Param.**: 0.33

End-to-End: ⑤ **Efficiency**:3.3333 ⑥ **Acc**: 0%

✓ **GT**

Tool 1 -> Tool 7 -> Tool 4 -> B

Tool 1: get_filelist
Tool 2: calc_batch_image_hotspot_percentage
Tool 3: threshold_segmentation
Tool 4: calculate_threshold_ratio
Tool 5: identify_fire_prone_areas
Tool 7: temperature_emissivity_separation
Tool 8: calc_batch_image_hotspot_tif
Tool 10: calc_batch_image_sum
Tool 11: calc_extreme_snow_loss_percentage_from_binary_map
Tool 12: count_pixels_satisfying_conditions
Tool 13: calculate_multi_band_threshold_ratio
Tool 14: get_percentile_value_from_image

Agent

GPT-5: Tool 1 😊 -> Tool 7 😊 -> Tool 4 😊 ×2 -> Tool 13 😢 ×3 -> Tool 4 😊 -> Tool 13 😢 ×3 -> C ✗

Kimi-K2: -> Fail ✗

Deepseek V3.1: Tool 1 😊 -> Tool 7 😢 -> Tool 5 😢 -> Tool 3 😢 -> Tool 8 😢 -> Tool 4 😢 ×2 -> Tool 6 😊 -> Tool 10 😢 -> Tool 9 😊 -> C ✗

Figure 19: **Example of Vegetation Monitoring with Spectrum Data under the Auto-Planning Regime.**

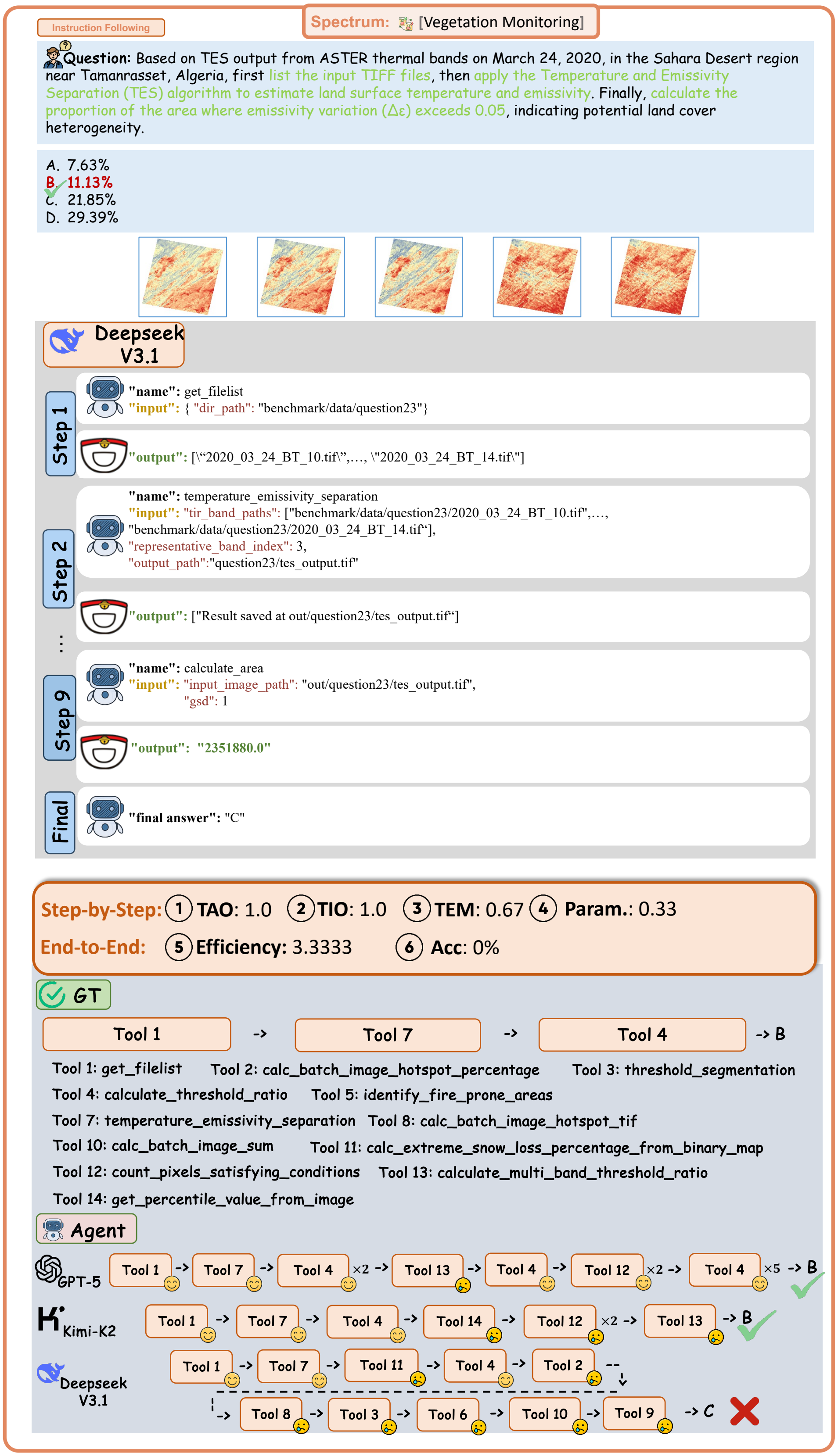

Question: Based on TES output from ASTER thermal bands on March 24, 2020, in the Sahara Desert region near Tamanrasset, Algeria, first list the input TIFF files, then apply the Temperature and Emissivity Separation (TES) algorithm to estimate land surface temperature and emissivity. Finally, calculate the proportion of the area where emissivity variation (Δε) exceeds 0.05, indicating potential land cover heterogeneity.

A. 7.63%
B. 11.13% ✓
C. 21.85%
D. 29.39%

Step 1

"name": get_filelist
"input": { "dir_path": "benchmark/data/question23"}

"output": [\"2020_03_24_BT_10.tif\",…, \"2020_03_24_BT_14.tif\"]

Step 2

"name": temperature_emissivity_separation
"input": "tir_band_paths": ["benchmark/data/question23/2020_03_24_BT_10.tif",…, "benchmark/data/question23/2020_03_24_BT_14.tif"],
"representative_band_index": 3,
"output_path":"question23/tes_output.tif"

"output": ["Result saved at out/question23/tes_output.tif"]

Step 9

"name": calculate_area
"input": "input_image_path": "out/question23/tes_output.tif",
"gsd": 1

"output": "2351880.0"

Final

"final answer": "C"

Step-by-Step: ① **TAO**: 1.0 ② **TIO**: 1.0 ③ **TEM**: 0.67 ④ **Param.**: 0.33

End-to-End: ⑤ **Efficiency:** 3.3333 ⑥ **Acc**: 0%

GT

Tool 1 -> Tool 7 -> Tool 4 -> B

Tool 1: get_filelist
Tool 2: calc_batch_image_hotspot_percentage
Tool 3: threshold_segmentation
Tool 4: calculate_threshold_ratio
Tool 5: identify_fire_prone_areas
Tool 7: temperature_emissivity_separation
Tool 8: calc_batch_image_hotspot_tif
Tool 10: calc_batch_image_sum
Tool 11: calc_extreme_snow_loss_percentage_from_binary_map
Tool 12: count_pixels_satisfying_conditions
Tool 13: calculate_multi_band_threshold_ratio
Tool 14: get_percentile_value_from_image

Agent

GPT-5: Tool 1 -> Tool 7 -> Tool 4 ×2 -> Tool 13 -> Tool 4 -> Tool 12 ×2 -> Tool 4 ×5 -> B ✓

Kimi-K2: Tool 1 -> Tool 7 -> Tool 4 -> Tool 14 -> Tool 12 ×2 -> Tool 13 -> B ✓

Deepseek V3.1: Tool 1 -> Tool 7 -> Tool 11 -> Tool 4 -> Tool 2 -> Tool 8 -> Tool 3 -> Tool 6 -> Tool 10 -> Tool 9 -> C ✗

Figure 20: **Example of Vegetation Monitoring with Spectrum Data under the Instruction-Following Regime.**

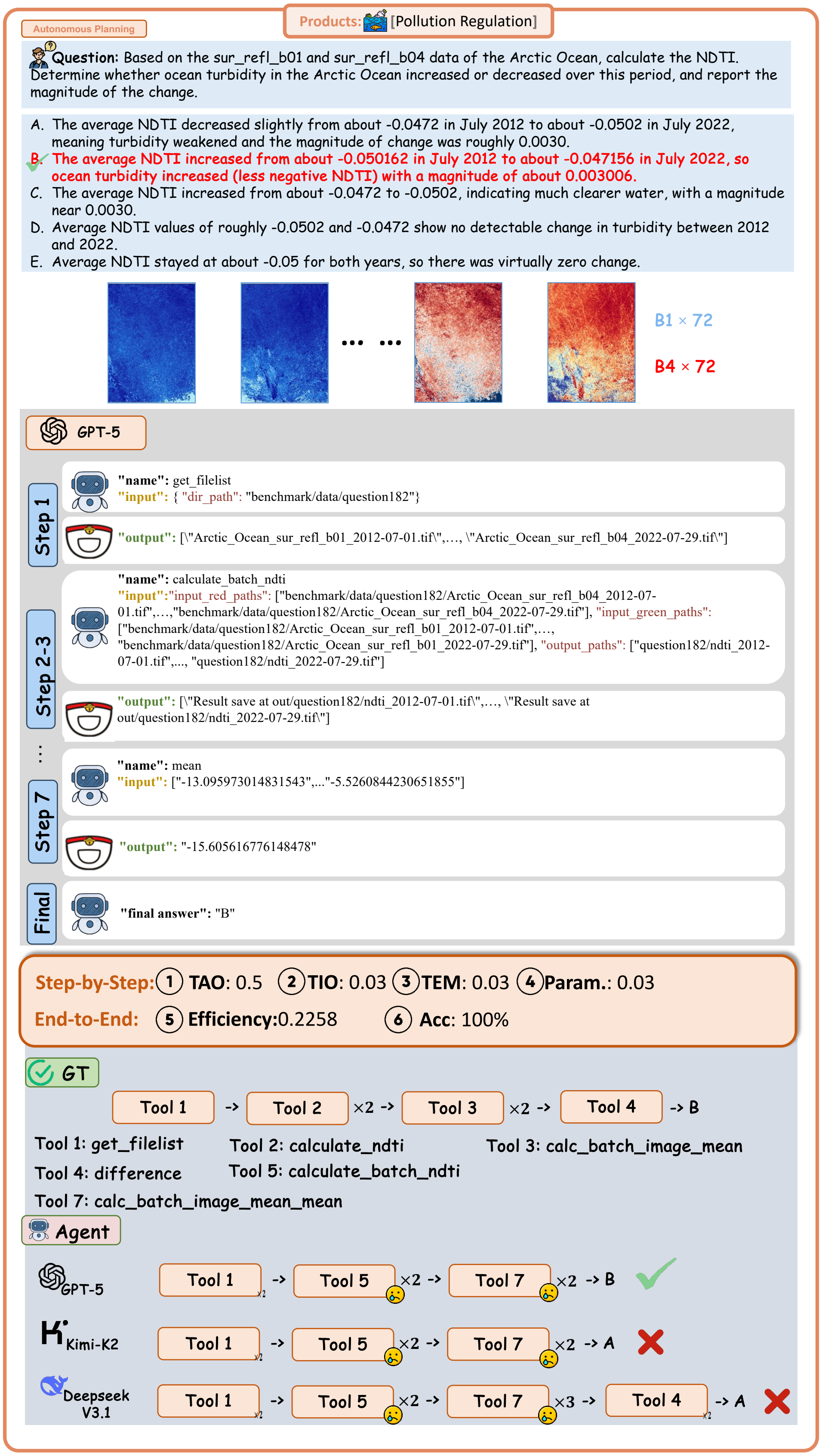

Question: Based on the sur_refl_b01 and sur_refl_b04 data of the Arctic Ocean, calculate the NDTI. Determine whether ocean turbidity in the Arctic Ocean increased or decreased over this period, and report the magnitude of the change.

A. The average NDTI decreased slightly from about -0.0472 in July 2012 to about -0.0502 in July 2022, meaning turbidity weakened and the magnitude of change was roughly 0.0030.
B. ✓ The average NDTI increased from about -0.050162 in July 2012 to about -0.047156 in July 2022, so ocean turbidity increased (less negative NDTI) with a magnitude of about 0.003006.
C. The average NDTI increased from about -0.0472 to -0.0502, indicating much clearer water, with a magnitude near 0.0030.
D. Average NDTI values of roughly -0.0502 and -0.0472 show no detectable change in turbidity between 2012 and 2022.
E. Average NDTI stayed at about -0.05 for both years, so there was virtually zero change.

Step 1

"name": get_filelist
"input": { "dir_path": "benchmark/data/question182"}

"output": [\"Arctic_Ocean_sur_refl_b01_2012-07-01.tif\",…, \"Arctic_Ocean_sur_refl_b04_2022-07-29.tif\"]

Step 2-3

"name": calculate_batch_ndti
"input":"input_red_paths": ["benchmark/data/question182/Arctic_Ocean_sur_refl_b04_2012-07-01.tif",…,"benchmark/data/question182/Arctic_Ocean_sur_refl_b04_2022-07-29.tif"], "input_green_paths": ["benchmark/data/question182/Arctic_Ocean_sur_refl_b01_2012-07-01.tif",…, "benchmark/data/question182/Arctic_Ocean_sur_refl_b01_2022-07-29.tif"], "output_paths": ["question182/ndti_2012-07-01.tif",..., "question182/ndti_2022-07-29.tif"]

"output": [\"Result save at out/question182/ndti_2012-07-01.tif\",…, \"Result save at out/question182/ndti_2022-07-29.tif\"]

⋮

Step 7

"name": mean
"input": ["-13.095973014831543",..."-5.5260844230651855"]

"output": "-15.605616776148478"

Final

"final answer": "B"

Step-by-Step: ① **TAO**: 0.5 ② **TIO**: 0.03 ③ **TEM**: 0.03 ④ **Param.**: 0.03

End-to-End: ⑤ **Efficiency**:0.2258 ⑥ **Acc**: 100%

✓ GT

Tool 1 -> Tool 2 ×2 -> Tool 3 ×2 -> Tool 4 -> B

Tool 1: get_filelist
Tool 2: calculate_ndti
Tool 3: calc_batch_image_mean
Tool 4: difference
Tool 5: calculate_batch_ndti
Tool 7: calc_batch_image_mean_mean

Agent

GPT-5: Tool 1 ×2 -> Tool 5 ×2 -> Tool 7 ×2 -> B ✓
Kimi-K2: Tool 1 ×2 -> Tool 5 ×2 -> Tool 7 ×2 -> A ✗
Deepseek V3.1: Tool 1 ×2 -> Tool 5 ×2 -> Tool 7 ×3 -> Tool 4 ×2 -> A ✗

Figure 21: **Example of Pollution Regulation with Products Data under the Auto-Planning Regime.**

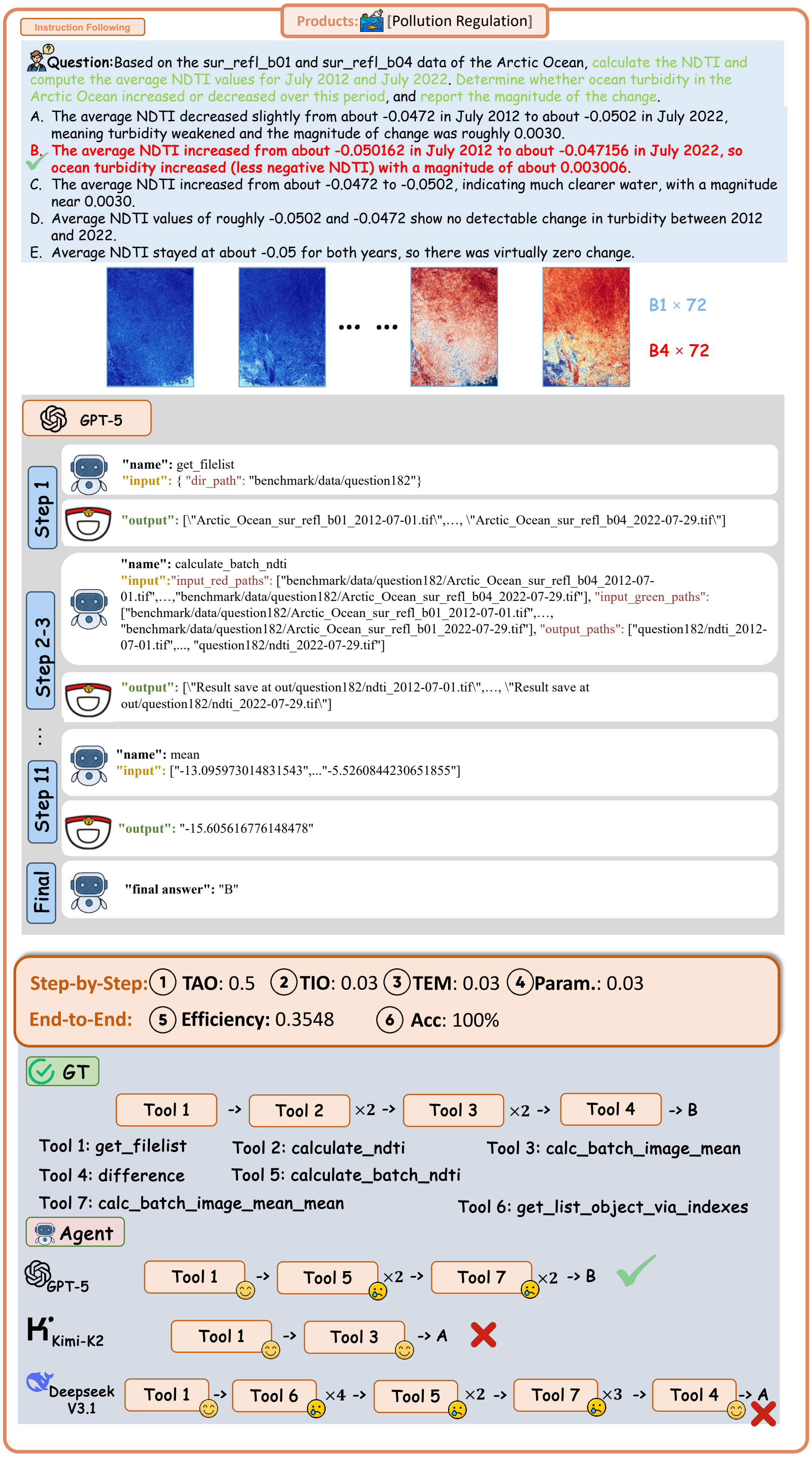

Question: Based on the sur_refl_b01 and sur_refl_b04 data of the Arctic Ocean, calculate the NDTI and compute the average NDTI values for July 2012 and July 2022. Determine whether ocean turbidity in the Arctic Ocean increased or decreased over this period, and report the magnitude of the change.

A. The average NDTI decreased slightly from about -0.0472 in July 2012 to about -0.0502 in July 2022, meaning turbidity weakened and the magnitude of change was roughly 0.0030.
B. ✓ The average NDTI increased from about -0.050162 in July 2012 to about -0.047156 in July 2022, so ocean turbidity increased (less negative NDTI) with a magnitude of about 0.003006.
C. The average NDTI increased from about -0.0472 to -0.0502, indicating much clearer water, with a magnitude near 0.0030.
D. Average NDTI values of roughly -0.0502 and -0.0472 show no detectable change in turbidity between 2012 and 2022.
E. Average NDTI stayed at about -0.05 for both years, so there was virtually zero change.

Step 1

"name": get_filelist
"input": { "dir_path": "benchmark/data/question182"}

"output": [\"Arctic_Ocean_sur_refl_b01_2012-07-01.tif\",…, \"Arctic_Ocean_sur_refl_b04_2022-07-29.tif\"]

Step 2-3

"name": calculate_batch_ndti
"input":"input_red_paths": ["benchmark/data/question182/Arctic_Ocean_sur_refl_b04_2012-07-01.tif",…,"benchmark/data/question182/Arctic_Ocean_sur_refl_b04_2022-07-29.tif"], "input_green_paths": ["benchmark/data/question182/Arctic_Ocean_sur_refl_b01_2012-07-01.tif",…, "benchmark/data/question182/Arctic_Ocean_sur_refl_b01_2022-07-29.tif"], "output_paths": ["question182/ndti_2012-07-01.tif",..., "question182/ndti_2022-07-29.tif"]

"output": [\"Result save at out/question182/ndti_2012-07-01.tif\",…, \"Result save at out/question182/ndti_2022-07-29.tif\"]

⋮

Step 11

"name": mean
"input": ["-13.095973014831543",..."-5.5260844230651855"]

"output": "-15.605616776148478"

Final

"final answer": "B"

Step-by-Step: ① **TAO**: 0.5 ② **TIO**: 0.03 ③ **TEM**: 0.03 ④ **Param.**: 0.03
End-to-End: ⑤ **Efficiency:** 0.3548 ⑥ **Acc**: 100%

GT

Tool 1 -> Tool 2 ×2 -> Tool 3 ×2 -> Tool 4 -> B

Tool 1: get_filelist
Tool 2: calculate_ndti
Tool 3: calc_batch_image_mean
Tool 4: difference
Tool 5: calculate_batch_ndti
Tool 6: get_list_object_via_indexes
Tool 7: calc_batch_image_mean_mean

Agent

GPT-5: Tool 1 -> Tool 5 ×2 -> Tool 7 ×2 -> B ✓
Kimi-K2: Tool 1 -> Tool 3 -> A ✗
Deepseek V3.1: Tool 1 -> Tool 6 ×4 -> Tool 5 ×2 -> Tool 7 ×3 -> Tool 4 -> A ✗

Figure 22: **Example of Pollution Regulation with Products Data under the Instruction-Following Regime.**

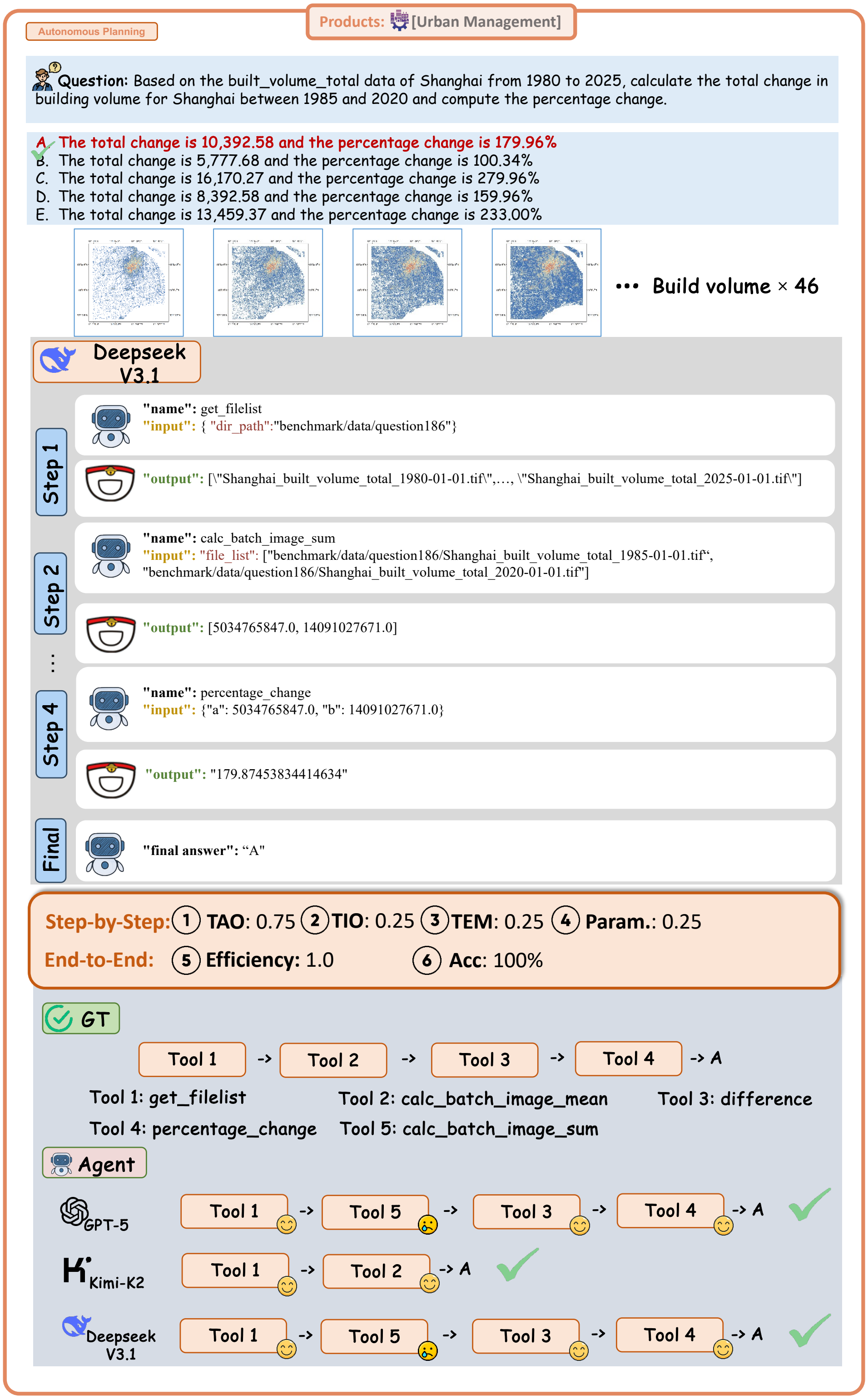

Question: Based on the built_volume_total data of Shanghai from 1980 to 2025, calculate the total change in building volume for Shanghai between 1985 and 2020 and compute the percentage change.

A. The total change is 10,392.58 and the percentage change is 179.96% ✓
B. The total change is 5,777.68 and the percentage change is 100.34%
C. The total change is 16,170.27 and the percentage change is 279.96%
D. The total change is 8,392.58 and the percentage change is 159.96%
E. The total change is 13,459.37 and the percentage change is 233.00%

Step 1

```
"name": get_filelist
"input": { "dir_path":"benchmark/data/question186"}
"output": [\"Shanghai_built_volume_total_1980-01-01.tif\",…, \"Shanghai_built_volume_total_2025-01-01.tif\"]
```

Step 2

```
"name": calc_batch_image_sum
"input": "file_list": ["benchmark/data/question186/Shanghai_built_volume_total_1985-01-01.tif“,
"benchmark/data/question186/Shanghai_built_volume_total_2020-01-01.tif"]
"output": [5034765847.0, 14091027671.0]
```

⋮

Step 4

```
"name": percentage_change
"input": {"a": 5034765847.0, "b": 14091027671.0}
"output": "179.87453834414634"
```

Final

```
"final answer": “A"
```

Step-by-Step: ① **TAO**: 0.75 ② **TIO**: 0.25 ③ **TEM**: 0.25 ④ **Param.**: 0.25

End-to-End: ⑤ **Efficiency:** 1.0 ⑥ **Acc**: 100%

GT

Tool 1 -> Tool 2 -> Tool 3 -> Tool 4 -> A

Tool 1: get_filelist
Tool 2: calc_batch_image_mean
Tool 3: difference
Tool 4: percentage_change
Tool 5: calc_batch_image_sum

Agent

GPT-5: Tool 1 -> Tool 5 -> Tool 3 -> Tool 4 -> A ✓
Kimi-K2: Tool 1 -> Tool 2 -> A ✓
Deepseek V3.1: Tool 1 -> Tool 5 -> Tool 3 -> Tool 4 -> A ✓

Figure 23: **Example of Urban Management with Products Data under the Auto-Planning Regime.**

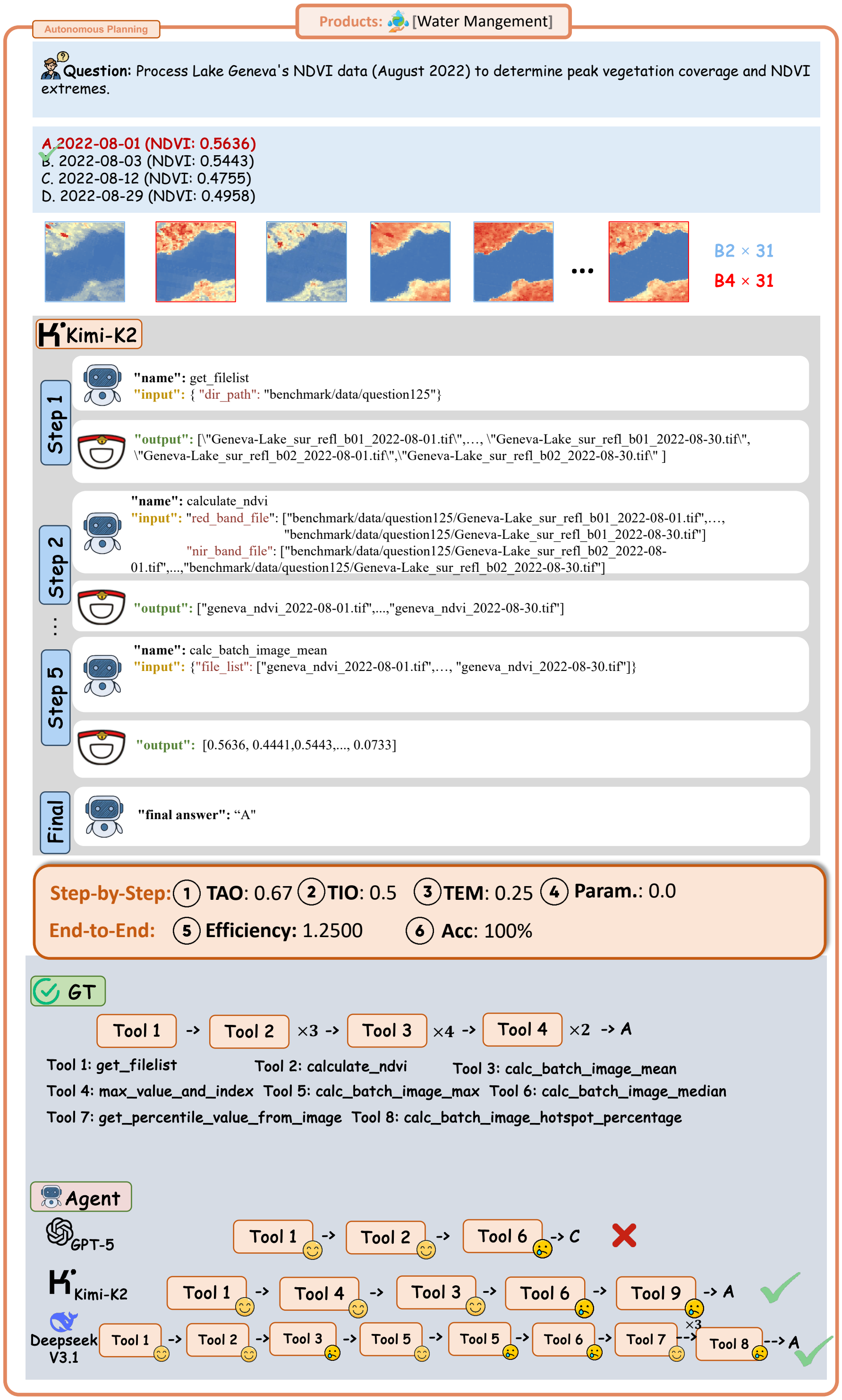

Question: Process Lake Geneva's NDVI data (August 2022) to determine peak vegetation coverage and NDVI extremes.

A. 2022-08-01 (NDVI: 0.5636) ✓
B. 2022-08-03 (NDVI: 0.5443)
C. 2022-08-12 (NDVI: 0.4755)
D. 2022-08-29 (NDVI: 0.4958)

Step 1

```
"name": get_filelist
"input": { "dir_path": "benchmark/data/question125"}
```

```
"output": [\"Geneva-Lake_sur_refl_b01_2022-08-01.tif\",…, \"Geneva-Lake_sur_refl_b01_2022-08-30.tif\",
\"Geneva-Lake_sur_refl_b02_2022-08-01.tif\",\"Geneva-Lake_sur_refl_b02_2022-08-30.tif\" ]
```

Step 2

```
"name": calculate_ndvi
"input": "red_band_file": ["benchmark/data/question125/Geneva-Lake_sur_refl_b01_2022-08-01.tif",…,
                          "benchmark/data/question125/Geneva-Lake_sur_refl_b01_2022-08-30.tif"]
         "nir_band_file": ["benchmark/data/question125/Geneva-Lake_sur_refl_b02_2022-08-
01.tif",...,"benchmark/data/question125/Geneva-Lake_sur_refl_b02_2022-08-30.tif"]
```

```
"output": ["geneva_ndvi_2022-08-01.tif",...,"geneva_ndvi_2022-08-30.tif"]
```

⋮

Step 5

```
"name": calc_batch_image_mean
"input": {"file_list": ["geneva_ndvi_2022-08-01.tif",…, "geneva_ndvi_2022-08-30.tif"]}
```

```
"output":  [0.5636, 0.4441,0.5443,..., 0.0733]
```

Final

```
"final answer": “A"
```

Step-by-Step: ① **TAO**: 0.67 ② **TIO**: 0.5 ③ **TEM**: 0.25 ④ **Param.**: 0.0

End-to-End: ⑤ **Efficiency:** 1.2500 ⑥ **Acc**: 100%

GT

Tool 1 -> Tool 2 ×3 -> Tool 3 ×4 -> Tool 4 ×2 -> A

Tool 1: get_filelist
Tool 2: calculate_ndvi
Tool 3: calc_batch_image_mean
Tool 4: max_value_and_index
Tool 5: calc_batch_image_max
Tool 6: calc_batch_image_median
Tool 7: get_percentile_value_from_image
Tool 8: calc_batch_image_hotspot_percentage

Agent

GPT-5: Tool 1 -> Tool 2 -> Tool 6 -> C ✗

Kimi-K2: Tool 1 -> Tool 4 -> Tool 3 -> Tool 6 -> Tool 9 -> A ✓

Deepseek V3.1: Tool 1 -> Tool 2 -> Tool 3 -> Tool 5 -> Tool 5 -> Tool 6 -> Tool 7 --> ×3 Tool 8 --> A ✓

Figure 24: **Example of Water Management with Products Data under the Auto-Planning Regime.**

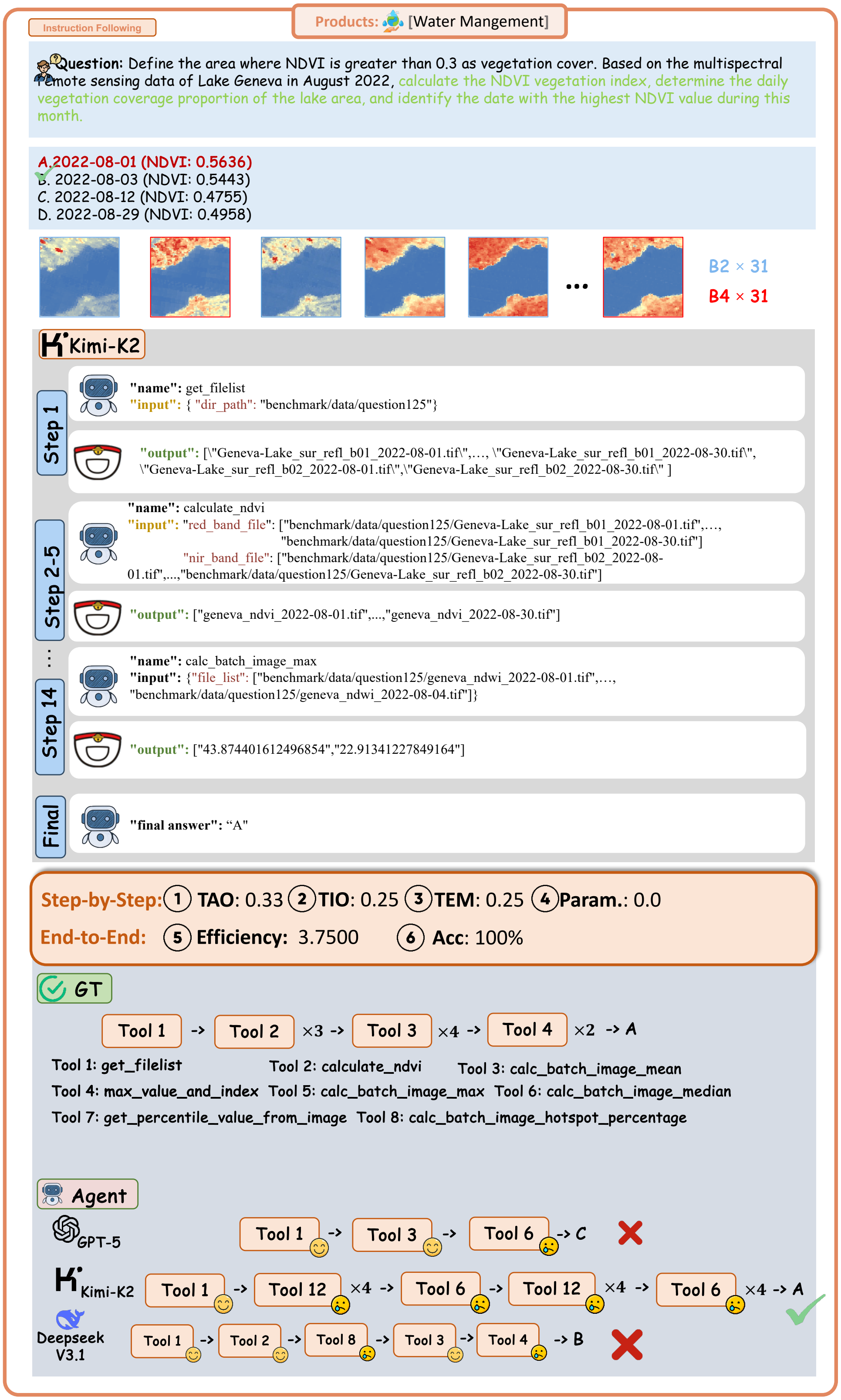

Question: Define the area where NDVI is greater than 0.3 as vegetation cover. Based on the multispectral remote sensing data of Lake Geneva in August 2022, calculate the NDVI vegetation index, determine the daily vegetation coverage proportion of the lake area, and identify the date with the highest NDVI value during this month.

A. 2022-08-01 (NDVI: 0.5636) ✓
B. 2022-08-03 (NDVI: 0.5443)
C. 2022-08-12 (NDVI: 0.4755)
D. 2022-08-29 (NDVI: 0.4958)

Step 1

```
"name": get_filelist
"input": { "dir_path": "benchmark/data/question125"}
```

```
"output": [\"Geneva-Lake_sur_refl_b01_2022-08-01.tif\",…, \"Geneva-Lake_sur_refl_b01_2022-08-30.tif\",
\"Geneva-Lake_sur_refl_b02_2022-08-01.tif\",\"Geneva-Lake_sur_refl_b02_2022-08-30.tif\" ]
```

Step 2-5

```
"name": calculate_ndvi
"input": "red_band_file": ["benchmark/data/question125/Geneva-Lake_sur_refl_b01_2022-08-01.tif",…,
                          "benchmark/data/question125/Geneva-Lake_sur_refl_b01_2022-08-30.tif"]
         "nir_band_file": ["benchmark/data/question125/Geneva-Lake_sur_refl_b02_2022-08-
01.tif",...,"benchmark/data/question125/Geneva-Lake_sur_refl_b02_2022-08-30.tif"]
```

```
"output": ["geneva_ndvi_2022-08-01.tif",...,"geneva_ndvi_2022-08-30.tif"]
```

⋮

Step 14

```
"name": calc_batch_image_max
"input": {"file_list": ["benchmark/data/question125/geneva_ndwi_2022-08-01.tif",…,
"benchmark/data/question125/geneva_ndwi_2022-08-04.tif"]}
```

```
"output": ["43.874401612496854","22.91341227849164"]
```

Final

```
"final answer": “A"
```

Step-by-Step: ① **TAO**: 0.33 ② **TIO**: 0.25 ③ **TEM**: 0.25 ④ **Param.**: 0.0

End-to-End: ⑤ **Efficiency:** 3.7500 ⑥ **Acc**: 100%

GT

Tool 1 -> Tool 2 ×3 -> Tool 3 ×4 -> Tool 4 ×2 -> A

Tool 1: get_filelist
Tool 2: calculate_ndvi
Tool 3: calc_batch_image_mean
Tool 4: max_value_and_index
Tool 5: calc_batch_image_max
Tool 6: calc_batch_image_median
Tool 7: get_percentile_value_from_image
Tool 8: calc_batch_image_hotspot_percentage

Agent

GPT-5: Tool 1 -> Tool 3 -> Tool 6 -> C ✗
Kimi-K2: Tool 1 -> Tool 12 ×4 -> Tool 6 -> Tool 12 ×4 -> Tool 6 ×4 -> A ✓
Deepseek V3.1: Tool 1 -> Tool 2 -> Tool 8 -> Tool 3 -> Tool 4 -> B ✗

Figure 25: **Example of Water Management with Products Data under the Instruction-Following Regime.**

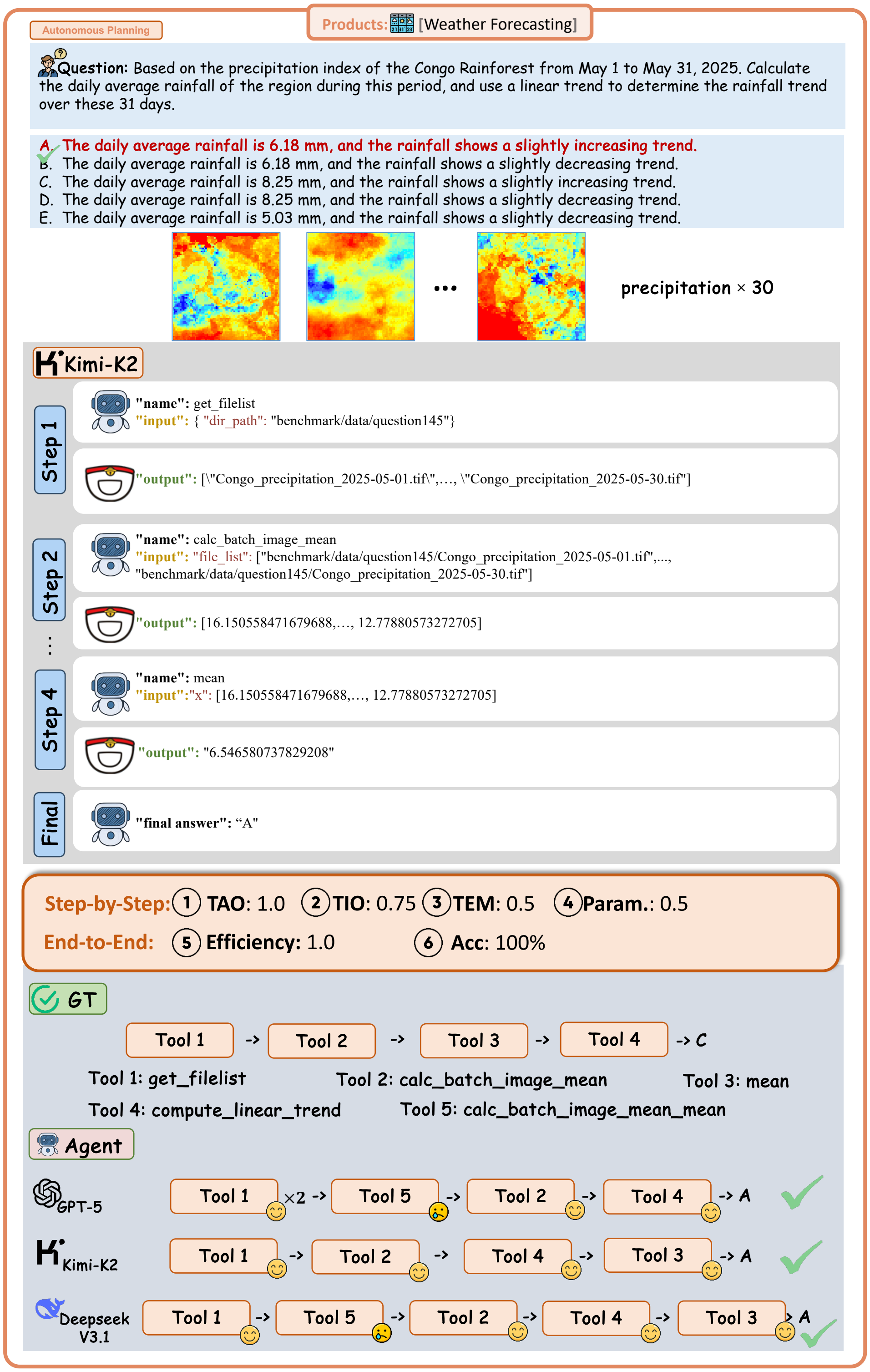

Question: Based on the precipitation index of the Congo Rainforest from May 1 to May 31, 2025. Calculate the daily average rainfall of the region during this period, and use a linear trend to determine the rainfall trend over these 31 days.

A. The daily average rainfall is 6.18 mm, and the rainfall shows a slightly increasing trend. ✓
B. The daily average rainfall is 6.18 mm, and the rainfall shows a slightly decreasing trend.
C. The daily average rainfall is 8.25 mm, and the rainfall shows a slightly increasing trend.
D. The daily average rainfall is 8.25 mm, and the rainfall shows a slightly decreasing trend.
E. The daily average rainfall is 5.03 mm, and the rainfall shows a slightly decreasing trend.

Step 1

"name": get_filelist
"input": { "dir_path": "benchmark/data/question145"}

"output": [\"Congo_precipitation_2025-05-01.tif\",..., \"Congo_precipitation_2025-05-30.tif"]

Step 2

"name": calc_batch_image_mean
"input": "file_list": ["benchmark/data/question145/Congo_precipitation_2025-05-01.tif",..., "benchmark/data/question145/Congo_precipitation_2025-05-30.tif"]

"output": [16.150558471679688,..., 12.77880573272705]

⋮

Step 4

"name": mean
"input":"x": [16.150558471679688,..., 12.77880573272705]

"output": "6.546580737829208"

Final

"final answer": "A"

Step-by-Step: ① **TAO**: 1.0 ② **TIO**: 0.75 ③ **TEM**: 0.5 ④ **Param.**: 0.5
End-to-End: ⑤ **Efficiency:** 1.0 ⑥ **Acc**: 100%

GT

Tool 1 -> Tool 2 -> Tool 3 -> Tool 4 -> C

Tool 1: get_filelist
Tool 2: calc_batch_image_mean
Tool 3: mean
Tool 4: compute_linear_trend
Tool 5: calc_batch_image_mean_mean

Agent

GPT-5: Tool 1 ×2 -> Tool 5 -> Tool 2 -> Tool 4 -> A ✓
Kimi-K2: Tool 1 -> Tool 2 -> Tool 4 -> Tool 3 -> A ✓
Deepseek V3.1: Tool 1 -> Tool 5 -> Tool 2 -> Tool 4 -> Tool 3 -> A ✓

Figure 26: **Example of Weather Management with Products Data under the Auto-Planning Regime.**

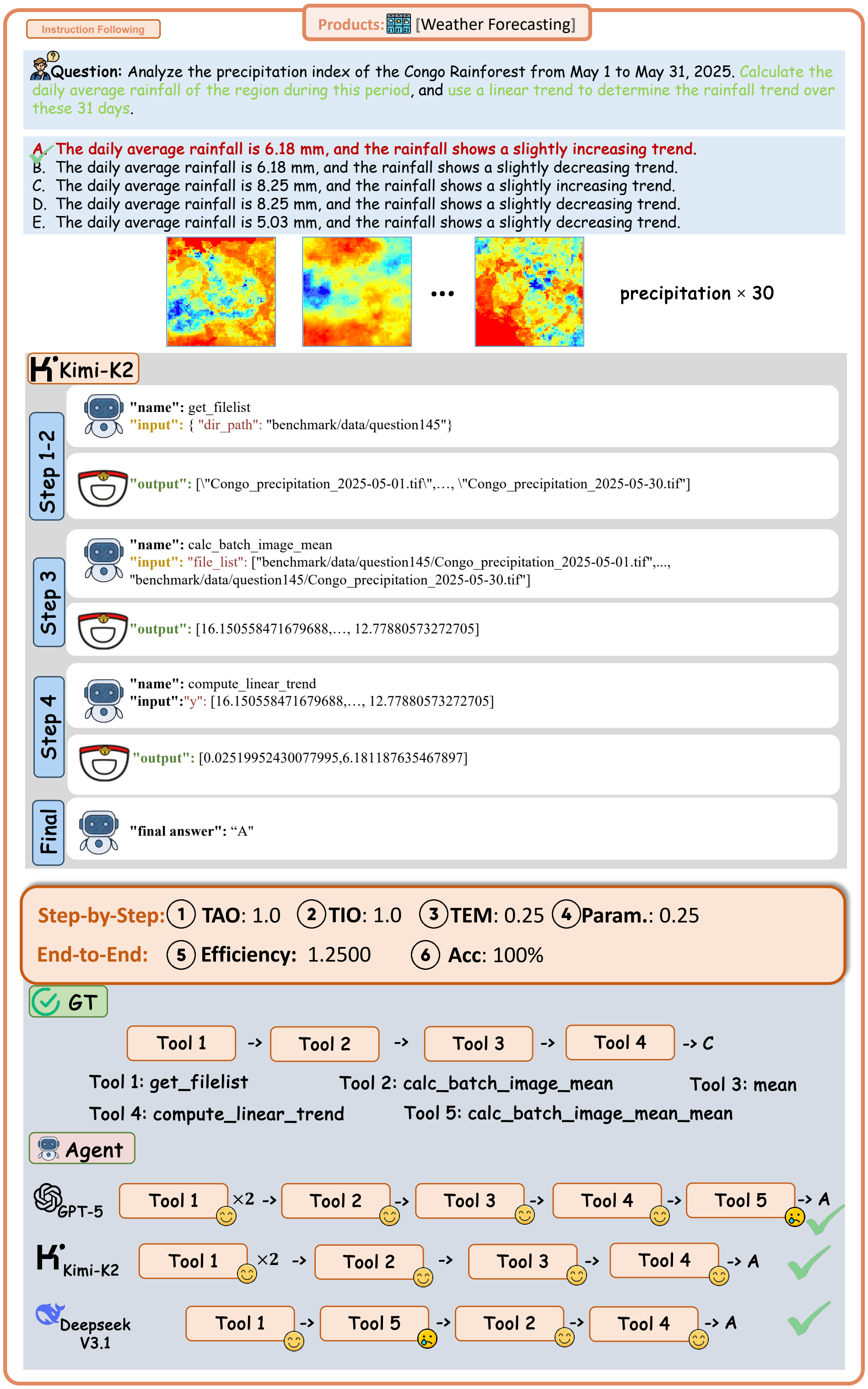

Question: Analyze the precipitation index of the Congo Rainforest from May 1 to May 31, 2025. Calculate the daily average rainfall of the region during this period, and use a linear trend to determine the rainfall trend over these 31 days.

A. ✓ The daily average rainfall is 6.18 mm, and the rainfall shows a slightly increasing trend.
B. The daily average rainfall is 6.18 mm, and the rainfall shows a slightly decreasing trend.
C. The daily average rainfall is 8.25 mm, and the rainfall shows a slightly increasing trend.
D. The daily average rainfall is 8.25 mm, and the rainfall shows a slightly decreasing trend.
E. The daily average rainfall is 5.03 mm, and the rainfall shows a slightly decreasing trend.

Step 1-2

```
"name": get_filelist
"input": { "dir_path": "benchmark/data/question145"}
```

```
"output": [\"Congo_precipitation_2025-05-01.tif\",…, \"Congo_precipitation_2025-05-30.tif"]
```

Step 3

```
"name": calc_batch_image_mean
"input": "file_list": ["benchmark/data/question145/Congo_precipitation_2025-05-01.tif",...,
"benchmark/data/question145/Congo_precipitation_2025-05-30.tif"]
```

```
"output": [16.150558471679688,…, 12.77880573272705]
```

Step 4

```
"name": compute_linear_trend
"input":"y": [16.150558471679688,…, 12.77880573272705]
```

```
"output": [0.02519952430077995,6.181187635467897]
```

Final

```
"final answer": “A"
```

Step-by-Step: ① **TAO**: 1.0 ② **TIO**: 1.0 ③ **TEM**: 0.25 ④ **Param.**: 0.25

End-to-End: ⑤ **Efficiency:** 1.2500 ⑥ **Acc**: 100%

Tool 1: get_filelist
Tool 2: calc_batch_image_mean
Tool 3: mean
Tool 4: compute_linear_trend
Tool 5: calc_batch_image_mean_mean

Agent
GPT-5
Tool 1 ×2 -> Tool 2 -> Tool 3 -> Tool 4 -> Tool 5 -> A ✓
Kimi-K2
Tool 1 ×2 -> Tool 2 -> Tool 3 -> Tool 4 -> A ✓
Deepseek V3.1
Tool 1 -> Tool 5 -> Tool 2 -> Tool 4 -> A ✓

Figure 27: **Example of Weather Management with Products Data under the Instruction-Following Regime.**

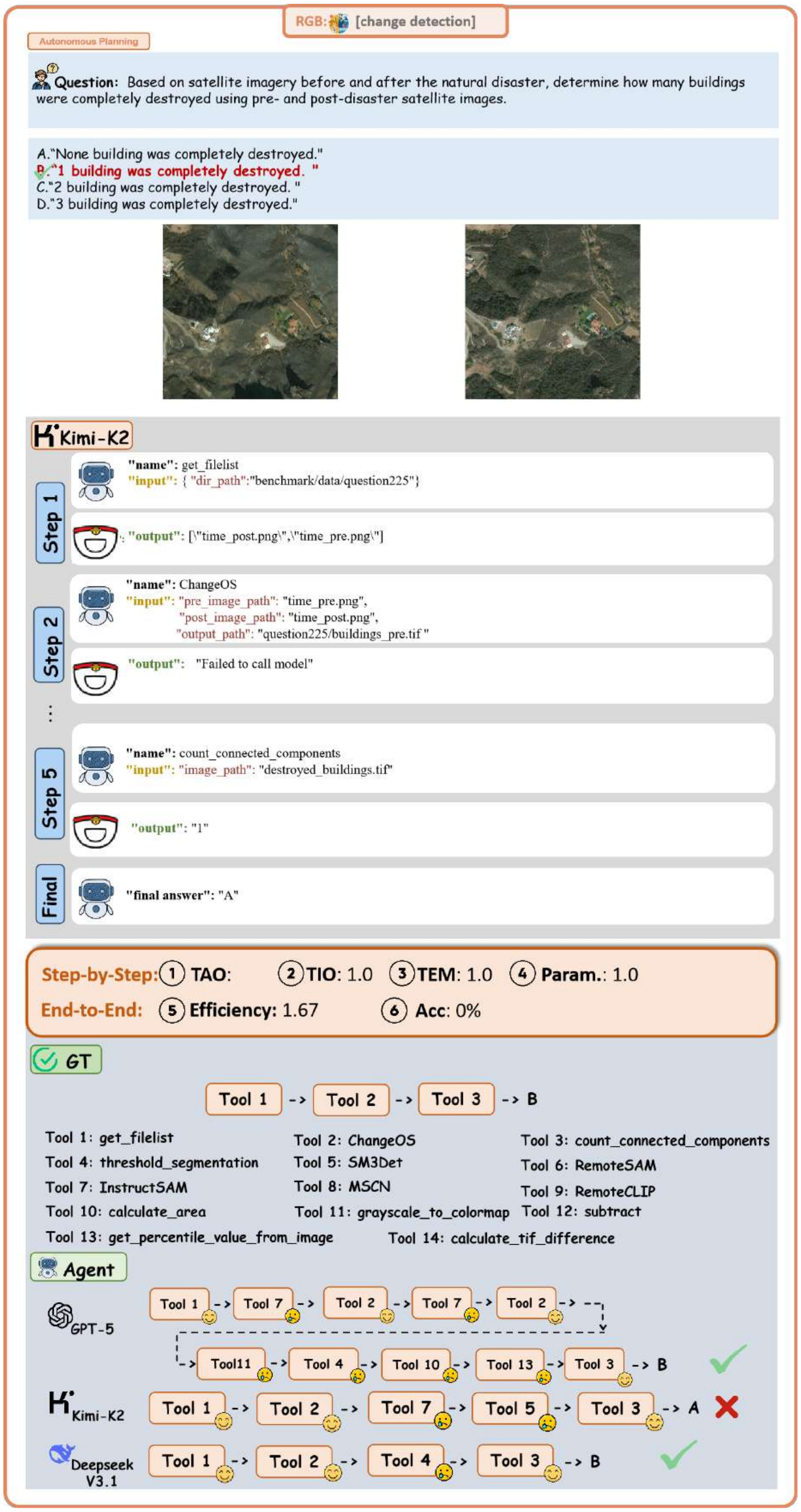

Question: Based on satellite imagery before and after the natural disaster, determine how many buildings were completely destroyed using pre- and post-disaster satellite images.

A."None building was completely destroyed."
✓ B."1 building was completely destroyed. "
C."2 building was completely destroyed. "
D."3 building was completely destroyed."

```
"name": get_filelist
"input": { "dir_path":"benchmark/data/question225"}
```

```
"output": [\"time_post.png\",\"time_pre.png\"]
```

```
"name": ChangeOS
"input": "pre_image_path": "time_pre.png",
         "post_image_path": "time_post.png",
        "output_path": "question225/buildings_pre.tif "
```

```
"output":   "Failed to call model"
```

```
"name": count_connected_components
"input": "image_path": "destroyed_buildings.tif"
```

```
"output": "1"
```

```
"final answer": "A"
```

Step-by-Step: ① TAO: ② TIO: 1.0 ③ TEM: 1.0 ④ Param.: 1.0
End-to-End: ⑤ Efficiency: 1.67 ⑥ Acc: 0%

Tool 1 -> Tool 2 -> Tool 3 -> B

Tool 1: get_filelist
Tool 2: ChangeOS
Tool 3: count_connected_components
Tool 4: threshold_segmentation
Tool 5: SM3Det
Tool 6: RemoteSAM
Tool 7: InstructSAM
Tool 8: MSCN
Tool 9: RemoteCLIP
Tool 10: calculate_area
Tool 11: grayscale_to_colormap
Tool 12: subtract
Tool 13: get_percentile_value_from_image
Tool 14: calculate_tif_difference

GPT-5: Tool 1 -> Tool 7 -> Tool 2 -> Tool 7 -> Tool 2 -> Tool11 -> Tool 4 -> Tool 10 -> Tool 13 -> Tool 3 -> B ✓
Kimi-K2: Tool 1 -> Tool 2 -> Tool 7 -> Tool 5 -> Tool 3 -> A ✗
Deepseek V3.1: Tool 1 -> Tool 2 -> Tool 4 -> Tool 3 -> B ✓

Figure 28: **Example of Change Detection with RGB Data under the Auto-Planning Regime.**

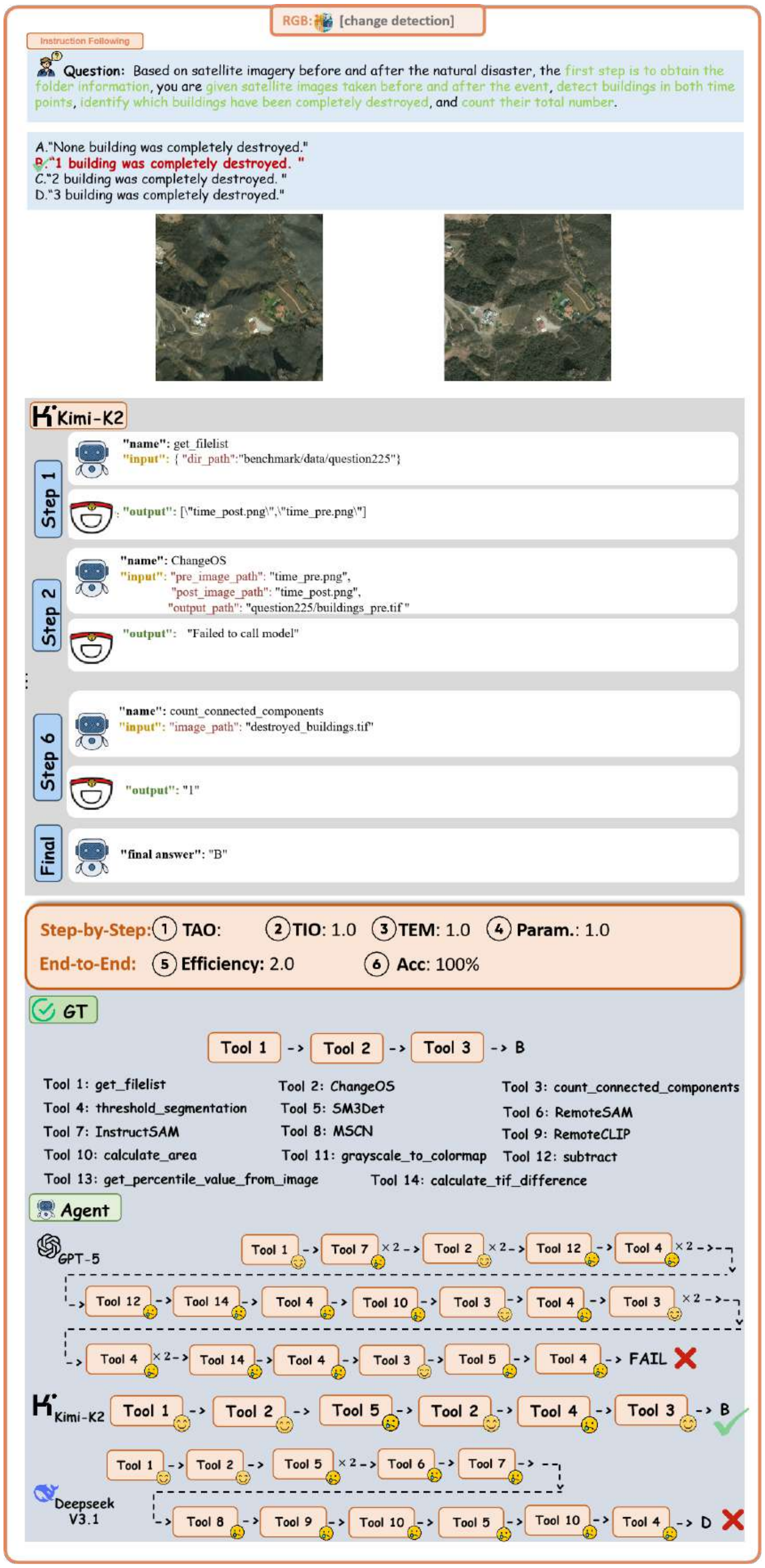
RGB: [change detection]
Instruction Following
Kimi-K2
Step 1
Step 2
Step 6
Final
GT
Tool 1 -> Tool 2 -> Tool 3 -> B
Agent
GPT-5
Tool 1 -> Tool 7 ×2 -> Tool 2 ×2 -> Tool 12 -> Tool 4 ×2 -> Tool 12 -> Tool 14 -> Tool 4 -> Tool 10 -> Tool 3 -> Tool 4 -> Tool 3 ×2 -> Tool 4 ×2 -> Tool 14 -> Tool 4 -> Tool 3 -> Tool 5 -> Tool 4 -> FAIL ✗
Kimi-K2
Tool 1 -> Tool 2 -> Tool 5 -> Tool 2 -> Tool 4 -> Tool 3 -> B ✓
Deepseek V3.1
Tool 1 -> Tool 2 -> Tool 5 ×2 -> Tool 6 -> Tool 7 -> Tool 8 -> Tool 9 -> Tool 10 -> Tool 5 -> Tool 10 -> Tool 4 -> D ✗

Question: Based on satellite imagery before and after the natural disaster, the first step is to obtain the folder information, you are given satellite images taken before and after the event, detect buildings in both time points, identify which buildings have been completely destroyed, and count their total number.

A."None building was completely destroyed."
B."1 building was completely destroyed. " ✓
C."2 building was completely destroyed. "
D."3 building was completely destroyed."

Step 1

"name": get_filelist
"input": { "dir_path":"benchmark/data/question225"}

"output": [\"time_post.png\",\"time_pre.png\"]

Step 2

"name": ChangeOS
"input": "pre_image_path": "time_pre.png",
"post_image_path": "time_post.png",
"output_path": "question225/buildings_pre.tif "

"output": "Failed to call model"

⋮

Step 6

"name": count_connected_components
"input": "image_path": "destroyed_buildings.tif"

"output": "1"

Final

"final answer": "B"

Step-by-Step: ① TAO: ② TIO: 1.0 ③ TEM: 1.0 ④ Param.: 1.0
End-to-End: ⑤ Efficiency: 2.0 ⑥ Acc: 100%

Tool 1: get_filelist
Tool 2: ChangeOS
Tool 3: count_connected_components
Tool 4: threshold_segmentation
Tool 5: SM3Det
Tool 6: RemoteSAM
Tool 7: InstructSAM
Tool 8: MSCN
Tool 9: RemoteCLIP
Tool 10: calculate_area
Tool 11: grayscale_to_colormap
Tool 12: subtract
Tool 13: get_percentile_value_from_image
Tool 14: calculate_tif_difference

Figure 29: **Example of Change Detection with RGB Data under the Instruction-Following Regime.**

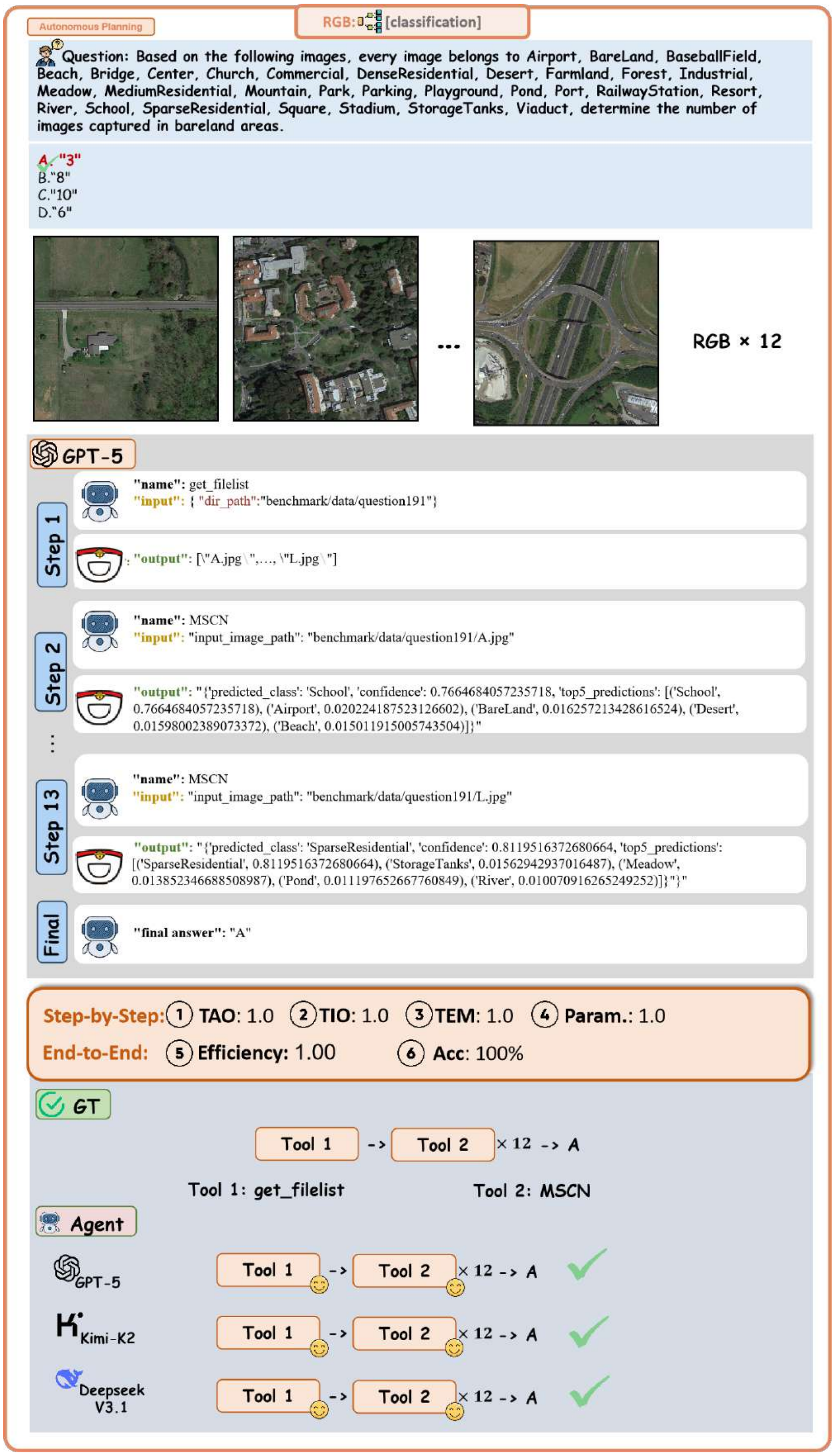

Question: Based on the following images, every image belongs to Airport, BareLand, BaseballField, Beach, Bridge, Center, Church, Commercial, DenseResidential, Desert, Farmland, Forest, Industrial, Meadow, MediumResidential, Mountain, Park, Parking, Playground, Pond, Port, RailwayStation, Resort, River, School, SparseResidential, Square, Stadium, StorageTanks, Viaduct, determine the number of images captured in bareland areas.

A. "3" ✓
B."8"
C."10"
D."6"

Step 1

```
"name": get_filelist
"input": { "dir_path":"benchmark/data/question191"}
```

```
"output": [\"A.jpg\",..., \"L.jpg\"]
```

Step 2

```
"name": MSCN
"input": "input_image_path": "benchmark/data/question191/A.jpg"
```

```
"output": "{'predicted_class': 'School', 'confidence': 0.7664684057235718, 'top5_predictions': [('School',
0.7664684057235718), ('Airport', 0.020224187523126602), ('BareLand', 0.016257213428616524), ('Desert',
0.01598002389073372), ('Beach', 0.015011915005743504)]}"
```

⋮

Step 13

```
"name": MSCN
"input": "input_image_path": "benchmark/data/question191/L.jpg"
```

```
"output": "{'predicted_class': 'SparseResidential', 'confidence': 0.8119516372680664, 'top5_predictions':
[('SparseResidential', 0.8119516372680664), ('StorageTanks', 0.01562942937016487), ('Meadow',
0.013852346688508987), ('Pond', 0.011197652667760849), ('River', 0.010070916265249252)]}"}"
```

Final

```
"final answer": "A"
```

Step-by-Step: ① TAO: 1.0 ② TIO: 1.0 ③ TEM: 1.0 ④ Param.: 1.0

End-to-End: ⑤ Efficiency: 1.00 ⑥ Acc: 100%

GT

Tool 1 -> Tool 2 × 12 -> A

Tool 1: get_filelist Tool 2: MSCN

Agent

GPT-5: Tool 1 -> Tool 2 × 12 -> A ✓

Kimi-K2: Tool 1 -> Tool 2 × 12 -> A ✓

Deepseek V3.1: Tool 1 -> Tool 2 × 12 -> A ✓

Figure 30: **Example of Classification with RGB Data under the Auto-Planning Regime.**

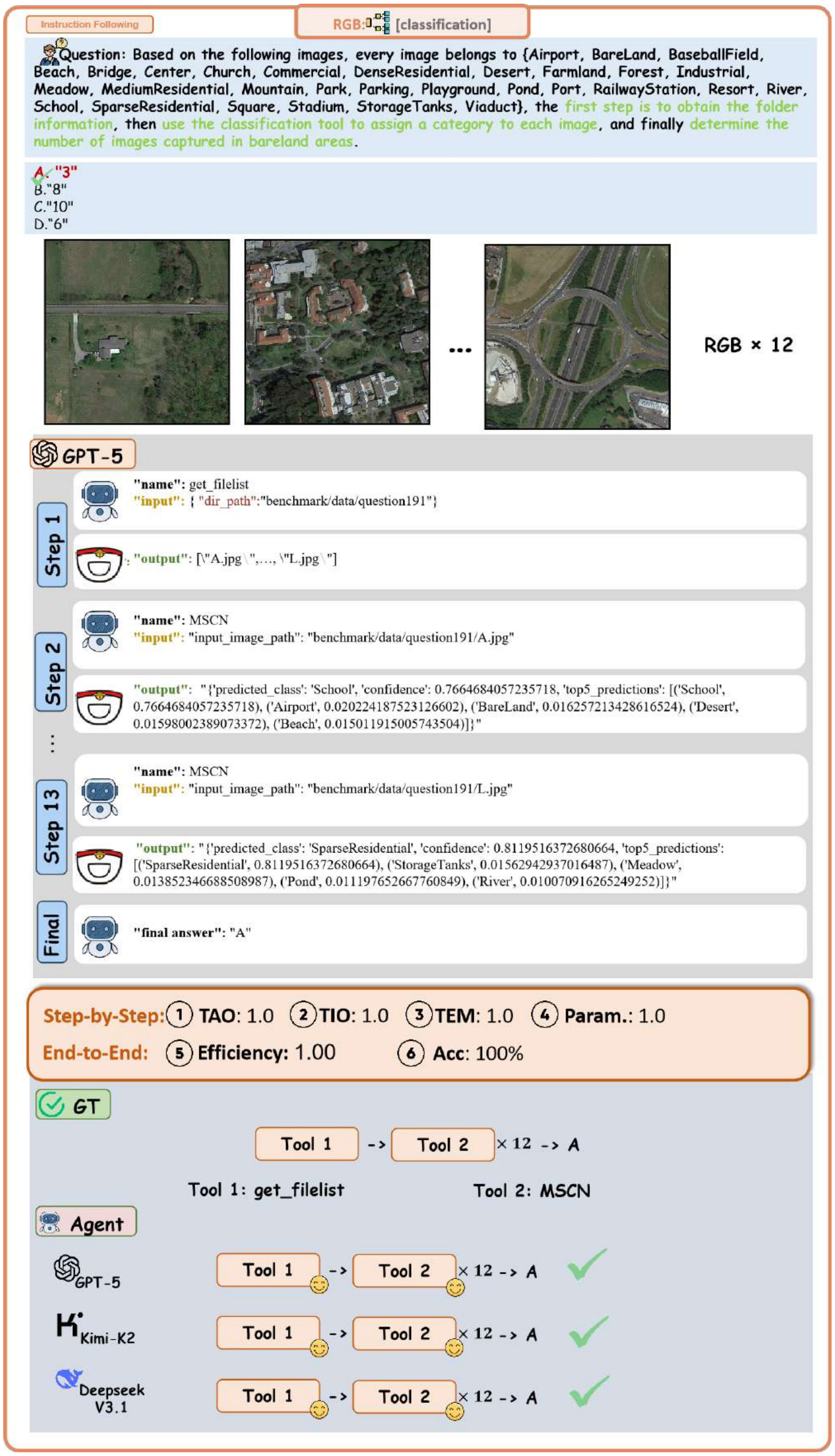

Question: Based on the following images, every image belongs to {Airport, BareLand, BaseballField, Beach, Bridge, Center, Church, Commercial, DenseResidential, Desert, Farmland, Forest, Industrial, Meadow, MediumResidential, Mountain, Park, Parking, Playground, Pond, Port, RailwayStation, Resort, River, School, SparseResidential, Square, Stadium, StorageTanks, Viaduct}, the first step is to obtain the folder information, then use the classification tool to assign a category to each image, and finally determine the number of images captured in bareland areas.

A."3"
B."8"
C."10"
D."6"

Step 1

```
"name": get_filelist
"input": { "dir_path":"benchmark/data/question191"}
```

```
"output": [\"A.jpg\",..., \"L.jpg\"]
```

Step 2

```
"name": MSCN
"input": "input_image_path": "benchmark/data/question191/A.jpg"
```

```
"output": "{'predicted_class': 'School', 'confidence': 0.7664684057235718, 'top5_predictions': [('School', 0.7664684057235718), ('Airport', 0.020224187523126602), ('BareLand', 0.016257213428616524), ('Desert', 0.01598002389073372), ('Beach', 0.015011915005743504)]}"
```

⋮

Step 13

```
"name": MSCN
"input": "input_image_path": "benchmark/data/question191/L.jpg"
```

```
"output": "{'predicted_class': 'SparseResidential', 'confidence': 0.8119516372680664, 'top5_predictions': [('SparseResidential', 0.8119516372680664), ('StorageTanks', 0.01562942937016487), ('Meadow', 0.013852346688508987), ('Pond', 0.011197652667760849), ('River', 0.010070916265249252)]}"
```

Final

```
"final answer": "A"
```

Step-by-Step: ① TAO: 1.0 ② TIO: 1.0 ③ TEM: 1.0 ④ Param.: 1.0

End-to-End: ⑤ Efficiency: 1.00 ⑥ Acc: 100%

GT
Tool 1 -> Tool 2 × 12 -> A
Tool 1: get_filelist
Tool 2: MSCN
Agent
GPT-5
Tool 1 -> Tool 2 × 12 -> A ✓
Kimi-K2
Tool 1 -> Tool 2 × 12 -> A ✓
Deepseek V3.1
Tool 1 -> Tool 2 × 12 -> A ✓

Figure 31: **Example of Classification with RGB Data under the Instruction-Following Regime.**

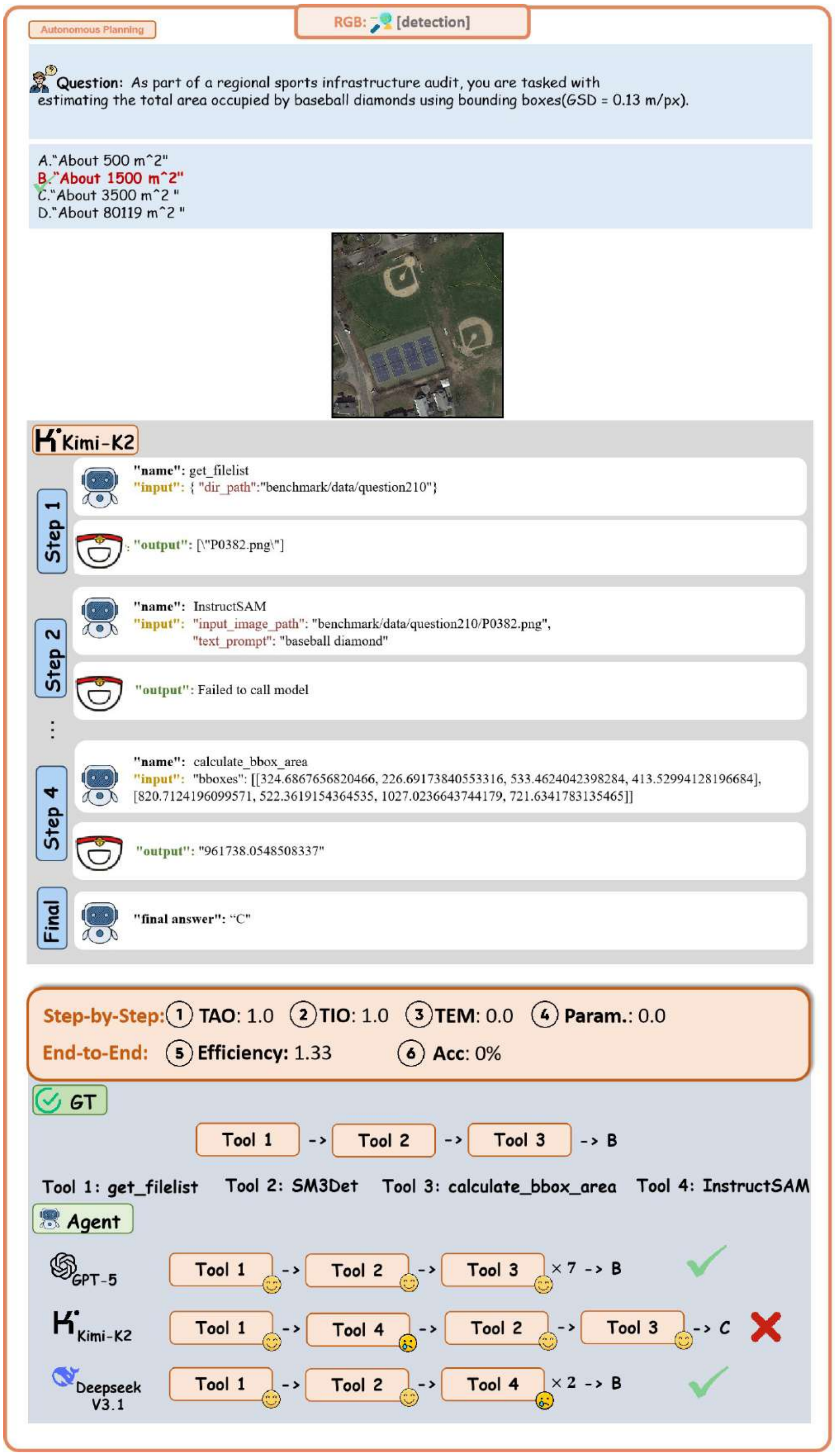

Question: As part of a regional sports infrastructure audit, you are tasked with estimating the total area occupied by baseball diamonds using bounding boxes(GSD = 0.13 m/px).

A."About 500 m^2"
B."About 1500 m^2" ✓
C."About 3500 m^2 "
D."About 80119 m^2 "

Kimi-K2

Step 1

"name": get_filelist
"input": { "dir_path":"benchmark/data/question210"}

"output": [\"P0382.png\"]

Step 2

"name": InstructSAM
"input": "input_image_path": "benchmark/data/question210/P0382.png",
"text_prompt": "baseball diamond"

"output": Failed to call model

⋮

Step 4

"name": calculate_bbox_area
"input": "bboxes": [[324.6867656820466, 226.69173840553316, 533.4624042398284, 413.52994128196684], [820.7124196099571, 522.3619154364535, 1027.0236643744179, 721.6341783135465]]

"output": "961738.0548508337"

Final

"final answer": "C"

Step-by-Step: ① TAO: 1.0 ② TIO: 1.0 ③ TEM: 0.0 ④ Param.: 0.0
End-to-End: ⑤ Efficiency: 1.33 ⑥ Acc: 0%

GT

Tool 1 -> Tool 2 -> Tool 3 -> B

Tool 1: get_filelist Tool 2: SM3Det Tool 3: calculate_bbox_area Tool 4: InstructSAM

Agent

GPT-5: Tool 1 -> Tool 2 -> Tool 3 × 7 -> B ✓
Kimi-K2: Tool 1 -> Tool 4 -> Tool 2 -> Tool 3 -> C ✗
Deepseek V3.1: Tool 1 -> Tool 2 -> Tool 4 × 2 -> B ✓

Figure 32: **Example of Detection with RGB Data under the Auto-Planning Regime.**

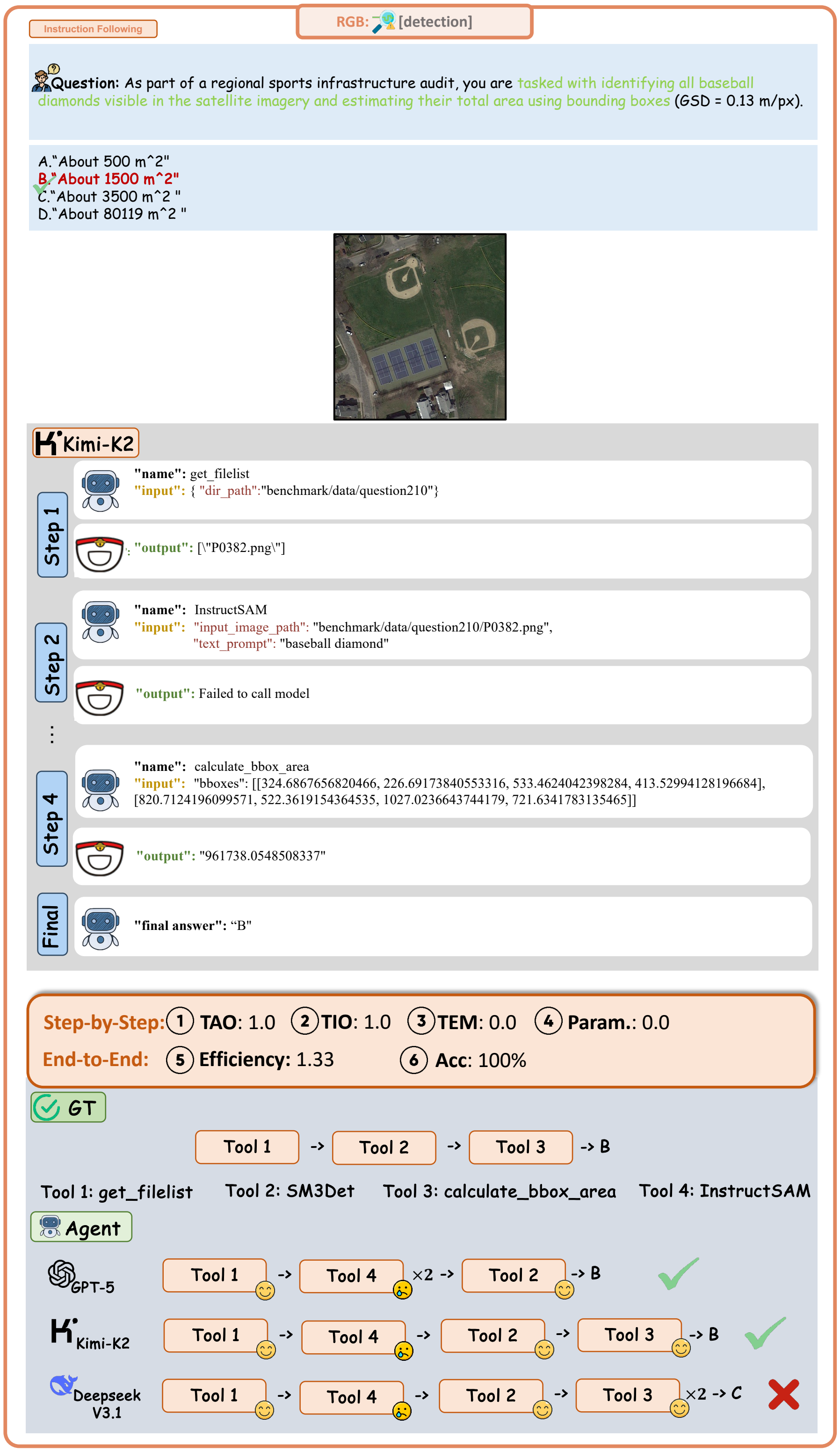

Instruction Following

RGB: [detection]

Question: As part of a regional sports infrastructure audit, you are tasked with identifying all baseball diamonds visible in the satellite imagery and estimating their total area using bounding boxes (GSD = 0.13 m/px).

A."About 500 m^2"
✓ B."About 1500 m^2"
C."About 3500 m^2 "
D."About 80119 m^2 "

Kimi-K2

Step 1

```
"name": get_filelist
"input": { "dir_path":"benchmark/data/question210"}
"output": [\"P0382.png\"]
```

Step 2

```
"name":  InstructSAM
"input":  "input_image_path": "benchmark/data/question210/P0382.png",
          "text_prompt": "baseball diamond"
"output": Failed to call model
```

⋮

Step 4

```
"name":  calculate_bbox_area
"input":  "bboxes": [[324.6867656820466, 226.69173840553316, 533.4624042398284, 413.52994128196684],
[820.7124196099571, 522.3619154364535, 1027.0236643744179, 721.6341783135465]]
"output": "961738.0548508337"
```

Final

```
"final answer": “B"
```

Step-by-Step: ① TAO: 1.0 ② TIO: 1.0 ③ TEM: 0.0 ④ Param.: 0.0
End-to-End: ⑤ Efficiency: 1.33 ⑥ Acc: 100%

GT

Tool 1 -> Tool 2 -> Tool 3 -> B

Tool 1: get_filelist Tool 2: SM3Det Tool 3: calculate_bbox_area Tool 4: InstructSAM

Agent

GPT-5: Tool 1 😊 -> Tool 4 😢 ×2 -> Tool 2 😊 -> B ✓
Kimi-K2: Tool 1 😊 -> Tool 4 😢 -> Tool 2 😊 -> Tool 3 😊 -> B ✓
Deepseek V3.1: Tool 1 😊 -> Tool 4 😢 -> Tool 2 😊 -> Tool 3 😊 ×2 -> C ✗

Figure 33: **Example of Detection with RGB Data under the Instruction-Following Regime.**

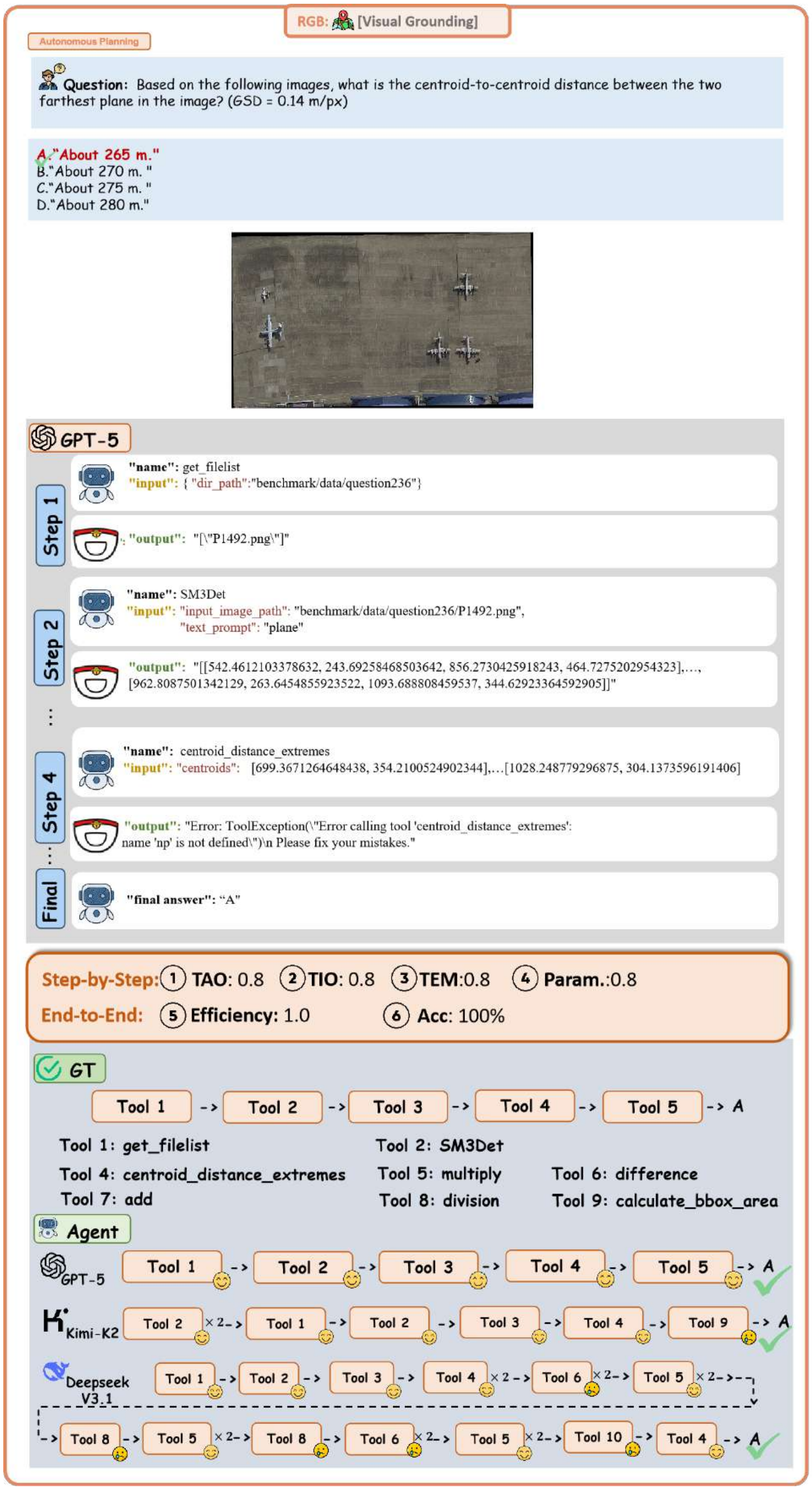

Question: Based on the following images, what is the centroid-to-centroid distance between the two farthest plane in the image? (GSD = 0.14 m/px)

A."About 265 m."
B."About 270 m. "
C."About 275 m. "
D."About 280 m."

GPT-5

Step 1

```
"name": get_filelist
"input": { "dir_path":"benchmark/data/question236"}
```

```
"output":  "[\"P1492.png\"]"
```

Step 2

```
"name": SM3Det
"input": "input_image_path": "benchmark/data/question236/P1492.png",
         "text_prompt": "plane"
```

```
"output":  "[[542.4612103378632, 243.69258468503642, 856.2730425918243, 464.7275202954323],…,
[962.8087501342129, 263.6454855923522, 1093.688808459537, 344.62923364592905]]"
```

⋮

Step 4

```
"name":  centroid_distance_extremes
"input": "centroids":   [699.3671264648438, 354.2100524902344],…[1028.248779296875, 304.1373596191406]
```

```
"output": "Error: ToolException(\"Error calling tool 'centroid_distance_extremes':
name 'np' is not defined\")\n Please fix your mistakes."
```

⋮

Final

```
"final answer": “A"
```

Step-by-Step: ① **TAO**: 0.8 ② **TIO**: 0.8 ③ **TEM**:0.8 ④ **Param.**:0.8

End-to-End: ⑤ **Efficiency:** 1.0 ⑥ **Acc**: 100%

Tool 1: get_filelist
Tool 2: SM3Det
Tool 4: centroid_distance_extremes
Tool 5: multiply
Tool 6: difference
Tool 7: add
Tool 8: division
Tool 9: calculate_bbox_area

Agent
GPT-5 Tool 1 -> Tool 2 -> Tool 3 -> Tool 4 -> Tool 5 -> A ✓
Kimi-K2 Tool 2 × 2-> Tool 1 -> Tool 2 -> Tool 3 -> Tool 4 -> Tool 9 -> A ✓
Deepseek V3.1 Tool 1 -> Tool 2 -> Tool 3 -> Tool 4 × 2 -> Tool 6 × 2-> Tool 5 × 2->
-> Tool 8 -> Tool 5 × 2-> Tool 8 -> Tool 6 × 2-> Tool 5 × 2-> Tool 10 -> Tool 4 -> A ✓

Figure 34: Example of Visual Grounding with RGB Data under the Auto-Planning Regime.

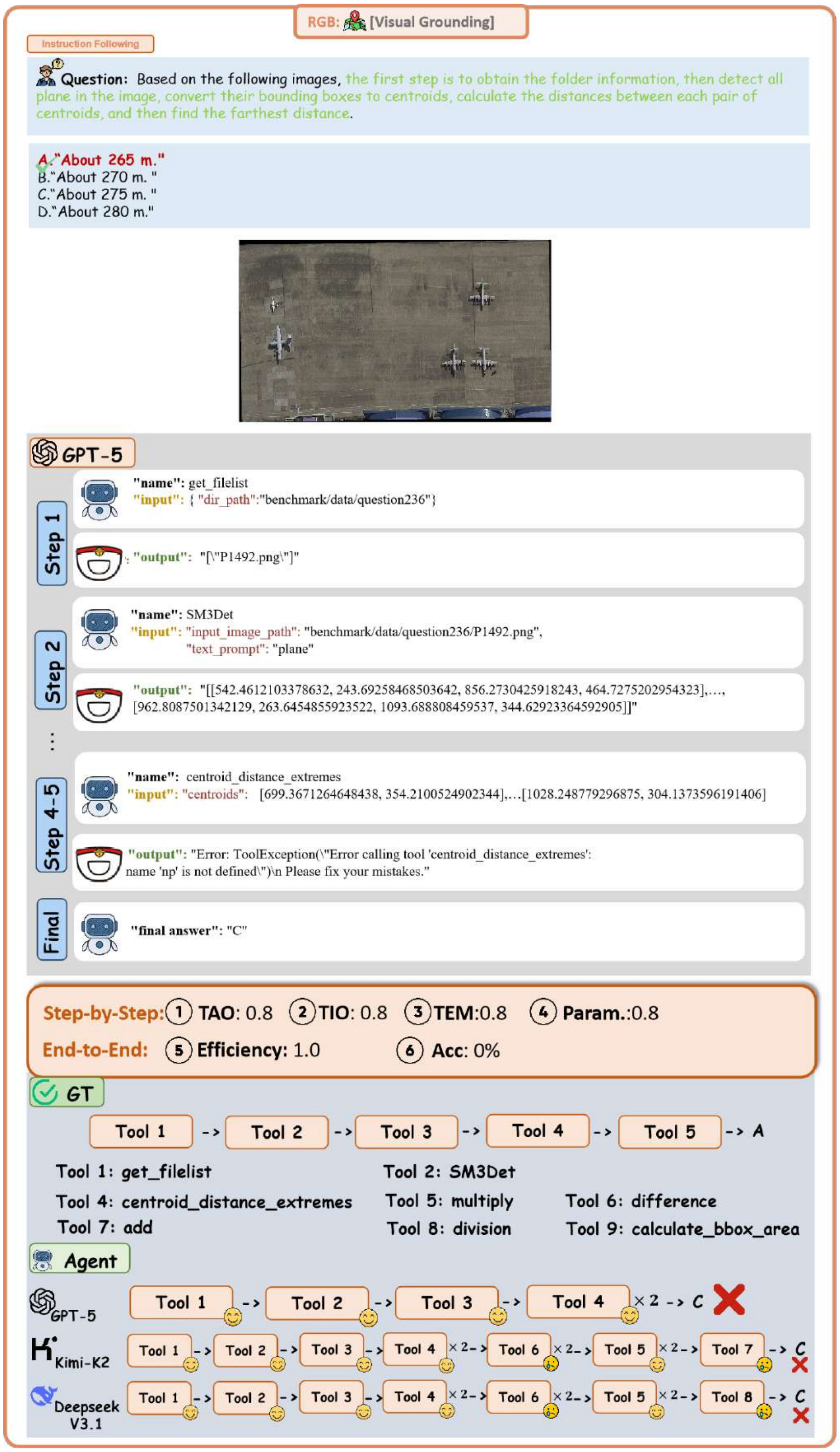

RGB: [Visual Grounding]

Instruction Following

Question: Based on the following images, the first step is to obtain the folder information, then detect all plane in the image, convert their bounding boxes to centroids, calculate the distances between each pair of centroids, and then find the farthest distance.

✓ A."About 265 m."
B."About 270 m. "
C."About 275 m. "
D."About 280 m."

GPT-5

Step 1

```
"name": get_filelist
"input": { "dir_path":"benchmark/data/question236"}
```

```
"output":  "[\"P1492.png\"]"
```

Step 2

```
"name": SM3Det
"input": "input_image_path": "benchmark/data/question236/P1492.png",
         "text_prompt": "plane"
```

```
"output":  "[[542.4612103378632, 243.69258468503642, 856.2730425918243, 464.7275202954323],…,
[962.8087501342129, 263.6454855923522, 1093.688808459537, 344.62923364592905]]"
```

⋮

Step 4-5

```
"name":  centroid_distance_extremes
"input": "centroids":  [699.3671264648438, 354.2100524902344],…[1028.248779296875, 304.1373596191406]
```

```
"output": "Error: ToolException(\"Error calling tool 'centroid_distance_extremes':
name 'np' is not defined\")\n Please fix your mistakes."
```

Final

```
"final answer": "C"
```

Step-by-Step: ① **TAO**: 0.8 ② **TIO**: 0.8 ③ **TEM**:0.8 ④ **Param.**:0.8

End-to-End: ⑤ **Efficiency:** 1.0 ⑥ **Acc**: 0%

GT

Tool 1 -> Tool 2 -> Tool 3 -> Tool 4 -> Tool 5 -> A

Tool 1: get_filelist
Tool 2: SM3Det
Tool 4: centroid_distance_extremes
Tool 5: multiply
Tool 6: difference
Tool 7: add
Tool 8: division
Tool 9: calculate_bbox_area

Agent

GPT-5: Tool 1 -> Tool 2 -> Tool 3 -> Tool 4 × 2 -> C ✗

Kimi-K2: Tool 1 -> Tool 2 -> Tool 3 -> Tool 4 × 2-> Tool 6 × 2-> Tool 5 × 2-> Tool 7 -> C ✗

Deepseek V3.1: Tool 1 -> Tool 2 -> Tool 3 -> Tool 4 × 2-> Tool 6 × 2-> Tool 5 × 2-> Tool 8 -> C ✗

Figure 35: **Example of Visual Grounding with RGB Data under the Instruction-Following Regime.**

I CASE STUDY: COMPARE WITH OTHER AGENTS

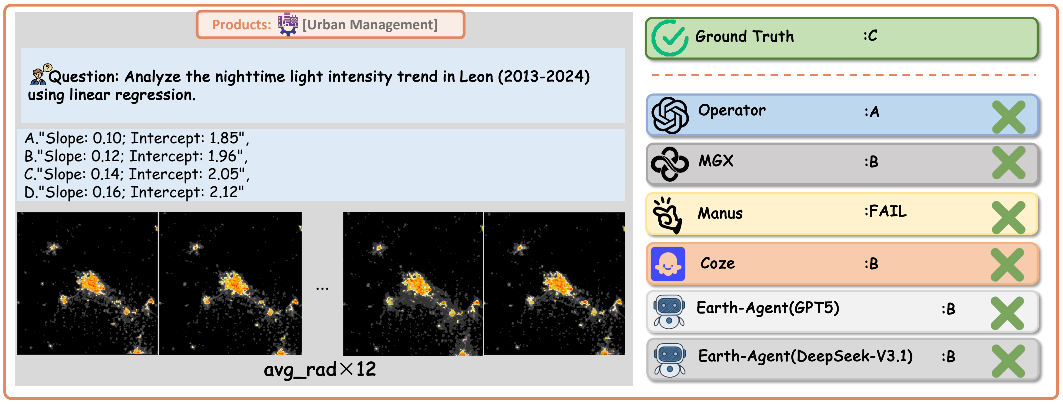

Question: Analyze the nighttime light intensity trend in Leon (2013-2024) using linear regression.

A."Slope: 0.10; Intercept: 1.85",
B."Slope: 0.12; Intercept: 1.96",
C."Slope: 0.14; Intercept: 2.05",
D."Slope: 0.16; Intercept: 2.12"

Ground Truth :C

Operator :A ✗
MGX :B ✗
Manus :FAIL ✗
Coze :B ✗
Earth-Agent(GPT5) :B ✗
Earth-Agent(DeepSeek-V3.1) :B ✗

Figure 36: **A Question Case of the Urban Management Task using Products Data with Responses from Different Agent.**

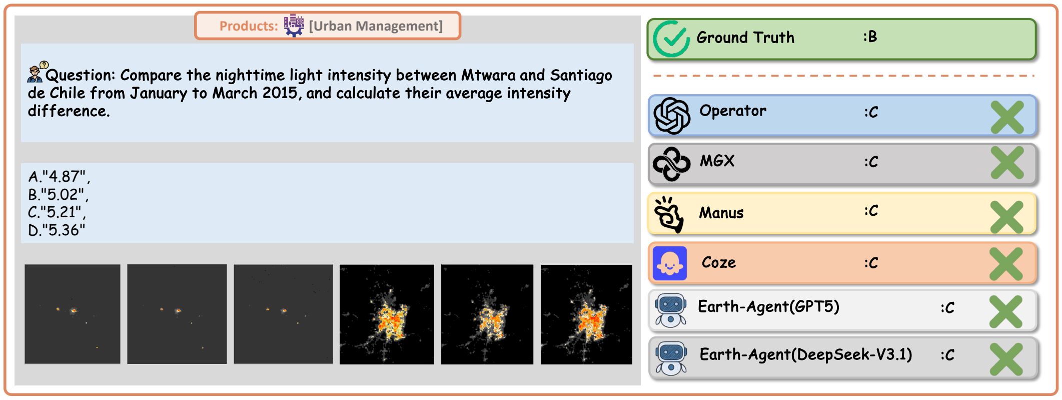

Question: Compare the nighttime light intensity between Mtwara and Santiago de Chile from January to March 2015, and calculate their average intensity difference.

A."4.87",
B."5.02",
C."5.21",
D."5.36"

Ground Truth :B

Operator :C ✗
MGX :C ✗
Manus :C ✗
Coze :C ✗
Earth-Agent(GPT5) :C ✗
Earth-Agent(DeepSeek-V3.1) :C ✗

Figure 37: **A Question Case of the Urban Management Task using Products Data with Responses from Different Agent.**

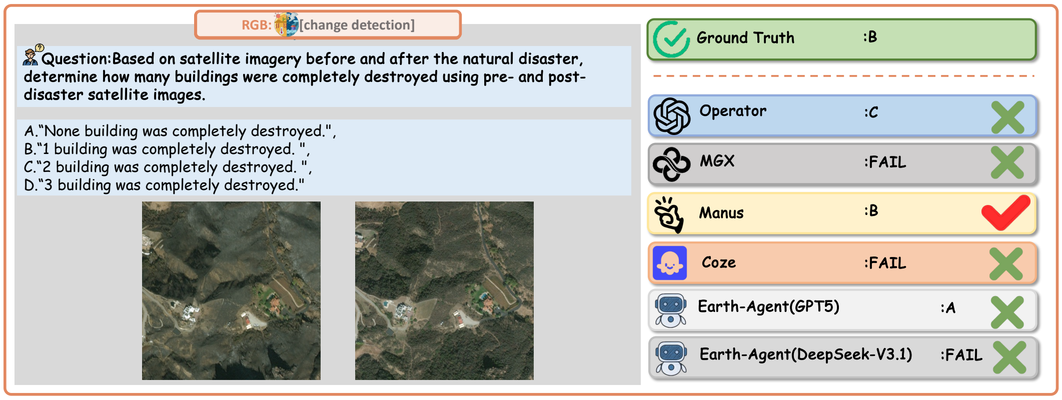

Question:Based on satellite imagery before and after the natural disaster, determine how many buildings were completely destroyed using pre- and post-disaster satellite images.

A."None building was completely destroyed.",
B."1 building was completely destroyed. ",
C."2 building was completely destroyed. ",
D."3 building was completely destroyed."

Ground Truth :B

Operator :C ✗
MGX :FAIL ✗
Manus :B ✓
Coze :FAIL ✗
Earth-Agent(GPT5) :A ✗
Earth-Agent(DeepSeek-V3.1) :FAIL ✗

Figure 38: **A Question Case of the Change Detection Task using RGB Data with Responses from Different Agent.**

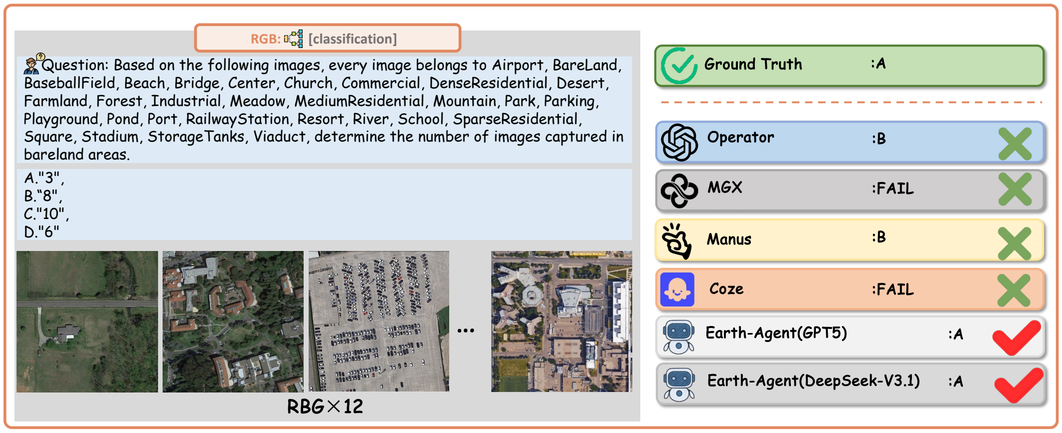

Question: Based on the following images, every image belongs to Airport, BareLand, BaseballField, Beach, Bridge, Center, Church, Commercial, DenseResidential, Desert, Farmland, Forest, Industrial, Meadow, MediumResidential, Mountain, Park, Parking, Playground, Pond, Port, RailwayStation, Resort, River, School, SparseResidential, Square, Stadium, StorageTanks, Viaduct, determine the number of images captured in bareland areas.

A."3",
B."8",
C."10",
D."6"

Ground Truth	:A	✓
Operator	:B	✗
MGX	:FAIL	✗
Manus	:B	✗
Coze	:FAIL	✗
Earth-Agent(GPT5)	:A	✓
Earth-Agent(DeepSeek-V3.1)	:A	✓

Figure 39: **A Question Case of the Classification Task using RGB Data with Responses from Different Agent.**

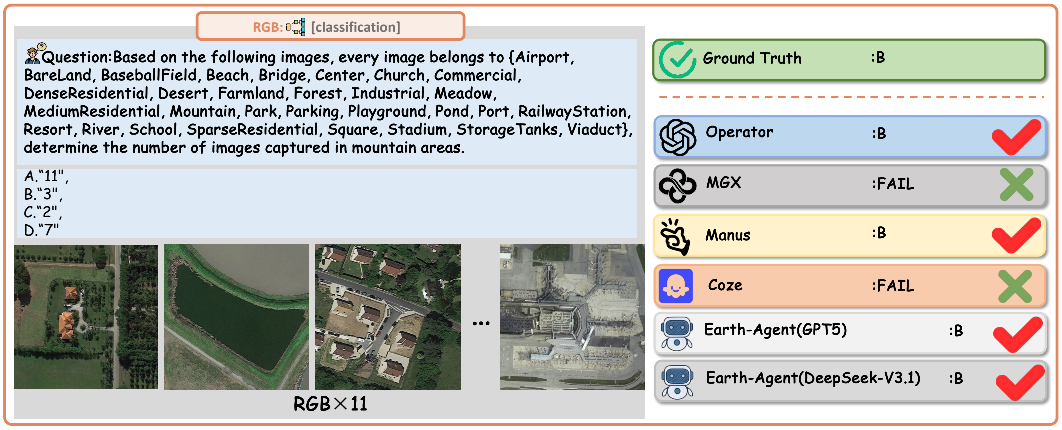

Question:Based on the following images, every image belongs to {Airport, BareLand, BaseballField, Beach, Bridge, Center, Church, Commercial, DenseResidential, Desert, Farmland, Forest, Industrial, Meadow, MediumResidential, Mountain, Park, Parking, Playground, Pond, Port, RailwayStation, Resort, River, School, SparseResidential, Square, Stadium, StorageTanks, Viaduct}, determine the number of images captured in mountain areas.

A."11",
B."3",
C."2",
D."7"

Ground Truth	:B	✓
Operator	:B	✓
MGX	:FAIL	✗
Manus	:B	✓
Coze	:FAIL	✗
Earth-Agent(GPT5)	:B	✓
Earth-Agent(DeepSeek-V3.1)	:B	✓

Figure 40: **A Question Case of the Classification Task using RGB Data with Responses from Different Agent.**

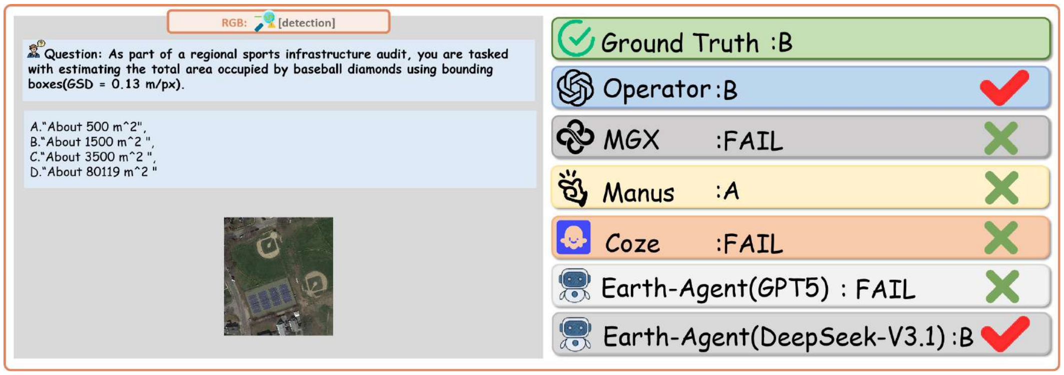

RGB: [detection]

Question: As part of a regional sports infrastructure audit, you are tasked with estimating the total area occupied by baseball diamonds using bounding boxes(GSD = 0.13 m/px).

A."About 500 m^2",
B."About 1500 m^2 ",
C."About 3500 m^2 ",
D."About 80119 m^2 "

Ground Truth :B
Operator :B ✓
MGX :FAIL ✗
Manus :A ✗
Coze :FAIL ✗
Earth-Agent(GPT5) : FAIL ✗
Earth-Agent(DeepSeek-V3.1) :B ✓

Figure 41: **A Question Case of the Detection Task using RGB Data with Responses from Different Agent.**

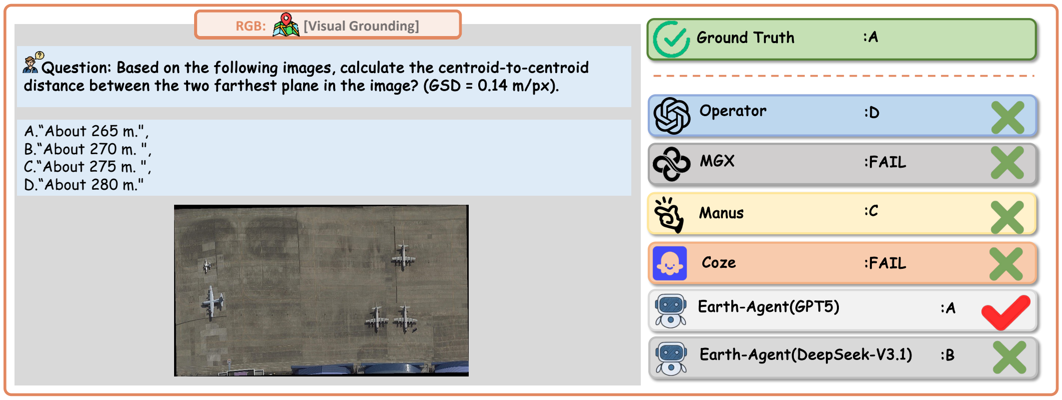

RGB: [Visual Grounding]

Question: Based on the following images, calculate the centroid-to-centroid distance between the two farthest plane in the image? (GSD = 0.14 m/px).

A."About 265 m.",
B."About 270 m. ",
C."About 275 m. ",
D."About 280 m."

Ground Truth :A
Operator :D ✗
MGX :FAIL ✗
Manus :C ✗
Coze :FAIL ✗
Earth-Agent(GPT5) :A ✓
Earth-Agent(DeepSeek-V3.1) :B ✗

Figure 42: **A Question Case of the Visual Grounding Task using RGB Data with Responses from Different Agent.**